THE UNIVERSITY OF QUEENSLAND

AUSTRALIA

Thermodynamics-Based Design of Creep Resistant Mg Solid Solutions Using the Miedema Scheme

Saeideh Abaspour

A thesis submitted for the degree of Doctor of Philosophy at

The University of Queensland in 2014

School of Mechanical and Mining Engineering

Abstract

Most current creep resistant alloy design methods for Mg alloys aim at incremental strengthening of existing alloys such as AZ91 thorough addition of ternary and quaternary elements, or alternatively through RE's additions. The most remarkable improvements has been through either Mg-Y or recently developed Mg-Gd-Y-Zr and Mg-Y-Nd-Zr alloys, although still below the strength of Mg-Th alloys, which are being phase out due to Th's radioactivity.

Many micromechanisms proposed to account for the observed improvements in either hardness or creep strength of Mg alloys including solid solution and/or precipitation hardening, dynamic precipitation, solute dragging/solute clustering and more importantly atomic size controlled diffusivity more often than not are little more than ad-hoc, after-the-fact explanations, valid at best for the particular system under consideration. Hence, extrapolation to other alloy-systems is either not possible or contradictory. In practice, a feasible path for systematic, either precipitation-hardened or creep-resistant Mg alloys, selection and design is still lacking.

The aim of the present work was to use atomic level thermodynamical arguments that suggest that extending the athermal regime through short range order (SRO) is a most feasible path to increasing the creep strength of Mg alloys. Potential solutes were sorted out and ranked based on their tendency to developing SRO using the Miedema's phenomenological scheme. The predictions were corroborated by experiments involving dilute binary alloys as well as through a collection of data from the literature.

Monotonic compression and stress relaxation tests were carried out on specimens of 6 cast binary alloys with (at.%) 2.5 Al, 0.6 Sn, 2.2 Zn, 0.8 Gd, 1.3 Y and 0.9 Nd, and of a similarly cast AZ91D alloy for reference. The solute concentration in the binary alloys was kept deliberately low to limit precipitation hardening effects during the testing. Compression testing was carried out at 298K (25°C), 373K (100°C) and 453K (180°C) for all of the alloys and at 493K (220°C) and 523K (250°C) for the Gd, Y and Nd containing ones. Stress relaxation testing was done at 453K (180°C) at either a predetermined strain (0.05) or stress (150 MPa).

The Mg-Al and the AZ91 alloys softened considerably above 373K (100°C), consistently with random solid solution by Al. The rest of the alloys exhibited increasing strength and reduced relaxation, in the order Sn, Zn, Nd, Gd and Y, an indication of a progressively extended athermal regime in the strength-temperature relationship of these alloys. The overall behaviour can be

accounted for through the respective solutes' tendency to develop short range order, lowest for Al and highest for Y, Gd and Nd, in agreement with what the respective phase diagrams suggest.

The relative tendency or lack of it, of most solutes to develop SRO rationalizes a number of observations in current multicomponent Mg alloys while it disputes the viability of several other micromechanisms often considered.

The feasibility of strengthening HPDC Mg alloys through a combination of percolating eutectics and residual solute in solution, or, more generally, age hardenable alloys through either homogeneously nucleated, coherent with the Mg matrix, precipitates, or via internally ordered precipitates mimicking Mg-Th alloy system, is also considered by making parallels with either the Al-Zn or the Al-Cu alloy systems. Examples of these approaches were discussed using data from the literature, such as experiments on alloys combining Mn and Sc to introduce order in the soft Mn precipitates, or the use of Na to provide finely dispersed, homogeneously nucleated clusters with the aim of refining the subsequent precipitation in alloys such as Mg-Sn.

Declaration by author

This thesis is composed of my original work, and contains no material previously published or written by another person except where due reference has been made in the text. I have clearly stated the contribution by others to jointly-authored works that I have included in my thesis.

I have clearly stated the contribution of others to my thesis as a whole, including statistical assistance, survey design, data analysis, significant technical procedures, professional editorial advice, and any other original research work used or reported in my thesis. The content of my thesis is the result of work I have carried out since the commencement of my research higher degree candidature and does not include a substantial part of work that has been submitted *to qualify for the award of any* other degree or diploma in any university or other tertiary institution. I have clearly stated which parts of my thesis, if any, have been submitted to qualify for another award.

I acknowledge that an electronic copy of my thesis must be lodged with the University Library and, subject to the General Award Rules of The University of Queensland, immediately made available for research and study in accordance with the Copyright Act 1968 unless a period of embargo has been approved by the Dean of the Graduate School.

I acknowledge that copyright of all material contained in my thesis resides with the copyright holder(s) of that material. Where appropriate I have obtained copyright permission from the copyright holder to reproduce material in this thesis.

Publications during candidature

- **Peer-reviewed conference papers:**

1) S. Abaspour and C. H. Caceres: The Athermal Component of the Strength of Binary Mg Solid Solutions. Edited by Martyn Alderman, Michele V. Manuel, Norbert Hort, Neale R. Neelameggham. Magnesium Technology 2014. TMS 2014 143rd Annual Meeting and Exhibition, February 16-20, San Diego Convention Centre, San Diego, California

2) S. Abaspour and C H Caceres: Creep Behaviour of Mg Binary Solid Solutions. Edited by Norbert Hort, Suveen N. Mathaudhu, Neale R. Neelameggham and Martyn Alderman. Magnesium Technology 2013. TMS 2013, 142nd Annual Meeting and Exhibition, San Antonio, United States, (17-20). 3-7 March 2013.

3) C. H. Caceres and S. Abaspour: Bounds to Hardening by Solid Solution, Precipitation and Short Range Order in Mg Binary Alloys. Edited by Norbert Hort, Suveen N. Mathaudhu, Neale R. Neelameggham and Martyn Alderman. Magnesium Technology 2013. TMS 2013, 142nd Annual Meeting and Exhibition, San Antonio, United States, (227-230). 3-7 March 2013.

Publications included in this thesis

Chapter 3

C. H. Caceres, **S. Abaspour**: Bounds to Hardening by Solid Solution, Precipitation and Short Range Order in Mg Binary Alloys. In Magnesium Technology 2013. TMS 2013.

Contributor	Statement of contribution
S. Abaspour (Candidate)	Designed / performed experiments (90%) Wrote and edited the paper (50%)
C. H. Caceres	Designed experiments (10%) Wrote and edited paper (50%)

Chapter 4

S. Abaspour, C. H. Caceres: Creep Behaviour of Mg Binary Solid Solutions. In: Magnesium Technology 2013. TMS 2013.

Contributor	Statement of contribution
S. Abaspour (Candidate)	Designed / performed experiments (90%) Wrote and edited the paper (90%)
C. H. Caceres	Designed experiments (10%) Wrote and edited paper (10%)

Chapter 5

S. Abaspour, C. H. Caceres: The Athermal Component of the Strength of Binary Mg Solid Solutions. In Magnesium Technology 2014. TMS 2014.

Contributor	Statement of contribution
S. Abaspour (Candidate)	Designed / performed experiments (90%) Wrote and edited the paper (90%)
C. H. Caceres	Designed experiments (10%) Wrote and edited paper (10%)

Contributions by others to the thesis

No contributions by others.

Statement of parts of the thesis submitted to qualify for the award of another degree

None.

Acknowledgements

I would like to express my sincere gratitude to my supervisor Dr. Carlos H Caceres for his guidance, encouragement and suggestions for carrying out the research.

I would also like to thank Graham Ruhle, Daniel Graham, Glenda Zemanek, Tharmalingam Sivarupan, Nagarajan Devarajan and Kun Yang, for assisting me in my experiments and also providing valuable suggestions.

I greatly acknowledge the financial support provided by the University of Queensland Research Scholarship (UQRS) and the ARC Centre of Excellence for Design in Light Metals throughout my candidature.

Keywords

Creep, Solid Solution Strengthening, Magnesium alloys, Stress Relaxation, Short Range Order, Miedema Scheme, Enthalpy of Formation, Athermal behaviour, Intermetallic, Phase Diagram.

Australian and New Zealand Standard Research Classifications (ANZSRC)

ANZSRC code: 091207, Metals and Alloy Materials, 100%

Fields of Research (FoR) Classification

FoR code: 0912, Materials Engineering, 100%

Table of Contents

List of figures

List of Tables

Introduction

Despite a good combination of room temperature mechanical and physical properties, excellent die-castability and, good corrosion resistance, the most commonly used Mg alloys, AZ and AM series, have restricted powertrain applications-where the most weight reduction is achievable- due to their low creep resistance. Several studies show that the poor elevated temperature performance of Mg-Al based alloys could be attributed to the coarsening of the eutectic β-$Mg_{17}Al_{12}$ phase, with a low melting point of 437°C, as well as dynamic discontinuous precipitation of $Mg_{17}Al_{12}$ from the α-Mg matrix which leads to grain boundary sliding [1, 2].

A continued research effort led to several new creep resistant alloys based on either the reinforcement of grain boundaries with thermally stable intermetallic particles, or the strengthening of α-Mg matrix by solid solution or precipitation hardening [3]. In the case of Mg-Al based alloys, addition of elements such as Ca[4], Sr[5], RE[2], Si[1, 6] and Sb[1] with higher affinity to Aluminum, suppresses the formation of $Mg_{17}Al_{12}$ phase and facilitates the formation of thermally stable intermetallic phases, strengthening the grain boundaries and consequently decreasing the creep rate of the alloys. On the other hand, Zhu *et al.* [3] have reported that the main strengthening mechanism in die-cast Mg-RE binary alloys is solid solution strengthening of the α-Mg matrix.

Solid solution strengthening of Mg alloys has been studied considering different solute- dislocation interactions. Akhtar and Teghtsoonian [7, 8] have reported that elastic and shear modulus interactions are the dominant strengthening mechanism in solid solution strengthening of dilute (less than 0.5 at.%) Mg-Zn alloys. In addition, chemical interaction has been introduced as the principle solid solution strengthening mechanism in Mg-Al (2.71 at.%) and Mg-Li [9]. Caceres and Blake[10] have also suggested that short range order (SRO) is the dominant strengthening mechanism in Mg-Zn concentrated alloys.

A distinguishing feature of the Mg alloys' field is that many micromechanisms proposed to account for the observed improvements in either hardness or creep strength more often than not are little more than ad-hoc, after-the-fact explanations, valid at best for the particular system under consideration. Hence, extrapolation to other alloy-systems is either not possible or contradictory. In practice, a feasible path for systematic, either precipitation-hardened or creep-resistant Mg alloys, selection and design is still lacking.

The aim of the current research is to quantify the effect of solid solution strengthening, focused on SRO, on the creep behaviour of dilute binary Mg alloys. Atomic level thermodynamics, through the

classical Miedema *et al.*'s [11-14] phenomenological scheme, is used to sort out solutes according to their expected strength of SRO behaviour during age hardening or to their potential effect on the extent of the athermal regime regarding creep. The scheme naturally suggests a rational approach to solute selection, hence, to alloy design, derived from the relevant binary phase diagrams.

Chapter 1 : Literature review

1.1 Creep in Pure Polycrystalline Magnesium

The deformation mechanisms of pure polycrystalline magnesium at elevated temperatures have been investigated [15] over a stress and temperature range of 20-50MPa and 150-250°C, respectively, and typical creep curves have been observed, revealing a decelerating creep rate in primary stage and steady state secondary creep. Several studies [4, 15, 16] have also shown the typical three creep stages in high temperature deformation of Mg and Mg-Al based alloys. It is generally accepted [4, 15, 17] that the steady state secondary creep rate of magnesium and Mg-Al alloys in the stress (σ) and temperature (T) ranges of 20 to 40 MPa and 100°C to 250°C can be described by a power-law equation:

$$\varepsilon^0 = A\sigma^n exp\left(\frac{-Q}{RT}\right) \qquad (1)$$

where *A*, *R*, *Q*, and *n* are a material constant, the gas constant, the activation energy for creep, and the stress exponent. Figure 1.1 shows the creep curves for pure polycrystalline magnesium indicating that the creep rate is increased with an increase in either applied stress at a constant temperature or temperature under constant stress. Shi and Northwood [15] have measured the stress exponent and activation energy of 5.86 and 106 KJ/mol, respectively, and dislocation climb stemming from diffusion of vacancies has been suggested as the dominant rate controlling mechanism in the steady state creep[15].

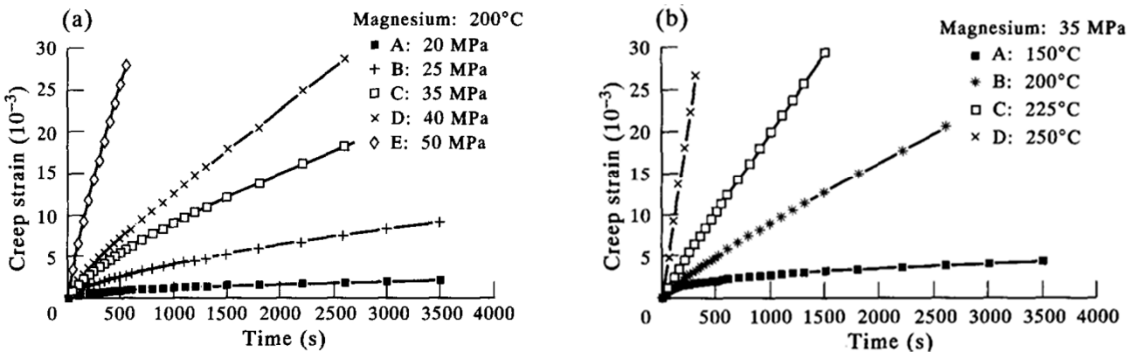

Figure 1-1 creep strain vs time curves for pure polycrystalline magnesium. (a) T=200°C and applied stress σ=20-50MPa, (b) σ=35Mpa and T=150-250°C [15].

Vagarali and Langdon [18] investigated the creep behaviour of polycrystalline magnesium, on a wider temperature range of 200-547°C. At lower temperatures (200-477°C), the activation energy for the creep was reported to be 135 KJ/mol which is consistent with the value for lattice self-diffusion. In addition, the stress exponent of 5.2 and extensive basal slip confirm that the creep rate is controlled by dislocation climb. At higher temperature (above 477°C), stress exponent was 6 and activation energy for creep increased with stress, due to the activation of non-basal slip. The creep rate was controlled by the cross slip of dislocations from the basal to the prismatic planes [18]. Creep behaviour of pure Mg at different strain rates also showed a transition from dislocation climb at strain rates $\leq 10^{-6} S^{-1}$ to cross-slip from the basal to prismatic planes at strain rates $\geq 10^{-6} S^{-1}$.

It has been suggested that diffusion-controlled dislocation climb is the principle creep mechanism in AZ91 under 150-180°C and 40-100MPa [17] and in AM60 at 180°C and 20-60MPa [19]. Dargusch *et al*. [6] also concluded that at low stresses (n=2) grain boundary sliding was the rate controlling mechanism while, at high stresses (n=5) dislocation climb dominated the deformation mechanism in AZ91, AS21, and AE42 alloys.

1.2 Creep of Solid Solution Alloys:

The creep of solid solution alloys is generally divided into class M (metal type) and class A (alloy type). Data of the former indicates a five-power-law creep, same as pure metals, with a normal primary stage of creep, and formation of subgrain structure. In this class, dislocation climbing is the rate controlling mechanism. The creep behaviour of alloy-type solid solutions is attributed to a viscous drag process involving three-power-law with a brief Primary stage [20, 21] In concentrated alloys dislocations are uniformly distributed [18, 22]. Mohamed [23] suggested that alloys with a large elastic modulus tend to show metal-type behaviour while class A behaviour is usually observed in alloys with a large atomic misfit ratio.

1.2.1 Creep of Class A (alloy type)

The dominant deformation mechanism in alloy-type solid solutions is viscous glide of dislocations controlled by solute-dislocation interactions. Solute atoms and dislocations show several types of interactions including the segregation of solute atoms to the core of the moving dislocation (Cottrell and Jaswon interaction), the destruction of short range order by dislocation motion creating an interface of positive energy (Fisher interaction), and chemical interaction leading to the segregation of solute atoms to stacking faults (Suzuki interaction). Diffusion-controlled glide mechanism

becomes slower than climb and therefore creep is controlled by the viscous glide of dislocations [20, 22, 24].

Of all the forms of solute-dislocation interactions, Cottrell and Jaswon interaction is the principle basis of different viscous-glide models. However, Mohamed [23] has suggested that the other interactions must be taken into consideration for a full account of the phenomenon. The solute dragging of dislocations has been formulated in different studies.

1.2.2 Weertman's Microcreep Theory:

In Weertman theory dislocation loops are emitted by sources and sweep until the interaction with the stress field of loops on different slip planes stops them, resulting in formation of dislocation pile-ups. At the same time, dislocations on other slip planes are annihilated by climb of the pile up's leading dislocations, generating new loops at the sources and leading to steady state creep [18, 20, 22]. The dislocations motion takes place as sequential glide and climb processes, and the rate-controlling mechanism is the slower of these two [18]. When the creep rate is controlled by dislocation glide, the creep rate is described by

$$\varepsilon^0 = \frac{0.35}{A} G \left(\frac{\sigma}{\varepsilon}\right)^3 \qquad (2)$$

where G is the shear modulus and A is an interaction parameter:

$$A = \frac{e^2 c b^5 G^2}{kT\tilde{D}} \qquad (3)$$

Where *e, c, b, k, T,* and *D* are the atom misfit parameter, the solute concentration, Burgers vector, Boltzmann's constant, the absolute temperature and the chemical interdiffusivity, respectively. If equation 3 is substituted into equation 2 the creep rate becomes:

$$\varepsilon_W^0 = \frac{kT\tilde{D}}{3e^2 c G b^5} \left(\frac{\sigma}{G}\right)^3 \qquad (4)$$

1.2.3 Takeuchi and Argon

In this model, with many points in common with Weertman's theory, Cottrell atmospheres are the retarding factor of dislocation motion. Since glide and climb occur sequentially, glide is the controlling step. The two theories differ in regards to the dislocation distribution. As soon as dislocation sources operate, emitted dislocations will disperse from their planes by climb, leading to

a homogenous distribution of dislocations [20, 25]. Takeuchi and Argon[25] suggested the following equation for steady state creep rate due to glide:

$$\varepsilon_{TA}^{0} = \frac{kT\tilde{D}}{8e^{2}cGb^{5}}\left(\frac{\sigma}{G}\right)^{3} \quad (5)$$

1.2.4 Creep of Class M (metal type)

The behaviour of class M indicates that the creep rate is controlled by a dislocation climb process. The creep curve exhibits an instantaneous strain after application of the load and normal primary creep stage. The steady state creep rate depends on the staking fault energy of the alloy. The steady state creep rate of many pure metals and solid solution alloys of class M can be described by:

$$\varepsilon^{0} = \mathrm{A}\frac{\mathrm{DGb}}{\mathrm{KT}}\left(\frac{\sigma}{\mathrm{G}}\right)^{\mathrm{n}} \quad (6)$$

where A is a dimensionless constant, D is the coefficient of self-diffusion, b is the Burgers vector, k is Boltzmann's constant, T is the absolute temperature, σ is the applied stress, G is the shear modulus, and n is a constant approximately equal to 5. Increasing the solute concentration changes the creep behaviour of solid solution alloys from class M to class A. This transition also occurs when the stress is increased above a certain critical value [20, 21].

1.3 Creep of Mg-based Solid Solution Alloys

The creep curves of Mg-based solid solution alloys such as Mg-Al [16], Mg-Zn[26] , Mg-Y[27] and Mg-Nd [28] reveal the typical three stages of creep: a decelerating primary creep followed by steady-state creep taking the minimum creep rate, and finally accelerated creep towards rupture [29].

1.3.1 Creep in Mg-Al

Aluminium increases the strength of the alloy by solution hardening mechanism [16] due to its large misfit. Several studies[16, 18] have shown that in Mg-Al solid solution alloys, creep is controlled by dislocation glide at low stresses whereas climb is the dominant mechanism at higher stresses, leading to the recovery of substructures. Even though the minimum creep rate of Mg-Al alloys decreases with increasing Al content at low stresses, the creep mechanism remains unchanged. At higher stresses and lower concentrations, dislocations are likely to escape from the solute atmosphere and the creep rate increases. Chino *et al.* [9] suggested that chemical interaction and

shear modulus effect account for the strengthening of Mg-at%2.71Al and Mg-0.036at%Ca solid solutions, respectively.

1.3.2 Creep in Mg-Y

Maruyama et al.[16] reported that solution hardening is the main strengthening mechanism in Mg-Y alloys, although forest-dislocation hardening and dynamic precipitation are also of great importance at higher Y contents. Operation of the non-basal slip system in supersaturated Mg-Y alloys at high temperatures leads to an increase in the critical stress for dislocation glide to pass through the forest dislocation and this effect is more pronounced at high Y contents [16, 27, 30]. Yttrium has been considered more effective than Al in strengthening Mg alloys at high temperature than Al, even though there is no considerable difference in size misfit of Y and of Al [27]. In Mg-Y solid solutions compared to Mg-Al, creep rate decreases by 3 orders of magnitude at a constant solute content [16].

1.3.3 Creep of Mg-Sn

Formation of thermally stable Mg_2Sn contributes to the strengthening of Mg-Sn alloys at both ambient and high temperature. The distribution of Mg_2Sn at grain boundaries along with its easy precipitation at 560°C are the main factors in improving the alloy strength [31]. Liu *et al.* [32] have reported that increasing tin content improves the creep resistance of Mg-(1-10%)Sn. In addition, the indentation creep behaviour of Mg-10%Sn at 150°C was found to be better than that of AE42 and Mg-7%Sn, providing the same creep resistance as AE42[32]. More recently, Nayyeri and Mahmoudi [33] showed that the addition of up to 0.4% Sb improves the creep behaviour of the alloy. During creep deformation, matrix and grain boundary regions are strengthened due to the formation of thermally stable Mg_3Sb_2 and Mg_2Sn phases. Dislocations movement is impeded by particles in the interior of the grains retarding dynamic recovery, while dynamic recrystallization is suppressed by stable phases at grain boundaries. Calcium has also been shown to have significant effect on creep resistance of Mg-5Sn. In this case, the decrease in secondary creep rate has been attributed to the formation of CaMgSn intermetallic phase. Surprisingly, binary Mg-Ca and Sn-Ca phases haven't been reported in their study[31].Wei *et al.* [34] showed that the creep resistance of Mg-5Sn which is controlled by dislocation creep, increased significantly with the addition of 2% La. The formation of Mg-Sn-La phase in feather-shaped, rod-like, and massive morphologies in the grain boundaries which effectively inhibit the grain boundary sliding was reported to be the main contributing factors to the improvement of creep properties

1.4 Solid Solution Strengthening

The critical resolved shear stress (CRSS) in solid solutions can be divided into two components

$$\tau = \tau_i + \tau^* \qquad (7)$$

where τ_i is the athermal component arising from long range stress fields and cannot be overcome with thermal energy. τ^* is the thermally activated component of stress which is connected with short range obstacles and can be overcome with thermal energy[9, 35].

According to Akhtar and Teghtsoonian [7] different solute-dislocation interactions can influence the athermal stress stemming from the long range stress fields. These interactions are as follows:

- Chemical interaction
- Short range order
- Elastic interactions involving shear modulus effect and atomic size misfit
- A change in dislocation density on the basal plane

Seeger [36] has studied the temperature dependence of the flow stress in a number of pure metals (Ag, Cu, Au). The flow stress at temperatures below one-third of the melting point consist of the two above-mentioned components; thermal and athermal components. While at temperatures above one-third of melting point the entire flow stress is represented by the latter [36].

The temperature dependence of flow stress in Ag-In solid solutions [37] is shown in Figure 1.2. The athermal flow stress model explains the general features of the Figure 1.2 [37, 38]. In the first stage (at temperatures lower than one-third of the melting temperature) the flow stress decreases when the temperature increases. The flow stress in this temperature range consists of a temperature dependent component and a temperature independent component which is called the plateau. At temperature ranges between two-third and one-third of the melting points, plateau stress is the main feature and is due to an athermal process involving solute-dislocation interactions. In the last stage (at temperatures above two-thirds of the melting temperature), the flow stress decreases rapidly with increasing temperature until it reaches the critical resolved shear stress of the pure metal. This behaviour can be attributed to an increase in the solute atoms mobility [37].

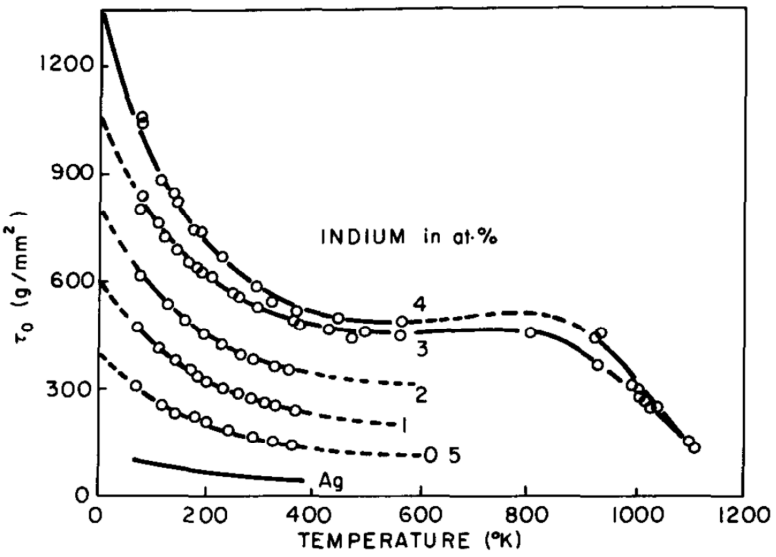

Figure 1-2. The temperature dependence of the flow stress of Ag-In binary alloys [37]

Akhtar and Teghtsoonian [7] pointed out that increasing the temperature up to 330K reduces the CRSS of Mg and Mg-Zn single crystals. The thermally activated behaviour of Mg-Zn has been shown in Figure 1.3.

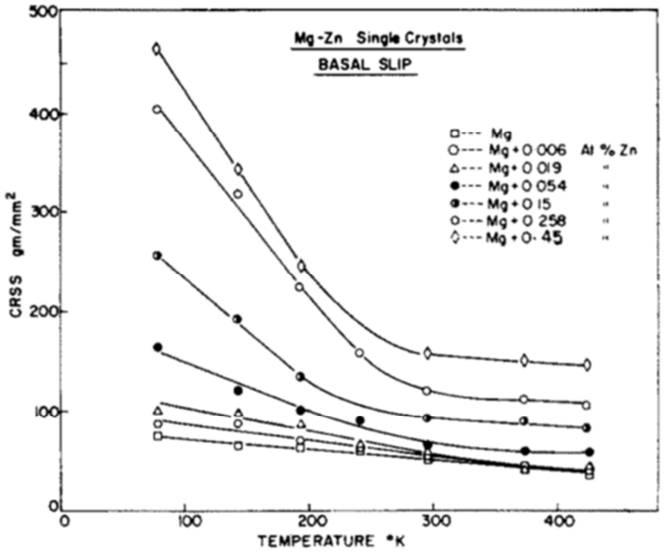

Figure 1-3. Critical resolved shear stress vs. temperature for Mg-Zn alloy crystals[7].

1.4.1 Short Range Order

Short range order[39] forms in concentrated solid solutions at certain temperatures and changes the physical and mechanical properties of the alloy. From the thermodynamical point of view, large negative heat of mixing of solute and solvent atoms leads to arrangement of atoms of different type producing local ordering [40]. Considering the energy of nearest-neighbour atoms, atomic strength of A-B bond is higher than that of A-A or B-B bonds [24] which consequently, rules out the possibility of short range clustering. When the energy of mixing becomes increasingly positive, a solubility gap appears then a congruently solidifying alloy and finally a eutectic system. Figure 1.4 shows changes in the phase diagram of alloys with increasingly positive heat of mixing [41].

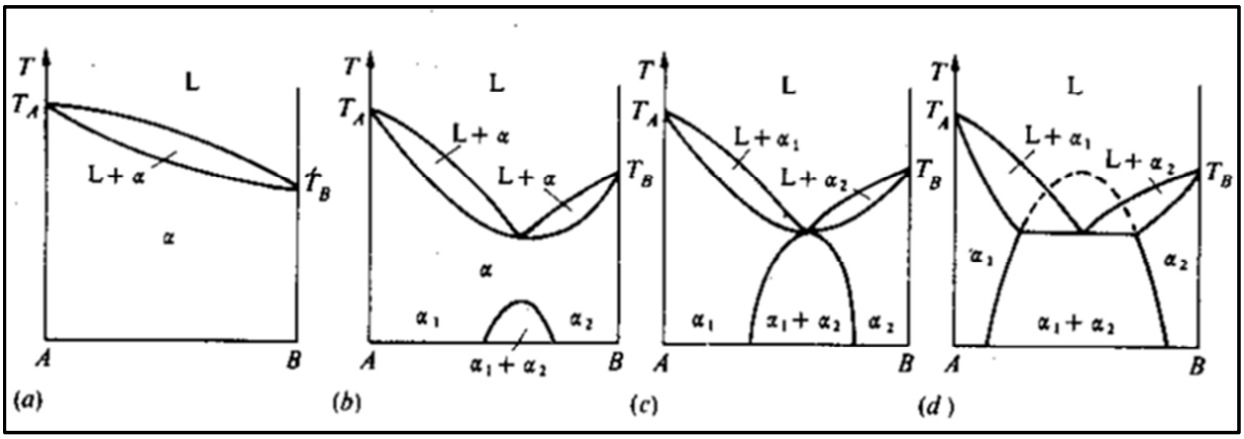

Figure 1-4. Changes in the phase diagram from (a) to (d) with increasingly positive energy of mixing EM>0 [41]

Deep eutectic in a phase diagram [41] indicates a tendency to form short range order. In the phase diagram of alloys forming intermetallic compounds, the negative heat of mixing leads to the formation of intermetallic phases from the melt in which the unlike nearest neighbour are energetically favourable. Changes in the phase diagram of alloys with increasingly negative heat of mixing are shown in Figure 1-5.

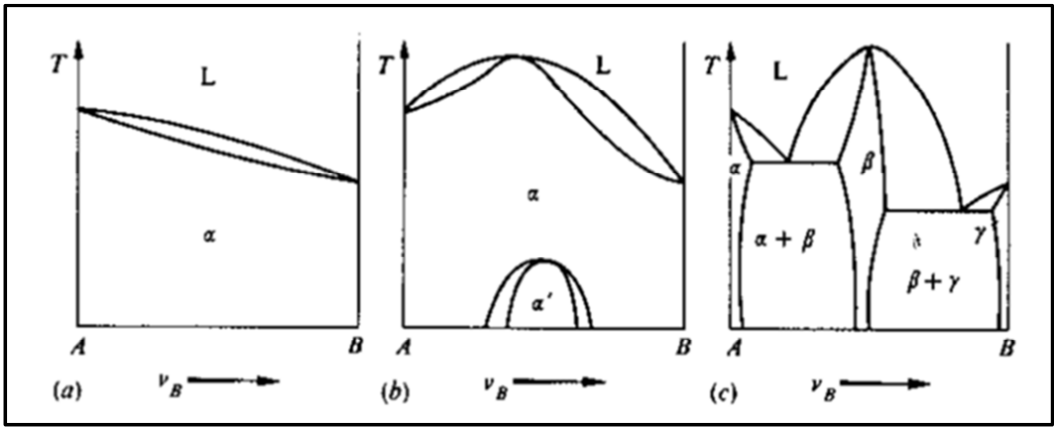

Figure 1-5. Changes in the phase diagram from (a) to (c) with increasingly negative energy of mixing EM<0 [41]

Short range order hardening has been studied in Zr-Al solid solutions in the temperature range of 20-502°C. In concentrated Zr-Al solid solutions with an aluminium concentration equal to or greater than 1.24 at%, significant strengthening is achieved due to short range order. The hardening effect of SRO is independent of temperature indicating that the thermal component of the flow stress remains unchanged while the athermal component increases [42].

The various possible strengthening mechanisms including Suzuki chemical locking; Guinier–Preston (G-P zones) and short range order in concentrated Mg-Zn alloys, have been discussed by Cáceres and Blake [10]. They pointed out that Suzuki's chemical locking of dislocations is unlikely to be significant as it's more prevalent in dilute alloys[39, 43]. G-P zones which are known to produce a very large increase in the strength in other systems by a micromechanism in many regards similar to SRO[44], were also considered unlikely, as the formation of GP zones requires prolonged ageing [45] at temperatures between 70 and 100°C whereas their as-quenched Mg-Zn alloy samples showed only a very little increase in the hardness at room temperature [10]. Chun and Byrne [46] considered clustering of Zn atoms as the possible source of strengthening in their as-quenched Mg-1.97at%Zn alloy based on the observed temperature dependence of the CRSS. However, based on thermodynamical considerations and TEM observations, the possibility of solute clustering was also ruled out [10].

The Mg-Zn phase diagram (Figure 1.6) is characterised by an intermetallic with the structure of a Laves phase, $MgZn_2$, forming from the melt which has a high melting point relative to the two bounding eutectics, indicating that its structure and composition are highly favoured energetically. The Mg-Zn phase diagram is typical of solutions with a large negative heat of mixing in which unlike nearest neighbours are energetically favourable, and in which SRO is established over a wide range of compositions[41]. Observations using diffuse X-ray scattering in Mg-In [47], Mg-Tb[48], Mg-Gd [49], Mg-Er [49] and Mg-Sn[50] alloys, whose phase diagrams closely resemble that of Mg-Zn have confirmed SRO in these alloys. Haasen [41] pointed out that the formation of a deep eutectic at ~30 at.%Zn alloy indicates a tendency to SRO or compound formation already in the melt in Mg-Zn alloys, a property used to produce a metallic glass with the composition Mg_7Zn_3.

TEM study of precipitation in Mg-3 at.%Zn [51], showed that upon ageing of the supersaturated solid solution, precipitation is initiated by segregation of Zn atoms along the c-axis, leading to the formation of rod-like ordered regions perpendicular to the basal plane. Over time, these regions evolve into the transitional β'-MgZn2 phase, eventually transforming into the equilibrium compound MgZn. This sequence indicates again that the $MgZn_2$ phase is highly favoured energetically, despite not being the equilibrium phase of the precipitation process. Eutectic decomposition of the Mg_7Zn_3 phase below 325°C leads to the formation of β'-MgZn2 phase which reveals the preference of the alloy to form an ordered structure at high temperature[10].

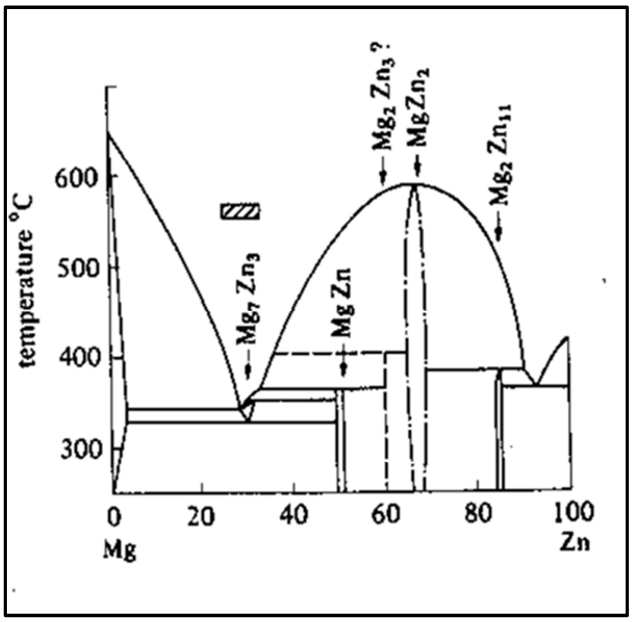

Figure 1-6 Mg-Zn phase diagram[41]

In alloys developing SRO the increase in the shear stress, $\Delta\tau s$, can be calculated from the following equation [9, 10]:

$$\Delta\tau_s = \frac{16}{\sqrt{3}}\frac{\{f(1-f)\}^2E^2}{a^3kT} \qquad (8)$$

where f is the solute concentration, k is Boltzmann's constant, E is the interaction energy and a is the lattice parameter .Figure 1.7 shows the concentration dependence of proof stress in Mg-Zn alloys.

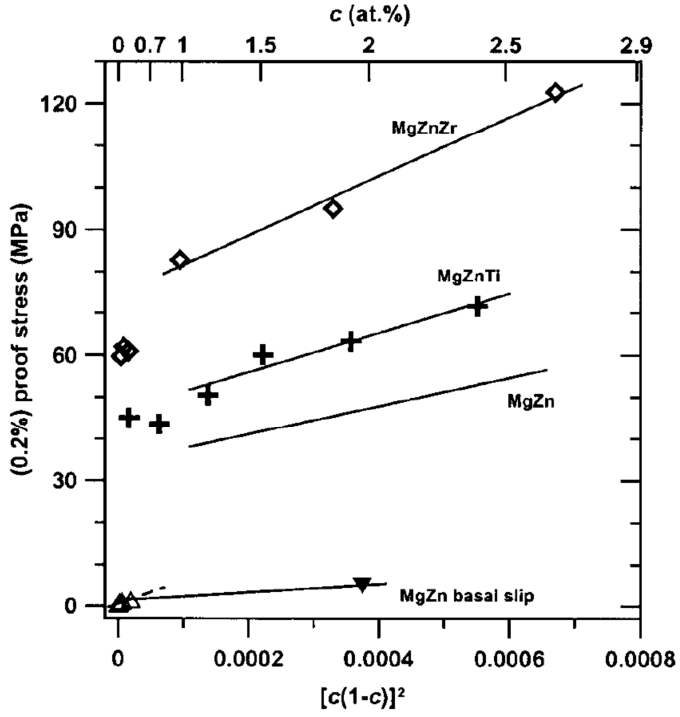

Figure 1-7. The concentration dependence of yield strength in Mg-Zn alloys[10]

1.4.2 Creep in Alloys with Short Range Order

Creep resistance of superalloys is said to be improved by short-range order. Short range order occurs in Ni-20%Cr and improves the performance of the alloy at 600°C[40]. Moreover, short-range order decreases the creep rate of Ti-6Wt%Al [52]. Mohamed[23] concluded that Fisher interaction considerably contributes to the creep resistance of Ni-25%Fe, Ni-20%Fe, and Al-10%Ag alloys. In Al-10%Ag and Al-10at%Zn, clustering rather than short range order has been

observed, however, the applicability of the Fisher interaction to clustering has been suggested by Mohamed [23].

Tiearney and Grant [24] have reported that even though the Cottrell solute atmosphere is the dominant strengthening mechanism in Ni-Mo, short range order significantly contributes to the creep resistance in concentrated alloys. The lower glide and climb rate in Ni-W alloys with less short range order than Ni-Mo, have been attributed to the lower diffusivity in this system [24].

1.5 Creep of intermetallics

High melting temperature due to the strong bonding and long range order are the main contributing factors to high creep resistance of intermetallics. Long range order reduces the diffusion rate so that when dislocation climb is the rate controlling mechanism the creep rate is decreased. Also for viscous glide of dislocations, long range order is destroyed by dislocation motion leading to an increase in the dragging force [20]. Long range order acts as obstacles to the dislocation motion. fully lamellar TiAl have the highest creep properties among other morphologies.

1.5.1 Secondary creep in FL TiAl

The stress exponent increases from n=1, at low stresses, to n=10 at high stresses in a Ti-48Al-2Cr-2Nb fully lamellar[20]. Figure 1-8 shows a minimum creep rate vs. stress plot for the alloy.

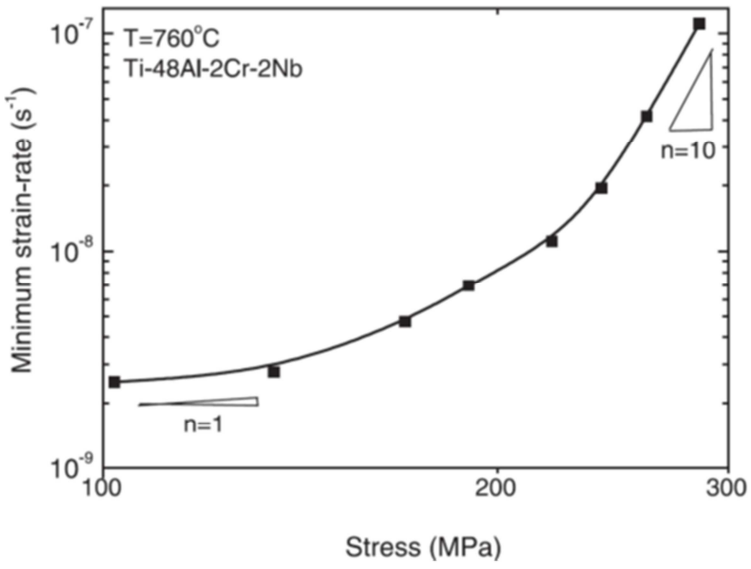

Figure 1-8. Minimum strain rate vs. stress curve of a Ti-48Al-2Cr-2Nb fully lamellar alloy deformed at 760°C.

The increase in the stress exponent with increasing stress is attributed to changes in the creep mechanism from diffusional creep at low stresses, to dislocation climb at higher stresses. At stresses above 200MPa and temperatures more than 700°C, creep is controlled by dislocation climb while dislocation glide is the rate-controlling mechanism when the stress increases[20].

The rate controlling creep mechanisms have been studied during secondary creep in a fully lamellae Ti-47Al-2Cr-2Nb alloy with a lamellar interface spacing of less than 300nm at low stresses[53]. It has been reported that at low stresses dislocation climb is less important. Grain boundary sliding as a possible deformation mechanism is being discarded due to the presence of interlocking grain boundaries. Dislocation slip by threading dislocations could not rationalize the creep strain in these alloys. Instead, it was proposed that the viscous glide of interfacial (Shockley) dislocations is the main deformation mechanism[53].

1.6 Increasing the Creep Strength of Mg-Al Alloys

The low melting point of β-$Mg_{17}Al_{12}$ intermetallic accounts for the poor high temperature performance of Mg-Al alloys[1, 2, 54-57]. Several commercial alloys have been developed using elements such as Si, Ca, RE and Sr which form thermally stable intermetallics in order to reduce the volume fraction or prevent the formation of β-Mg17Al12 phase[5, 6, 58, 59].

1.6.1 Creep of Mg-Al-Si

Improved creep properties of Mg-Al-Si alloys are mainly attributed to the presence of high melting point Mg_2Si particles[6, 58]. Likewise, a previous study[6] on die-cast AS21 and AM20 with approximately the same amount of α-Mg and β-$Mg_{17}Al_{12}$ indicated that the formation of Mg_2Si improved creep resistance of AS21. Figure 1.9 shows the effect of Si on the creep behaviour of AM20 alloy tested at 150°C applied stress of 50MPa.

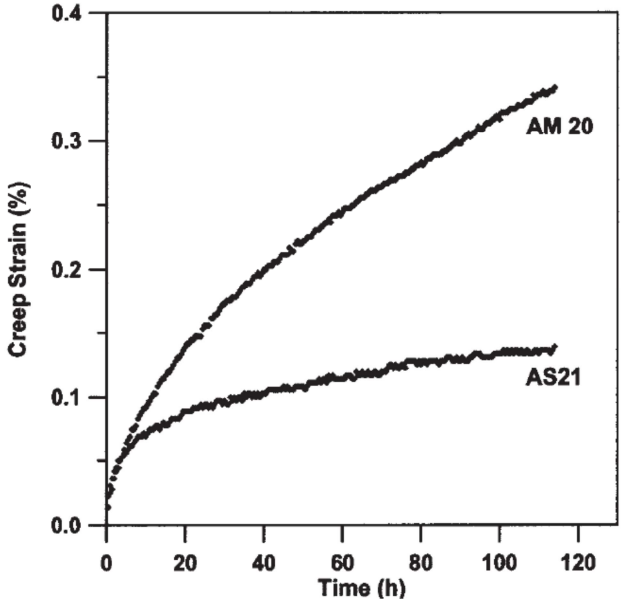

Figure 1-9. Creep curves of die-cast AM20 and AS21 (0.86wt pct Si) alloys[6].

By adding Si to AZ91, continuous precipitation is encouraged, suppressing discontinuous precipitation, which according to Dargush *et al.*[6], is detrimental to the alloy's creep resistance. The morphology of the Mg_2Si intermetallic phase has been found to be of great importance to both tensile and creep properties of Mg alloy [6]. Mg_2Si with branched Chinese script morphology increases the creep resistance of the alloy by preventing grain boundary sliding [1, 6]. Nevertheless, the low yield strength and poor castability of AS21 have restricted its application. Effect of silicon additions on the creep behaviour of AM50 was investigated at 150°C and 100MPa [60]. Figure 1.10 shows the effect of silicon on the creep behaviour of AM50 alloy.

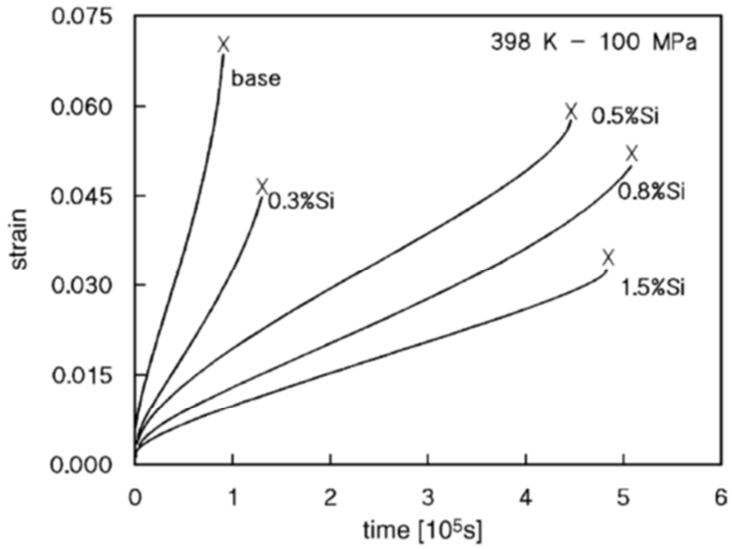

Figure 1-10. Effect of silicon content on the creep behaviour of AM50[60]

1.6.2 Creep of Mg-Al-RE

The addition of rare earth elements effectively improves the creep properties of Mg alloys [2, 58, 61]. However, solid solution strengthening is limited due to the low solid solubility of rare earth elements in Mg. Zhu *et al*. [3] have shown that in binary Mg-La, Mg-Ce and Mg-Nd alloys, increasing the alloy content reduces the minimum creep rate by reinforcing the grain boundaries with higher amount of intermetallics. Solid solution strengthening has been considered to be the main strengthening mechanism in these alloys [3]. In ternary Mg-Al-RE alloys formation of the high melting temperature intermetallics such as Al_3RE and $Al_{11}RE$ depending on the Al/RE ratio, leads to an improvement in creep performance of the alloys.

It has been reported that solid solution and precipitation hardening are the principle mechanisms increasing the creep resistance of Mg-2%Nd[28] .As the atomic size misfit of Nd in Mg is 13.8%, remarkable solid solution strengthening is achievable. At high temperatures, dynamic precipitation restricts dislocation movement, becoming the dominant strengthening mechanism [28].

1.6.3 Creep of Mg-Al-Sr

Mg-Al-Sr alloys have been developed in various compositions, namely, AJ51, AJ52, AJ62, AJ52 showed high creep resistance [5]. Sr addition to Mg-Al alloys has been shown to reduce or even prevent β phase formation. Instead, by Sr addition high melting temperature intermetallics form which are the main reason in improving the creep properties. The type of intermetallic (Al_4Sr and $Al_3Mg_{13}Sr$) which forms in these alloys depends on the Al/Sr concentration ratio. At ratio below 0.3, Al_4Sr is the only intermetallic whereas $Al_3Mg_{13}Sr$ appears at higher ratios[5]. Based on the values for activation energy Jing *et al*.[59] have suggested that dislocation climb and grain boundary sliding are responsible for creep mechanisms. Grain boundary sliding and grain boundary migration are inhibited due to the formation of continuous grain boundary networks [59].

1.6.4 Creep of Mg-Al- Ca

In Mg-Al-Ca systems, the type of the intermetallic phase is determined by the Ca/Al ratio. Thermally stable Al_2Ca precipitates form when the Ca/Al ratio is below 0.8, while at ratios above 0.8, Mg_2Ca forms, in both cases at the grain boundaries. The crystallographic structure of both phases is hexagonal [59].Concentrations of less than 1% cause hot cracking, die-sticking and cold shuts; increasing Ca content up to 2% eliminates such problems[2]. Grain boundary sliding and dislocation creep are the creep mechanisms at low (<70 MPa) and high stresses (>70 MPa),

respectively. Improved creep resistance of the Mg-Al-Ca- alloys has been mainly attributed to the thermal stability and the interfacial coherency of the intermetallic phases which create a pinning effect at grain boundaries [4]. Simultaneous addition of Ca and Sr significantly improves the creep properties of AZ91. Adding Ca and Sr to ZA (Mg-Zn-Al) alloys also improved the creep resistance, due to a reduction in the rate of dislocation climb and modifications to the $Mg_xZn_yAl_z$ phase [62].

1.7 Miedema Scheme

In 1970s a simple atomic model was developed by Miedema *et al*. [13, 14, 63] to formulate the enthalpy of mixing in binary metallic alloys. In their model, atomic cells of each atom in a binary system and in the pure elemental state are assumed to be similar. The first assumption in this model is that the volume of the atomic cells remain unchanged, however boundary condition between dissimilar cells changes, leading to a redistribution of electrons to achieve equilibrium in two steps. First, the discontinuity of electron density, n_{ws}, at the boundary of the Wigner-Seitz cells should be smoothed. A positive contribution,$(\Delta n_{ws}^{1/3})^2$, to the heat of formation, ΔH, arises by the elimination of electron mismatch. Next, difference in chemical potentials of the alloying elements leads to a charge transfer from the more electronegative element to the less electronegative one causing the atoms of each element to be compressed and expanded respectively. A negative contribution, $(\Delta\varphi^*)^2$, to the heat of formation stems from the equalization of the chemical potential which provides the driving force for alloying.

Figure 1-11 reveals the two steps by which boundary condition reach equilibrium when to atoms of different cells are brought into contact.

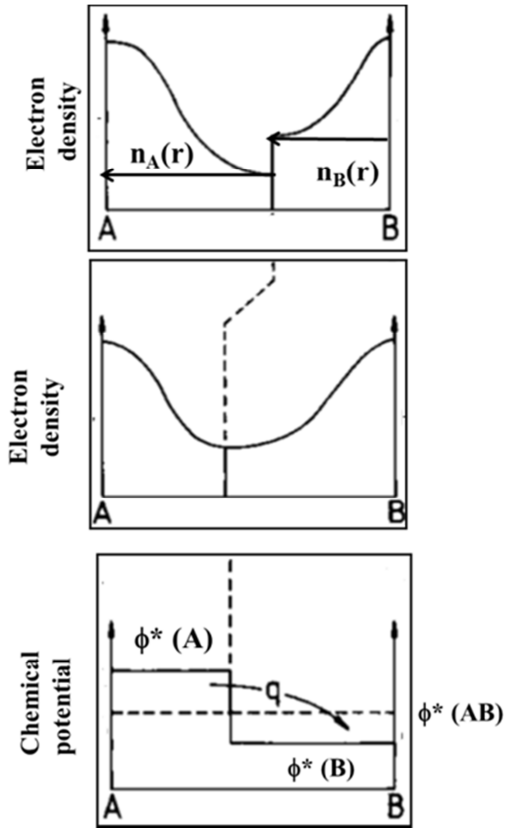

Figure 1-11. Two steps in the energy of alloys formation.[64].

Miedema's coordinates, $n_{ws}^{1/3}$ and φ^* are semi-empirical parameters [65, 66] obtained from experimental bulk modulus of the elements and from Pauling's electronegativity respectively [14, 65-67]. A linear correlation between Pauling's electronegativity and work function has been reported[66].,

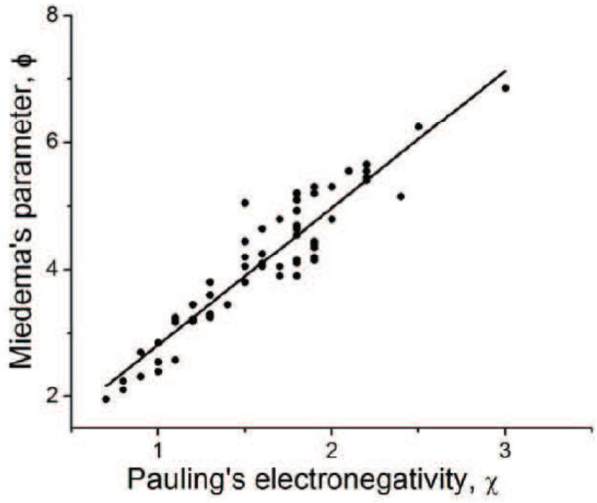

Figure 1-12. The linear correlation between Pauling's electronegativity and work function[66].

It's to be noted that size factor is not included in Miedema's model though, it contributes to the heat of formation in amorphous alloys [65]. In liquid metals and intermetallic compounds size mismatch is not an important factor to cause elastic energy[12]. For liquid alloys and disordered solid solutions, the model predicts the same values of heat of mixing. However, ΔH for disordered solid solution is more positive associated with the size-mismatch energy. Likewise, ΔH is more negative in ordered solid solutions compared to liquid alloy. Brillouin- zone effect is also neglected in the model though it might be of importance in solid alloys[68]. Heat of formation of transition metals doesn't depend on their crystal structure[11]. As a result accuracy of Miedema's model is more reliable when applied to liquid than to solid systems [68]. To overcome these limitation ab-initio methods have been developed [69].

1.7.1 Alloys of two transition metals or two non-transition metals

The sign and magnitude of the heat of formation for an equi-atomic compound can be calculated by addition of the two contributions [14, 63, 64, 67]:

$$\Delta H = -P(\Delta\varphi^*)^2 + Q(\Delta n_{WS}^{1/3})^2$$

Where, P and Q are constant for a given group of alloy system or equivalently Q/P= ± 9/4 for all alloying systems representing the slope of the line corresponded to $\Delta H=0$.

The sign of ΔH can be predicted using the binary phase diagrams and equation 1. Interrmetallic compounds in a phase diagram represents the negative energy of formation. If there are no compounds in a binary system the enthalpy of formation is positive providing that, the mutual solubilities don't exceed 10% [13, 14, 67].

To predict the sign and magnitude of the enthalpy of mixing of a given host with other solutes a plot can be created using Miedema's coordinates. The two perpendicular lines through the host separate metals that have a negative heat of alloying with the given host from metals with positive heat of formation with the host. The enthalpy of formation of any other host with solutes can be obtained by shifting the lines maintaining the same slope until they pass through the desired host [12]. Such plot has been created for Fe in [12], Mg in [67] and generic one in [70].

1.8 References

[1] A. Srinivasan, U.T.S. Pillai, B.C. Pai, Materials Science & Engineering A, 527 (2010) 6543-6550. 10.1016/j.msea.2010.07.020

[2] Z. Yang, J.P. Li, J.X. Zhang, G.W. Lorimer, J. Robson, Acta Metallurgica Sinica (English Letters), 21 (2008) 313-328. 10.1016/s1006-7191(08)60054-x

[3] S.M. Zhu, M.A. Gibson, M.A. Easton, J.F. Nie, Scripta Materialia, 63 (2010) 698-703. http://dx.doi.org/10.1016/j.scriptamat.2010.02.005

[4] A.A. Luo, B.R. Powell, M.P. Balogh, Metallurgical and Materials Transactions A, 33 (2002) 567-574. 10.1007/s11661-002-0118-1

[5] M. Pekguleryuz, P. Labelle, D. Argo, E. Baril, in: (Ed.) *PSTAM*, 2003, pp.

[6] M.S. Dargusch, G.L. Dunlop, A.L. Bowles, K. Pettersen, P. Bakke, Metallurgical and Materials Transactions A, 35 (2004) 1905-1909. 10.1007/s11661-004-0099-3

[7] A. Akhtar, E. Teghtsoonian, Acta Metallurgica, 17 (1969) 1339-1349. 10.1016/0001-6160(69)90151-5

[8] A. Akhtar, E. Teghtsoonian, Acta Metallurgica, 17 (1969) 1351-1356.

[9] Y. Chino, M. Kado, T. Ueda, M. Mabuchi, Metallurgical and Materials Transactions A, 42 (2011) 1965-1973. 10.1007/s11661-010-0563-1

[10] C.H. Cáceres, A. Blake, physica status solidi, 194 (a) (2002) 147-158.

[11] A. Miedema, Journal of the Less Common Metals, 46 (1976) 67-83.

[12] A.R. Miedema, P.F. de Châtel, F.R. de Boer, Physica B+C, 100 (1980) 1-28. http://dx.doi.org/10.1016/0378-4363(80)90054-6

[13] A.R. Miedema, F.R. de Boer, R. Boom, Calphad, 1 (1977) 341-359. 10.1016/0364-5916(77)90011-6

[14] A.R. Miedema, R. Boom, F.R. De Boer, Journal of the Less Common Metals, 41 (1975) 283-298. 10.1016/0022-5088(75)90034-x

[15] L. Shi, D.O. Northwood, Acta Metallurgica et Materialia, 42 (1994) 871-877. 10.1016/0956-7151(94)90282-8

[16] K. Maruyama, M. Suzuki, S. HIROYUKI, Metallurgical and Materials Transactions A, 33 (2002) 875-882.

[17] W.S. Miller, F.J. Humphreys, Scripta Metallurgica et Materialia, 25 (1991) 33-38.

[18] S.S. Vagarali, T.G. Langdon, Acta Metallurgica, 30 (1982) 1157-1170. 10.1016/0001-6160(82)90009-8

[19] S.R. Agnew, K.C. Liu, E.A. Kenik, S. Viswanathan, in: H.I. Kaplan, J. Hryn, B. Clow (Ed.) *Magnesium Technology 2000*, The Minerals, Metals and Materials Society (TMS), 2000, pp. 285-290.

[20] M.E. Kassner, Elsevier, 2009.

[21] F.A. Mohamed, T.G. Langdon, Acta Metallurgica, 22 (1974) 779-788. 10.1016/0001-6160(74)90088-1

[22] F.A. Mohamed, Materials Science and Engineering, 38 (1979) 73-80. 10.1016/0025-5416(79)90034-x

[23] F.A. Mohamed, Materials Science and Engineering, 61 (1983) 149-165. 10.1016/0025-5416(83)90197-0

[24] T.C. Tiearney, N.J. Grant, Metallurgical Transactions A, 13 (1982) 1827-1836. 10.1007/bf02647839

[25] S. Takeuchi, A.S. Argon, Journal of Materials Science, 11 (1976) 1542-1566. 10.1007/bf00540888

[26] C.J. Boehlert, K. Knittel, Materials Science and Engineering: A, 417 (2006) 315-321. 10.1016/j.msea.2005.11.006

[27] M. Suzuki, H. Sato, K. Maruyama, H. Oikawa, MATERIALS SCIENCE AND ENGINEERING A-STRUCTURAL MATERIALS PROPERTIES MICROSTRUCTURE AND PROCESSING, 252 (1998) 248-255.

[28] J. Yan, Y. Sun, F. Xue, S. Xue, Y. Xiao, W. Tao, Materials Science and Engineering: A, 524 (2009) 102-107. 10.1016/j.msea.2009.06.008

[29] F.R.N. Nabarro, H.L. de Villiers, Taylor and Francis London, 1995.

[30] L. Gao, R.S. Chen, E.H. Han, Journal of Alloys and Compounds, 472 (2009) 234-240.

[31] G. Nayyeri, R. Mahmudi, Materials Science & Engineering A, 527 (2010) 2087-2098. 10.1016/j.msea.2009.11.053

[32] H. Liu, Y. Chen, Y. Tang, S. Wei, G. Niu, Journal of Alloys and Compounds, 440 (2007) 122-126. 10.1016/j.jallcom.2006.09.024

[33] G. Nayyeri, R. Mahmudi, Materials Science & Engineering A, 527 (2010) 669-678. 10.1016/j.msea.2009.08.056

[34] S. Wei, Y. Chen, Y. Tang, X. Zhang, M. Liu, S. Xiao, Y. Zhao, Materials Science & Engineering A, 508 (2009) 59-63. 10.1016/j.msea.2008.12.049

[35] A. Akhtar, in: Department of Metallurgy, University of British Columbia, Vancouver, 1968.

[36] A. Seeger, in: J.C. Fisher, W.G. Johnston, R. Thomson, T. Vreeland (Eds.) Dislocations and mechanical properties of crystals, Chapman and Hall, London, 1957, pp. 243-329.

[37] O. Boser, Metallurgical and Materials Transactions B, 3 (1972) 843-849. 10.1007/bf02647658

[38] C.G. Schmidt, A.K. Miller, Acta Metallurgica, 30 (1982) 615-625.

[39] J.C. Fisher, Acta Metallurgica, 2 (1954) 9-10.

[40] N.R. Dudova, R.O. Kaibyshev, V.A. Valitov, PHYSICS OF METALS AND METALLOGRAPHY, 108 (2009) 625-633. 10.1134/s0031918x0912014x

[41] P. Haasen, Cambridge University Press, Cambridge, 1996.

[42] S.N. Tiwari, K. Tangri, Materials Science and Engineering, 57 (1983) 31-37. 10.1016/0025-5416(83)90024-1

[43] P.A. Flinn, Acta Metallurgica, 6 (1958) 631-635.

[44] A. Kelly, Philosophical Magazine, 3 (1958) 1472-1474.

[45] J.B. Clark, Acta Metallurgica, 13 (1965) 1281-1289.

[46] J.S. Chun, J.G. Byrne, Journal of Materials Science, 4 (1969) 861-872.

[47] L.A. Safronova, A.A. Katsnel'son, S.V. Sveshnikov, Y.M. L'Vov, Fiz. metal. metalloved., 43 (1977) 76-80.

[48] V. Silonov, E. Evlyukhina, L. Rokhlin, Russian Physics Journal, 39 (1996) 622-625. 10.1007/bf02439089

[49] D.S. Gencheva, A.A. Katsnel'son, L.L. Rokhlin, V.M. Silonov, F.A. Khavadzha, Fiz. metal. metalloved., 51 (1981) 788-793.

[50] S. Henes, V. Gerold, Zeitschrift fur Metallkunde, 53 (1962) 703-708.

[51] L. Sturkey, J.B. Clark, Journal of the Institute of Metals, 88 (1959) 177-181.

[52] T. Neeraj, M.J. Mills, Materials Science & Engineering A, 319 (2001) 415-419. 10.1016/s0921-5093(01)01045-0

[53] L. Hsiung, T. Nieh, Intermetallics, 7 (1999) 821-827.

[54] M.S. Dargusch, M.A. Easton, S.M. Zhu, G. Wang, Materials Science and Engineering A, 523 (2009) 282-288. 10.1016/j.msea.2009.06.015

[55] M.S. Dargusch, K. Pettersen, K. Nogita, M.D. Nave, G.L. Dunlop, Materials Transactions (JIM), 47 (2006) 977-982.

[56] M.O. Pekguleryuz, A.A. Kaya, ADVANCED ENGINEERING MATERIALS, 5 (2003) 866-878. 10.1002/adem.200300403

[57] M. Regev, A. Rosen, M. Bamberger, E. Aghion, Materials Science and Engineering, 252A (1998) 6-16.

[58] M. Pekguleryuz, M. Celikin, International Materials Reviews, 55 (2010) 197-217. doi:10.1179/095066010X12646898728327

[59] B. Jing, S. Yangshan, X. Shan, X. Feng, Z. Tianbai, Materials Science & Engineering A, 419 (2006) 181-188. 10.1016/j.msea.2005.12.017

[60] E. Evangelista, S. Spigarelli, M. Cabibbo, C. Scalabroni, O. Lohne, P. Ulseth, Materials Science & Engineering A, 410 (2005) 62-66. 10.1016/j.msea.2005.08.150

[61] J.-F. Nie, Metallurgical and Materials Transactions A, 43 (2012) 3891-3939. 10.1007/s11661-012-1217-2

[62] Z. Zhang, A. Couture, A. Luo, Scripta Materialia, 39 (1998) 45-53.

[63] F.R. de Boer, R. Boom, W.C.M. Mattens, A.R. Miedema, A.K. Niessen, North-Holland, Amsterdam, 1989.

[64] A.R. Miedema, Physica B: Condensed Matter, 182 (1992) 1-17. http://dx.doi.org/10.1016/0921-4526(92)90565-A

[65] Z. Bangwei, Physica B+C, 121 (1983) 405-408. http://dx.doi.org/10.1016/0378-4363(83)90071-2

[66] T. Rajasekharan, V. Seshubai, arXiv preprint arXiv:0907.1799, (2009)

[67] A.R. Miedema, Journal of the Less Common Metals, 32 (1973) 117-136. 10.1016/0022-5088(73)90078-7

[68] R. Boom, F.R. De Boer, A.R. Miedema, Journal of the Less Common Metals, 46 (1976) 271-284. http://dx.doi.org/10.1016/0022-5088(76)90215-0

[69] R.F. Zhang, S.H. Sheng, B.X. Liu, Chemical Physics Letters 442 (2007) 511.

[70] K.C. Russell, in, DTIC Document, 1989.

Chapter 2 Experimental Details

2.1 Alloy composition

Binary alloys with nominal composition listed in Table 5-1, were selected based on the phase diagrams and the soluts' maximum solubility at 473K (200°C) in order to limit precipitation hardening effects during the mechanical testing. The alloys were prepared by melting commercially pure Mg, Zn, Al, Sn, Nd, Y and a Mg-Gd master alloy (2:3 Gd:Mg) in a steel crucible coated with boron nitride in an electric furnace under a protective atmosphere of SF6+CO2.

The liquid metals were stirred mechanically for ~20 minutes to ensure the dissolution of the alloy components and subsequently poured at 1008-1023K (735-750°C) under an argon atmosphere into 80 x 80 x 10 mm^3 steel moulds preheated to 573K (300°C). Commercial AZ91D alloy was similarly cast for reference. Chemical composition analysis was done using an inductively coupled plasma atomic emission spectroscopy (ICP-AES). The actual compositions are listed in Table 5-1

2.2 Solution Heat Treatment

The cast plates were solution heat treated under Ar atmosphere as per the times and temperatures given in Table 2-1, and quenched into water. Samples for grain size measurement were polished following standard procedures and etched using an acetic–picric acid mixture [20 ml acetic acid, 3 g picric acid, 20 ml H_2O and 50 ml Ethanol] for Mg-Zn and Nital [5% nitric acid and 95% ethanol] for the rest of the alloys. The linear intercept method in accordance with ASTM E112-88 was used to determine the grain size, counting not fewer than 200 boundaries (see Table 5-1).

2.3 Mechanical Testing

Compression testing was carried out using cylindrical specimens, 18 mm in height and 9 mm in diameter, on a screw-driven machine at 298K (25°C), 373K (100°C) and 453K (180°C) in a temperature controlled chamber. The more creep resistant solid solutions, namely, specimens containing Gd, Y and Nd, were also tested at 493K (220°C) and 523K (250°C). The crosshead speed was 0.016 mm/min for all the tests (initial strain rate = $1.5x10^{-5}s^{-1}$). All tests were repeated at least 2 times.

Stress relaxation tests were performed at 453K (180°C). The specimens were deformed at an applied crosshead speed of 0.2 mm/min (initial strain rate = $1.85x10^{-4}$ s^{-1}) up to a predetermined

strain and stress, and the machine stopped allowing the stress to relax for 30 minutes for the less creep resistant alloys (Al, Zn and AZ91) or 60 minutes for the rest.

Chapter 3 Bounds to Hardening by Precipitation and Short Range Ordering in Mg Binary Alloys

Bounds to hardening by Precipitation and Short Range Ordering in Mg Binary Alloys

C.H. Cáceres, Saeideh Abaspour

ARC Centre of Excellence for Design in Light Metals

Materials Engineering, School of Engineering

The University of Queensland, QLD 4072, Australia

Abstract

Miedema's coordinates are used to rank 4 model binary alloys considering the respective values of enthalpy of formation and the tendency to developing short range order (SRO) and intermetallic compounds. The terminal solid solubility generally increases whereas the tendency to order decreases with decreasing heat of formation, and hardening by near-random solid solution and precipitation is expected to be dominant for solutes with low tendency to order, such as Al. For solutes with an intermediate tendency to order, such as Zn, or to form compounds, such as Gd, SRO is predicted to dominate the hardening. For solutes, whose very large heat of formation leads to very high melting point intermetallics forming straight from the liquid, such as Sb, the terminal solid solubility is too low for any solute based hardening to be feasible. Implications for alloy design and selection regarding precipitation hardening and creep resistance are discussed.

Keywords: Miedema's Coordinates, Mg alloys, Precipitation Hardening; Short Range Order

3.1 Introduction

Magnesium's locus on the group IIA manifests in highly attractive pairing with most other metals, i.e., the interaction energy of mixing is strongly negative. A strongly negative interaction energy normally [1] leads to a high melting point intermetallic bounded by two eutectics, of the type illustrated by Fig. 3-1(a), and to which many binary Mg alloys closely conform to. Cases in point are, in order of increasingly negative interaction energy, Mg-Al, Mg-Zn and Mg-Sb alloys. In the opposite case, i.e., strongly positive energy, limited solubility and a single eutectic is observed, as in Fig. 3-1(b). An example is Mg-Th.

When the interaction energy is negative, the ensuing tendency to pairing between unlike atoms in a solution of X atoms in Mg introduces an ordering effect in an otherwise random solid solution, with a pre-eminence of pairs Mg-X, in detriment of X-X or Mg-Mg pairs [2]. In a dilute alloy, the net result is the development of short range order (SRO), whereas in the concentrated ones it leads to compound formation. In some alloys SRO is observed already in the liquid, leading to highly viscous melts, and a propensity to form metallic glasses [1] (pp. 81–82). SRO has been confirmed by X-ray diffraction in a number of Mg-based solid solutions, namely: Mg-Sn, Mg-Gd, Mg-In and Mg-Er [3, 4], whereas indirect evidence has been presented for Mg-Zn [5] and Mg-Y [6, 7]. SRO has also been predicted from first principles and experimentally confirmed in liquid Mg-Zn [8]. The formation of SRO in a solid solution leads to increased hardening well above that of random solid solution [5, 9, 10]. For a metal like Mg whose alloys are reluctant to develop precipitation hardening [11-13], the development of SRO is an important alternative.

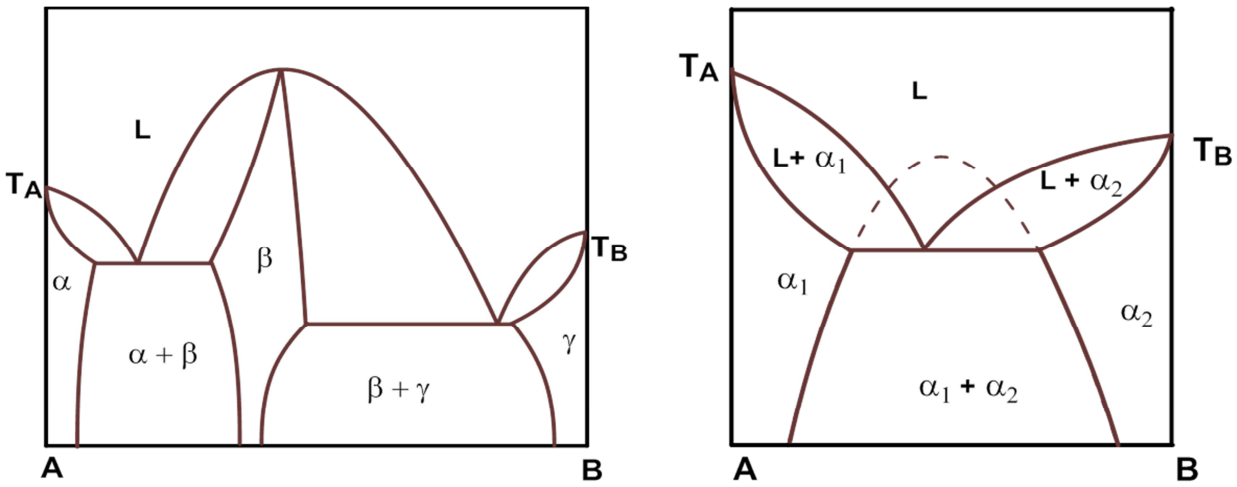

(a) (b)

Figure 3-1.The phase diagrams for (a) highly negative and (b) highly positive interaction energy between solute and solvent

Predicting the possibility of having SRO is immediate from a phase diagram like that of Fig. 3-1(a), but not all phase diagrams of Mg alloys are so amenable of interpretation even when the interaction energy with the solute is manifestly negative. This is the case of Mg-Gd, Mg-Y or Mg-Nd alloys, amongst others, which are characterized by a sequence of intermetallic compounds, some forming from the solid solution and some straight from the liquid. These intermetallics are often associated with particular size ratios between host and solute, i.e., the formation of intermetallic compounds at

given concentrations normally takes pre-eminence; the same applies for particular electron concentrations [2]. That is, electronegativity is not the only factor at play.

The sign and magnitude of the enthalpy of mixing can be used to sort out alloys of a given host, Mg in this case, predicting, among other things, the relative solubility. These predictions can be made regardless of the details of the alloy's phase diagram, i.e., regardless of whether it conforms to those of Fig. 3-1 or exhibits a complex sequence of compounds. This sorting method, developed on the principles laid out in the 1970's by Miedema *et al.* [14-17] will be used in this work to anticipate which alloys are more amenable of developing either strong solid solution, precipitation, short range order or, in some extreme cases, no solute based hardening at all. A set of four model alloys will be used for the analysis: Mg-Al, Mg-Zn, Mg-Sb and Mg-Gd. The phase diagrams of the first three systems closely conform to that of Fig. 3-1(a), whereas the one for Mg-Gd exhibits a series of intermetallic compounds.

3.2 Miedema's cellular model

Miedema *et al.*'s [14-18] phenomenological approach, in its simpler form involves only two parameters, and is valid for transition metals and the divalent metals such as Mg and Zn. It combines a work function, ϕ^*, (closely related to Pauling's electronegativity value), and the electron density at the boundary of the Wigner–Seitz (WS) cell, $n_{WS}^{1/3}$. The approach enables calculating the enthalpy of formation of dilute solutions in the liquid state, predicting the sign and magnitude of the interaction, hence the relative tendency to form either ordered, random or immiscible solutions. Ab-initio and Calphad calculations normally reproduce closely Miedema *et al.*'s, providing the approach with strong independent support. A limitation often pointed out is its fundamentally isotropic nature, i.e., the method applies most accurately to metals in the liquid state, where size related elastic energy effects can be neglected. Further developments in the ab-initio methods enabled overcoming some of these limitations (e.g., see Zhang et al. [19]).

The enthalpy of formation [16], ΔH, of a given alloy results from a negative contribution from the difference between the host's and solute's work functions, measuring the main driving force either to form a solution or an intermetallic compound by charge transfer, and a positive contribution stemming from the need to smooth any discontinuity of the electron density at the boundary of the WS cell between solute and solvent.

Using values from [17, 20] (see Table 3-1), a diagram using Miedema's coordinates was created for Mg in Fig. 3-2. The two perpendicular lines through Mg sort out solutes as follows: elements sitting right on the lines have no enthalpy of mixing with Mg; the upper (or "north) and lower, (or "south") sectors identify solutes with a negative energy of mixing; those lying on the east or west sectors have a positive energy of mixing.

Solutes located right on the lines are expected exhibit complete miscibility, those on the north or south sections alloy readily with the host and show a tendency to develop phase diagrams similar to that of Fig. 3-1(a), whereas diagrams for solutes on the east-west sections should form simple eutectics akin to that of Fig. 3-1(b). The correctness of these predictions can be easily verified for the solutes considered in this work, as well as for many others.

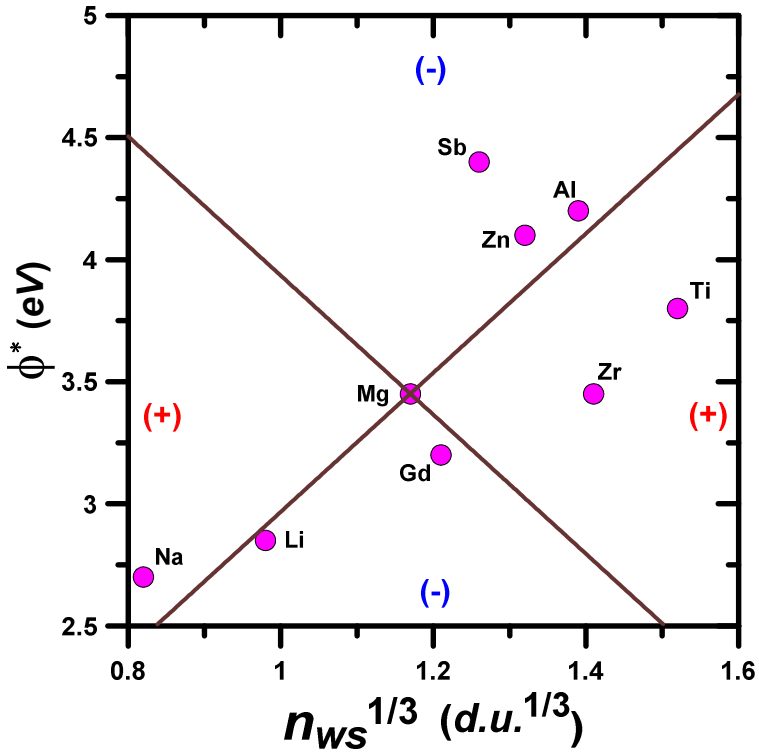

Figure 3-2. Miedema plot for Mg with the work function, φ, and the electronic density, $n_{WS}^{1/3}$, as coordinates (see Table 3-1).*

Increasing values of ϕ^* are associated with a tendency to develop SRO and an attendant decrease in the terminal solubility. (The later follows as well from the Hume-Rothery's law involving electronegativity.) This illustrated in Fig. 3-3, where Al, with the smallest ΔH-value, has the largest terminal solubility, whereas Sb, with the largest one, exhibits virtually no solubility.

3.3 Solid solution hardening

In Fig. 3-4 the RT strength of Mg-Al, Mg-Zn and Mg-Gd is compared. The respective rate of the solid solution hardening correlates well with the alloys' ΔH value, i.e., a rather weak hardening rate, consistent with a near random solid solution [7, 10], is observed for Al, whereas the much stronger hardening in Mg-Zn and Mg-Gd is consistent with a well-developed SRO [5].

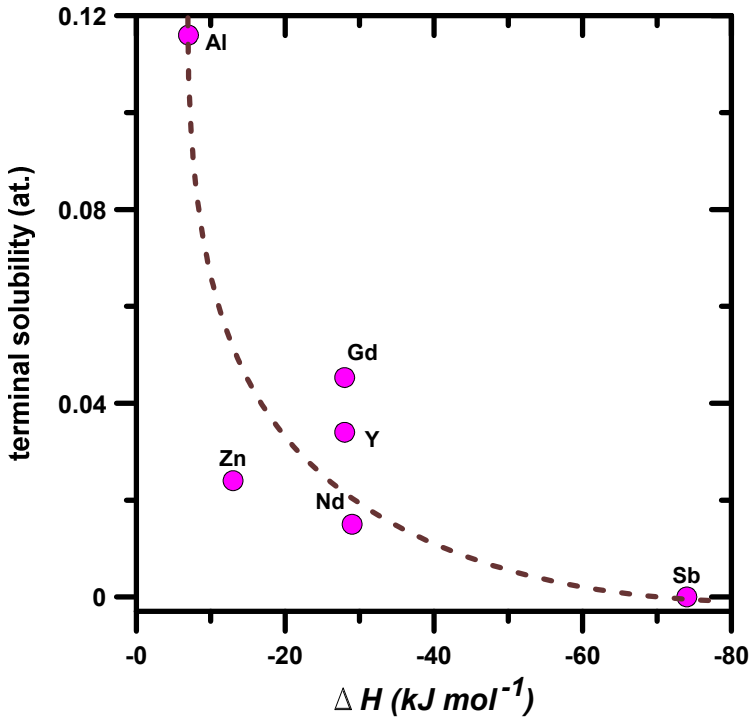

Figure 3-3. The terminal solid solubility as a function the enthalpy of formation for the solutes studied

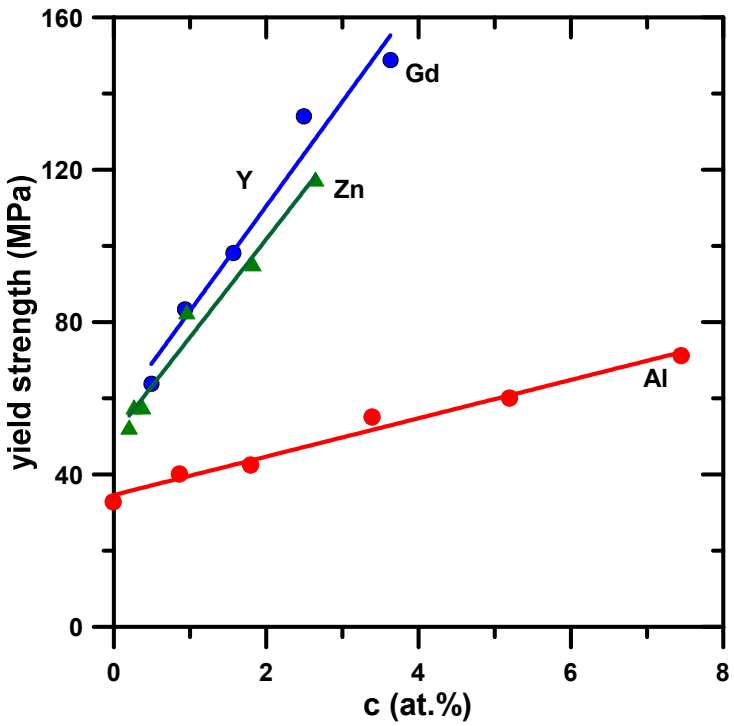

Figure 3-4. The strength of Mg-based solid solutions. Mg-Zn data from [88]; Mg-Al from [79] and Mg-Gd from [82].

3.4 Ranking of alloys

A straightforward way of ranking the strength of Mg alloys within the north-south sectors of Fig. 3.4, i.e., those with negative interaction energy, and regardless of whether the phase diagram conforms to that of Fig. 3-1(a) or not, can be easily developed based on the potential strength of the SRO. For a solute concentration c , the strength of the SRO, $\tau_{SRO,}$ can be assumed to obey the relationship [5]:

$$\tau_{SRO} \sim [\Delta H^* c(1-c)]^2. \qquad (1)$$

SRO is a typical athermal hardening mechanism, and alloys which develop it can be expected to be more creep resistant than those exhibiting only random solid solution [21, 22]. Thus, to make the ranking valid for predicting creep strength, and in order to prevent any precipitation hardening effects that might arise when testing a supersaturated solid solution at high temperature, the analysis was done for the respective solute solubilities at ~200^{o}C. These c-values are listed in Table 3-2.

Table 3-1. Miedema's coordinates values for Figures 3-2, 3-3 and 3-5 .

Solute	Al	Zn	Gd	Sb
ϕ^*	4.2	4.1	3.2	4.4
$n_{WS}^{1/3}$	1.39	1.32	1.21	1.26
ΔH	-7	-13	-35.3	-74

Table 3-2. Approximate solute solubilities (at.%) at 200^{o}C for the alloys studied.

Solute	Al	Zn	Gd	Sb
c @ 200^{o}C	2.5	1.5	1.0	0.05

The ranking of the alloys as per Eq. 1 is shown in Fig. 3-5. Accordingly, the Mg-Al alloy are expected to exhibit the lowest strengthening by SRO, in this case due to its low ΔH-value. Zn and Gd containing alloys should exhibit increased strength due to the larger ΔH despite the somewhat reduced c. At the other end, for Mg-Sb the c-value drops to nearly zero, i.e., the alloy should exhibit no solute based strengthening despite its large ΔH. The latter is obviously an upper bound, as Mg-Al is a lower bound. Other Mg alloy systems within the north-south sectors of Fig. 3-2 can be expected to fit in between these two bounds, with some systems exhibiting SRO strengths matching or surpassing that of Mg-Gd.

The alloys' behavior at RT depicted in Fig. 3-4 is closely consistent with the ranking of Fig. 3-5. Regarding the creep behavior, Mg-Gd should exhibit a well-defined athermal behavior as expected from the strong SRO, whereas Mg-Al should not, and Mg-Zn should lie in between. Creep data confirming these predictions are presented in another session in this symposium [20].

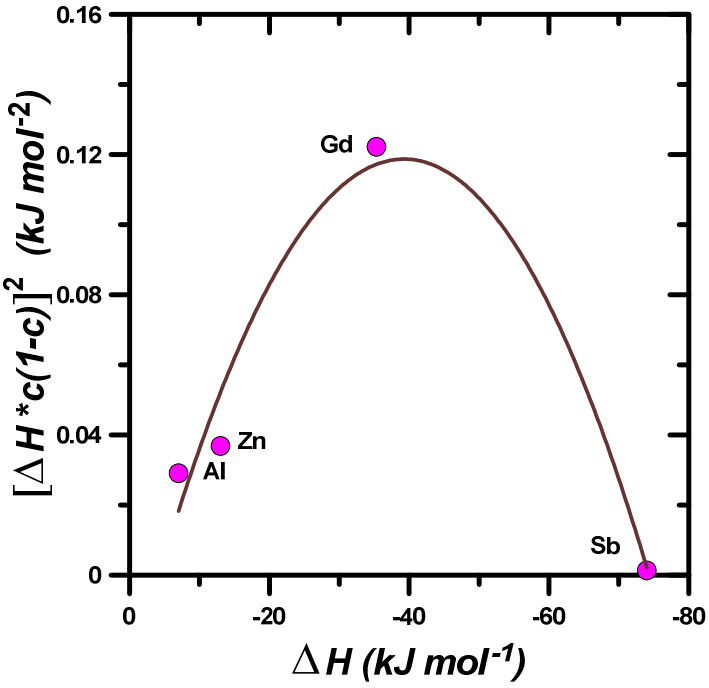

Figure 3-5. .The predicted strength of the SRO (Eq. 1) versus the heat of formation for the alloys studied.

Figures 3-3 and 3-5 allow making predictions concerning the feasibility of precipitation hardening. A strong tendency to order, as opposed to clustering, is expected to interfere with the homogeneous nucleation of small and finely distributed precipitates upon ageing of the supersaturated solid solution. The feasibility of developing strong precipitation hardening is thus expected to be opposite to the tendency to develop SRO. That is, alloys to the left of the maximum in Fig. 3-5 should be increasingly prone to exhibit precipitation hardening. Classical ageing experiments on Mg-Al and Mg-Zn support this assertion [20-22], i.e., of the alloys considered here Mg-Al exhibits the strongest response to ageing at intermediate temperatures.

3.5 Conclusions

- Meidema et al.'s phenomenological approach has been used to rank the potential strength of four model Mg binary alloys considering the alloys' enthalpy of mixing.

- A maximum in the random solid solutions effects and precipitation hardening is predicted for solutes with low heat of formation, such as Al.

- Solutes with an intermediate heat of formation, such as Zn or Gd, are expected to exhibit strong SRO. These alloys should exhibit maximum strength at high temperature as a result of an extended athermal stress range.

- For extreme values of heat of formation, e.g., Mg-Sb alloys, the very limited terminal solubility implies negligible solute based hardening effects.

3.6 References

[1] P. Haasen, Cambridge University Press, Cambridge, 1996.

[2] W. Hume-Rothery, Institute of Metals, London, 1946.

[3] D.S. Gencheva, A.A. Katsnel'son, L.L. Rokhlin, V.M. Silonov, F.A. Khavadzha, Fiz. metal. metalloved., 51 (1981) 788-793.

[4] L.A. Safronova, A.A. Katsnel'son, S.V. Sveshnikov, Y.M. L'Vov, Fiz. metal. metalloved., 43 (1977) 76-80.

[5] C.H. Cáceres, A. Blake, physica status solidi, 194 (a) (2002) 147-158.

[6] L. Gao, R.S. Chen, E.H. Han, Journal of Alloys and Compounds, 472 (2009) 234-240.

[7] L. Gao, R.S. Chen, E.H. Han, Journal of Alloys and Compounds, 481 (2009) 379-384. 10.1016/j.jallcom.2009.02.131

[8] N. Jha, A.K. Mishra, Journal of Alloys and Compounds, 329 (2001) 224-229.

[9] A. Akhtar, E. Teghtsoonian, Metallurgical Transactions A, 2 (1971) 2757-2763.

[10] C.H. Cáceres, D.M. Rovera, Journal of Light Metals, 1/3 (2001) 151-156.

[11] J.B. Clark, Acta Metall., 13 (1965) 1281-1289.

[12] J.B. Clark, Acta Metall., 16 (1968) 141-152.

[13] J.B. Clark, Transactions of Japan Institute of Metals, 9 Supplement (1968) 354-355.

[14] A.R. Miedema, F.R. de Boer, R. Boom, Calphad, 1 (1977) 341-359. 10.1016/0364-5916(77)90011-6

[15] A.R. Miedema, Journal of the Less Common Metals, 32 (1973) 117-136. 10.1016/0022-5088(73)90078-7

[16] A.R. Miedema, R. Boom, F.R. De Boer, Journal of the Less Common Metals, 41 (1975) 283-298. 10.1016/0022-5088(75)90034-x

[17] F.R. de Boer, R. Boom, W.C.M. Mattens, A.R. Miedema, A.K. Niessen, North-Holland, Amsterdam, 1989.

[18] K.C. Russell, in, DTIC Document, 1989.

[19] R.F. Zhang, S.H. Sheng, B.X. Liu, Chemical Physics Letters 442 (2007) 511.

[20] R.F. Zhang, in, 2012.

[21] D. Kuhlmann-Wilsdorf, Metallurgical and Materials Transactions, 35A (2004) 369-418.

[22] A. Seeger, in: J.C. Fisher, W.G. Johnston, R. Thomson, T. Vreeland (Eds.) Dislocations and mechanical properties of crystals, Chapman and Hall, London, 1957, pp. 243-329.

Chapter 4 Creep Behaviour of Mg Binary Solid Solutions

Creep Behaviour of Mg Binary Solid Solutions

*Saeideh Abaspour, C.H. Cáceres**

ARC-Centre of Excellence for Design in Light Metals

Materials Engineering, School of Engineering

The University of Queensland, QLD 4072, Australia

Abstract

Specimens of cast Mg-0.8 at.%Gd, Mg-2.2 at.%Zn and Mg-2.5at.%Al alloys were tested in compression at an initial strain rate of ~$1.5x10^{-5}s^{-1}$ at room temperature and 180°C. The Mg-Zn alloy, and more so the Mg-Gd alloy, exhibited a largely athermal behaviour, in contrast with the Mg-Al alloy which softened considerably at the higher temperature. The athermal behaviour of the Zn- and Gd-containing alloys can be accounted for by their strong tendency to developing short range order.

Keywords: Solid solution strengthening, Short Range Order, Mg Alloys, Creep

4.1 Introduction

A plot of the strength of a solid solution versus temperature normally takes the shape of Fig. 4-1. At low temperatures the strength decreases rapidly, whereas at intermediate temperatures it becomes virtually insensitive to temperature. The behaviour can be rationalised by dividing the strength into two components [1-3]:

$$\tau = \tau i + \tau^*$$

where τi is the athermal component of the stress arising from long range stress fields and which cannot be overcome through thermal activation, and τ^* is the thermally activated component connected with short range obstacles that can be overcome by thermal energy. At temperatures above two-thirds of the melting point the flow stress decreases rapidly again, approaching the critical resolved shear stress of the pure metal, a behaviour attributed to an increase in the mobility

of the solute atoms. The extent of the athermal regime determines the resistance to dislocation creep of any solid solution [4]. Ideally, the athermal regime should extend well past the service temperature of the alloy.

The strength of a solid solution is determined by a number of solute-dislocation interactions, among them [1-3, 5, 6]

- Elastic interactions involving the shear modulus and atomic size misfit (random solid solution effects). These are considered short range interactions, i.e., amenable of thermal activation.

- Short range order (SRO). This is a typical long range, i.e., athermal, hardening mechanism [7].

Random solid solution effects dominate the strength of Mg-Al [8]; SRO, in turn, has been confirmed by x-ray scattering Mg-In, Mg-Gd, Mg-Er and Mg-Sn [9-11], whereas theoretical and experimental evidence suggests that it is present in Mg-Zn alloys as well [8, 12]. On a parallel presentation in this symposium [13] thermodynamical arguments are used to rank Mg-based binary alloys considering their relative tendency to develop SRO. Taking Mg-Al, Mg-Zn and Mg-Gd as model alloys, it is predicted that Gd in solution should develop the strongest SRO, hence it should produce the most creep resistant alloy, followed by Zn and Al, in that order. The object of this paper is to present experimental evidence in support of those predictions.

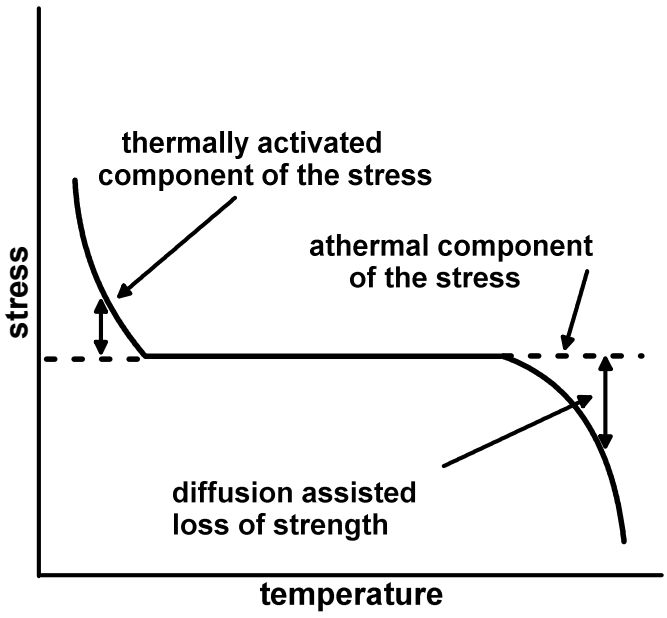

Figure 4-1. The temperature dependence of the flow strenght (schematic).

4.2 Experimental Details

Castings with nominal compositions 1.5 at%Zn, 2.5 at%Al and 1 at% Gd were produced. The amount of solute for each alloy was set to approximately match the solubility at 200°C in order to limit precipitation hardening effects during the testing at the higher temperature. The actual compositions are listed in Table 4-1.

Commercially pure Mg, Zn, Al and a Mg-Gd master alloy (2:3 Gd:Mg) were melted in steel crucibles coated with boron nitride in an electric furnace under a SF6+CO2 protective atmosphere.

The liquids were stirred mechanically for 20 minutes to ensure the dissolution of the solute and subsequently poured at 735-750°C under an argon atmosphere into steel moulds of size 80 x 80 x 10 mm^3, preheated to 300°C. The cast plates were solution heat treated under Ar atmosphere as per the times and temperatures given in Table 4-1, and quenched into water. Compression tests were carried out on cylindrical specimens, 18 mm in height and 9 mm in diameter, on a screw driven machine at 25°C and 180°C in a temperature controlled chamber. The crosshead speed was 0.016 mm/min for all the tests (initial strain rate = $1.5*10^{-5}s^{-1}$).

Table 4-1.Chemical composition of the alloys studied determined by inductively coupled plasma atomic emission spectroscopy (ICP-AES), and the respective grain sizes and solution heat treatment schedule.

Alloy	Solute (at.%)	Grain size (µm)	Time (h)	Temperature (°C)
Mg-1.5%Zn	2.2	123	4	470
Mg-1%Gd	0.8	119	4	535
Mg-2.5%Al	-	129	10	413

4.3 Results

Figures 4-2 to 4-4 show the deformation flow curves of Mg-2.5Al, Mg-2.2Zn and Mg-0.8Gd, respectively, at room and high temperature. Serrated flow was observed in Mg-Zn at room temperature (Fig. 4-3) and at 180°C in Mg-Gd (Fig .4-4). Figure 4-5 compares the alloys' behaviour at room temperature and figure 4-6 at 180°C.

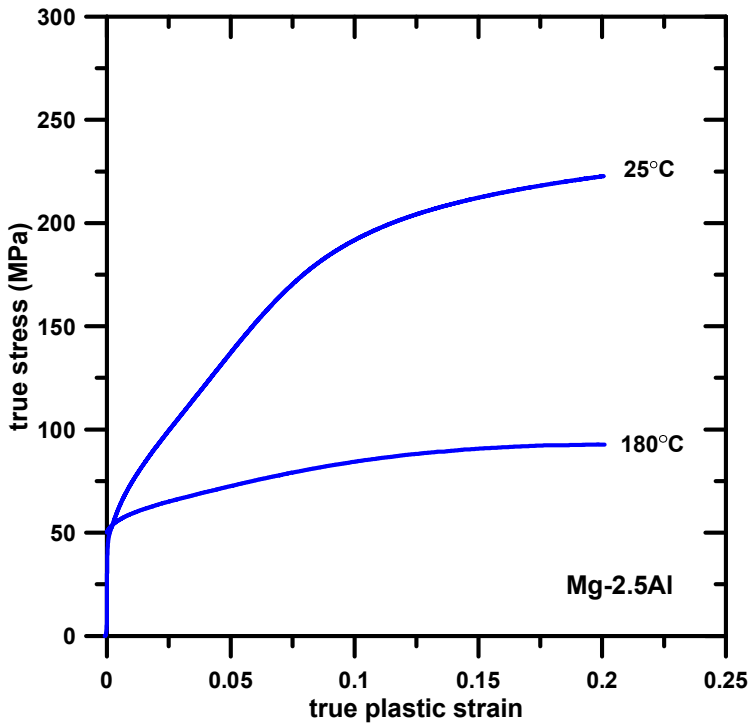

Figure 4-2. Compressive flow curves of Mg-2.5Al

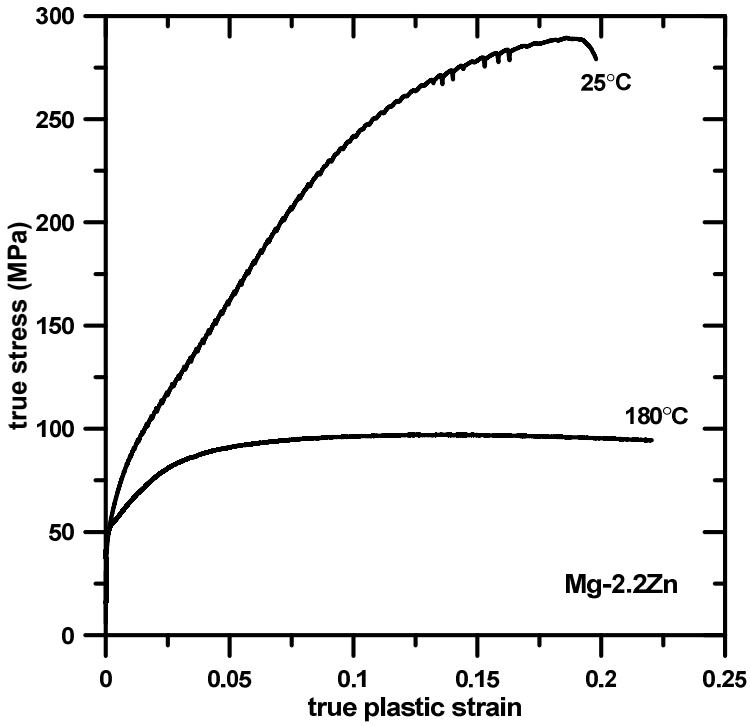

Figure 4-3. Compressive flow curves of Mg-2.2Zn

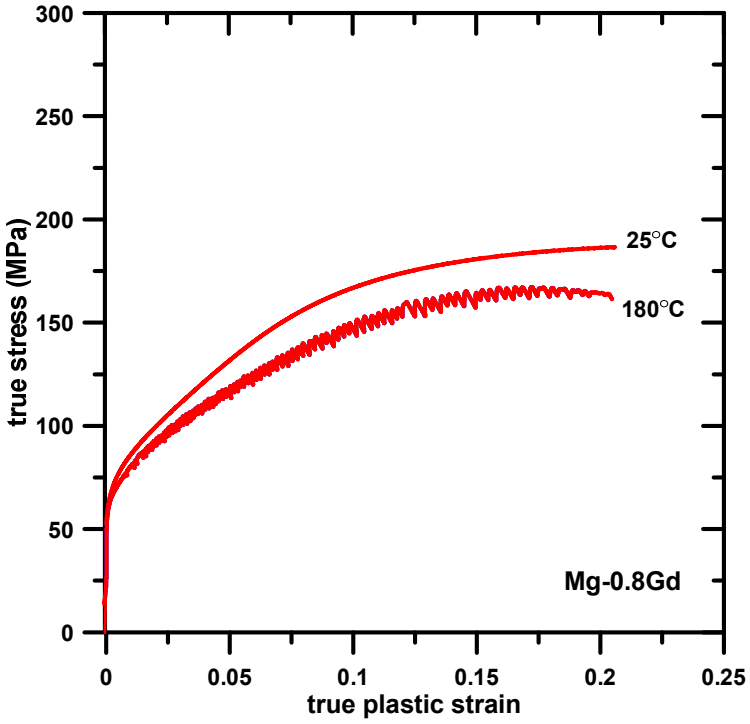

Figure 4-4.Compression flow curves of Mg-0.8Gd

At room temperature all three alloys exhibited an extended linear hardening regime, which reached saturation at about 10 % strain. The saturation stress was largest in the Mg-Zn alloy. At 180°C the loss of strength was very limited in the Mg-Gd alloy, whereas it was extensive in the Mg-Al alloy. The Mg-Zn alloy exhibited a short linear hardening regime, saturating at a strength level which was matched by the Mg-Al alloy at large strains. Figure 4-7 compares the flow stress at 0.05 strain, showing that the behaviour of the Mg-Gd is nearly athermal, followed by Mg-Zn and Mg-Al, in that order, and line with the expectations from the theoretical analysis of the companion publication[13].

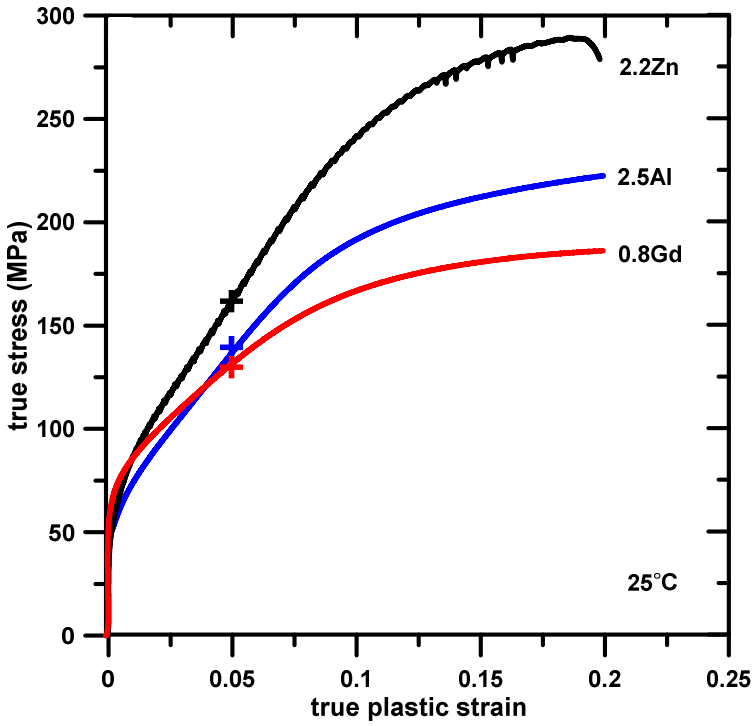

Figure 4-5. The flow behavior of the alloys studied, at 25°C. The crosses identify the strength values plotted in figure 4-7.

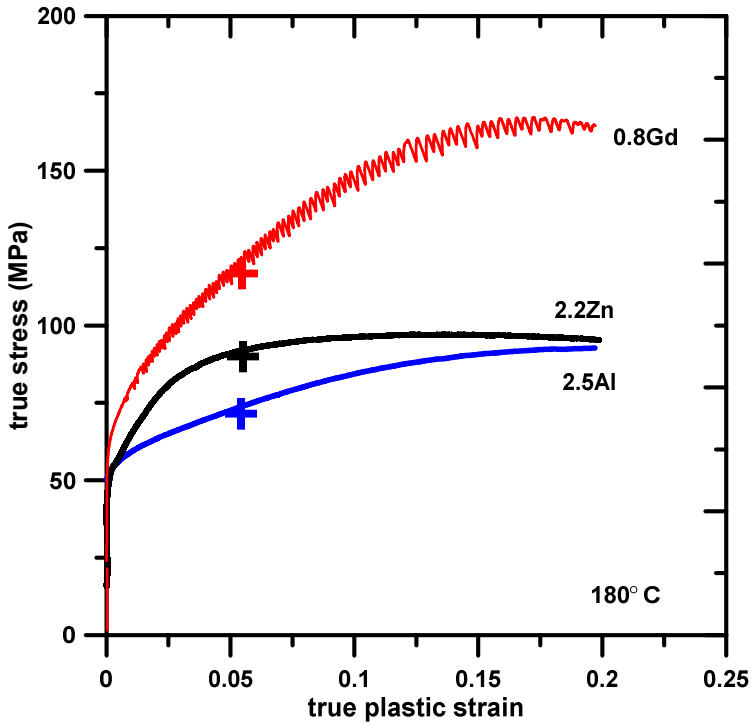

Figure 4-6. The flow behavior of the alloys studied, at 180°C. The crosses identify the strength values plotted in figure 4-7.

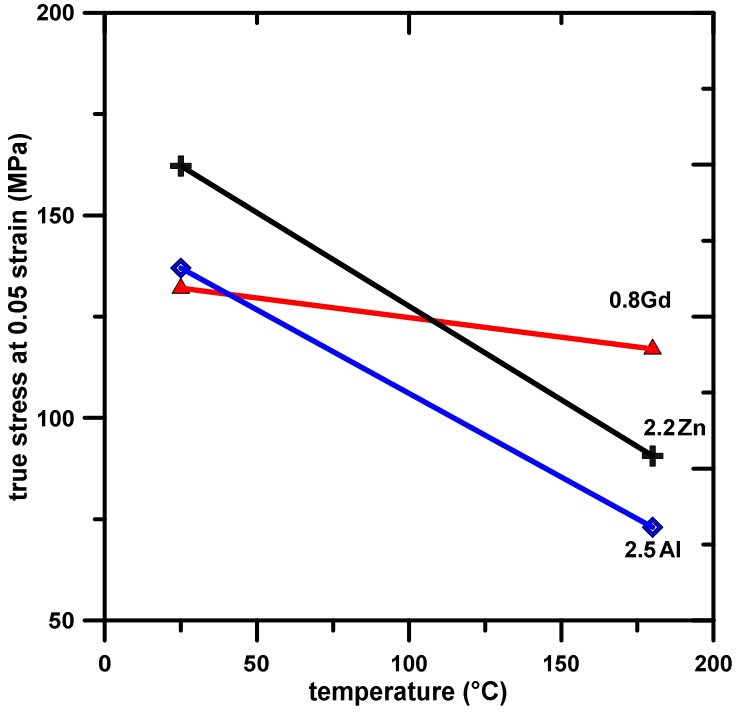

Figure 4-7. The strength of the alloys studied, at 25 and 180°C, at a strain of 5% (the crosses in Figures 4-3 and 4-4).

4.4 Discussion

The remarkably athermal behaviour of the Mg-Gd alloy, indicated both by the extended linear hardening regime [1, 14] at both temperatures in figures 4-2 to 4-4 and the small decrease in strength in figure 4-7, constitutes strong evidence of the presence of SRO which remains stable at the higher temperature. The Mg-Zn alloy partly reproduces the behaviour of the Mg-Gd, with a shorter linear hardening stage and a larger drop in strength at the higher temperature. This behaviour is consistent with a lower intensity of SRO, which makes it less thermally stable in comparison with the Mg-Gd. The Mg-Al alloy, as expected from its virtual absence of SRO, although it still exhibits a linear hardening at the higher temperature, the hardening rate is much lower and it suffers a substantial drop in strength despite its larger alloy content.

4.5 Conclusions

Mg-0.8at.%Gd, Mg-2.2at.%Zn and Mg-2.5at.%Al solid solutions were tested at RT and 180^{o}C.

- The solute contents were kept deliberately low to prevent precipitation hardening at the higher testing temperature.

- The Mg-Gd lost very little strength at the higher temperature. The loss of strength was larger for the Mg-Zn and substantial for the Mg-Al.

- The extent of the athermal behaviour is consistent with the relative strength of short range order in each of the alloys, largest in the Mg-Gd and lowest in the Mg-Al.

4.6 References

[1] D. Kuhlmann-Wilsdorf, H.G.F. Wilsdorf, J.A. Wert, Scripta Metallurgica et Materialia, 31 (1994) 729-734.

[2] D. Hull, D.J. Bacon, 3rd ed., Pergamon Press, Oxford, 1984.

[3] A. Seeger, in: J.C. Fisher, W.G. Johnston, R. Thomson, T. Vreeland (Eds.) Dislocations and mechanical properties of crystals, Chapman and Hall, London, 1957, pp. 243-329.

[4] F.R.N. Nabarro, H.L. de Villiers, Taylor and Francis London, 1995.

[5] Y. Chino, M. Kado, T. Ueda, M. Mabuchi, Metallurgical and Materials Transactions A, 42 (2011) 1965-1973. 10.1007/s11661-010-0563-1

[6] A. Akhtar, E. Teghtsoonian, Philosophical Magazine, 25 (1972) 897-916.

[7] A. Akhtar, E. Teghtsoonian, Acta Metallurgica, 17 (1969) 1339-1349. 10.1016/0001-6160(69)90151-5

[8] C.H. Cáceres, A. Blake, physica status solidi, 194 (a) (2002) 147-158.

[9] S. Henes, V. Gerold, Zeitschrift fur Metallkunde, 53 (1962) 703-708.

[10] D.S. Gencheva, A.A. Katsnel'son, L.L. Rokhlin, V.M. Silonov, F.A. Khavadzha, Fiz. metal. metalloved., 51 (1981) 788-793.

[11] L.A. Safronova, A.A. Katsnel'son, S.V. Sveshnikov, Y.M. L'Vov, Fiz. metal. metalloved., 43 (1977) 76-80.

[12] N. Jha, A.K. Mishra, Journal of Alloys and Compounds, 329 (2001) 224-229.

[13] C.H. Caceres, S. Abaspour, in: (Ed.) *TMS 2013*, 2013, pp.

[14] U.F. Kocks, H. Mecking, Progress in Materials Science, 48 (2003) 171-273.

Chapter 5 The Athermal Component of the Strength of Mg Binary Solid Solutions

The Athermal Component of the Strength of Binary Mg Solid Solutions

Saeideh Abaspour, C.H. Cáceres

ARC-Centre of Excellence for Design in Light Metals

Materials Engineering, School of Engineering

The University of Queensland, QLD 4072, Australia

Abstract

Stress relaxation tests at predetermined strain/stress were used to assess the athermal stress, σ_a, component of the flow stress between room temperature and 180°C for Mg-0.8at% Gd, Mg-0.87at% Nd, Mg-1.3at% Y and Mg-2.5at %Al solid solutions. σa decreased monotonically with increasing temperature for the Mg-2.5at%Al whereas it remained constant for Mg-Gd or increased for Mg-Y and Mg-Nd. The limited athermal behaviour of Mg-2.5at% Al alloy can be attributed to the random solid solution introduced by the Al. The remarkably athermal behaviour of the Mg-RE alloys is consistent with an increasingly strong tendency to develop short range order in conjunction with strain induced precipitation hardening.

Key words: Solid solution strengthening, Stress relaxation, Athermal behaviour, Short range order, Mg alloys

5.1 Introduction

The strength of an alloy is normally split into two components [1-3]:

$$\sigma = \sigma^* + \sigma_a$$

σ^*identifies the thermally activated component and σ_a the athermal component of the strength. The thermal nature of the stress arises from the interaction of dislocations with short range obstacles which can be overcome with help from the available thermal energy. In binary solid solutions of Mg the thermally activated component is closely connected to the solid solution softening of the prismatic and pyramidal slip systems [4, 5]. The athermal component results from the interaction

between dislocations and long range obstacles, such as short range order (SRO) when present. Short range interactions involving atomic size and shear modulus misfit, as expected for random solid solution effects are dominant in Mg-Al alloys [6] and in general in dilute (<0.4at.%) solid solutions. In concentrated alloys, the phase diagram of most Mg binary solid solutions suggests that SRO should be the dominant strengthening mechanism[7, 8] .SRO is a textbook example of an athermal strengthening mechanism that increases the creep strength of the alloy by preventing climb and cross slip and lowering the stacking fault energy [9].

The extent of the athermal regime determines the alloy creep strength [1-3, 7, 9, 10] and thus, extending the athermal regime to as high a temperature as possible, for instance by introducing or maximizing SRO, can be considered as a basic criterion for designing a creep resistant alloy.

The tendency for developing SRO is evident from the phase diagram [8, 11] through either two deep eutectics separated by a high melting point intermetallic, as in Mg-Zn alloys, or through the formation of multiple compounds as in Mg-RE alloys. Order in the solid solution, as opposed to the tendency to phase separation leading to precipitation hardening, stems from a negative enthalpy of mixing between solute and the host [8].

The sign and magnitude of the enthalpy of mixing can be predicted using the so called Miedema's scheme[8]. Mg-Al alloys with a low enthalpy of mixing show the weakest tendency to form, and hence the lowest strengthening from, SRO[8]. The larger (negative) enthalpy of mixing in Mg-Zn and Mg-Gd binary solid solutions should lead to stronger SRO effects and are thus expected to exhibit extended athermal behaviour, well beyond that of Mg-Al solid solutions. The behavior of other rare earth (RE) elements which are widely used to enhance the creep performance of Mg alloys, such as Nd and Y, with similar phase diagrams and enthalpy of mixing to that of Mg-Gd is expected to be similar to that of Mg-Gd.

In the current work stress relaxation tests were used to determine the athermal component of the strength of several Mg-RE binary solid solutions. The results are then discussed in terms of the expected strength of SRO.

5.2 Experimental Details

Mg binary alloys with nominal compositions (at.%) 2.5 Al, 1.0 Gd, 1.0 Nd and 1.6 Y were prepared by melting commercially pure Mg, Al, Gd, Nd and Y in steel crucibles coated with boron nitride in an electric furnace. The actual compositions are given in Table 5-1. The molten alloys were

protected with SF6+CO_2 atmosphere. A mechanical stirrer was used to mix the melt for 20 minutes to ensure the dissolution of the solutes. Castings were made in steel moulds of size 80 x 80 x 10 mm^3, preheated to 300°C under an argon atmosphere. Solution treatments were performed on the cast plates under Ar atmosphere as per the times and temperatures given in Table 1, and quenched into water. Compression tests were carried out on cylindrical specimens, 18 mm in height and 9 mm in diameter, on a screw driven machine at 25°C, 100°C and 180°C in a temperature controlled chamber. The crosshead speed was 0.016 mm/min for all the tests (initial strain rate = $1.5x10^{-5}s^{-1}$). Stress relaxation tests were carried out at 180°C during the compression test at 0.2mm/min. In sequential stress relaxation tests the alloys were deformed to a certain predetermined strain/stress, the test stopped and the stress monitored for 30 minutes in Mg-Al, and for 60 minutes in Mg-Gd, Mg-Y and Mg-Nd. The specimens were then reloaded to a higher stress/strain and the test was repeated.

Table 5-1.Chemical composition of the alloys studied determined by inductively coupled plasma atomic emission spectroscopy (ICP-AES), and the respective grain sizes and solution heat treatment schedule.

Alloy	Solute (at.%)	Grain size (µm)	Time (h)	Temperature (°C)
Mg-2.5%Al	-	129	10	413
Mg-1%Gd	0.8	119	4	535
Mg-1.6%Y	1.3	108.4	2	540
Mg-1%Nd	0.87	120	6	540

5.3 Results

Figure 5-1 shows the deformation flow curves of Mg-2.5Al, Mg-0.8Gd, Mg-1.3Y and Mg-0.87Nd at 25 and 180°C. An Extended linear hardening regime was observed in all the alloys at room temperature. Mg-Al exhibited an extensive loss of strength at 180°C, whereas it was limited in Mg-Gd alloy. Mg-Y and Mg-Nd alloys showed no loss of strength. Figure 5-2 compares the flow stress at 0.005 and 0.05 strains, showing that the behavior of the Mg-1.3Y and Mg-0.87Nd is athermal, and Mg-0.8Gd is nearly athermal, followed by Mg-2.5Al. There was a limited increase in the strength of Mg-2.5Al at lower strain at 100°C. The strength of the Mg-0.87Nd and Mg-1.3Y alloys remained constant between room temperature and 100°C and increased at 180°C. Figure 5-3 reveals the relaxation behavior of the alloys. The slope of the curves at a given time determines the stress relaxation rate. There was a dramatic decrease in the strength of the Mg-2.5Al alloy while, Mg-0.8Gd, Mg-1.3Y and Mg-0.87Nd hardly showed any stress relaxation

5.4 Discussion

In the Mg-2.5Al alloy the substantial drop in strength at high temperature (Fig. 5-2) and the high stress relaxation rate (Fig. 5-3) both are consistent with the absence of SRO. Stress relaxation near to zero (Fig. 5-3) corresponds well with the athermal behaviour of the Mg-0.8Gd alloy and constitutes further evidence of the presence of SRO already confirmed by diffuse X-ray scattering [12]. The extended linear hardening regime (Fig. 5-1), the remarkably athermal behaviour of Mg-1.3Y and Mg-0.87Nd (Fig. 5-2) and a nil stress relaxation (Fig. 5-3) are also consistent with a strong tendency to develop short range.

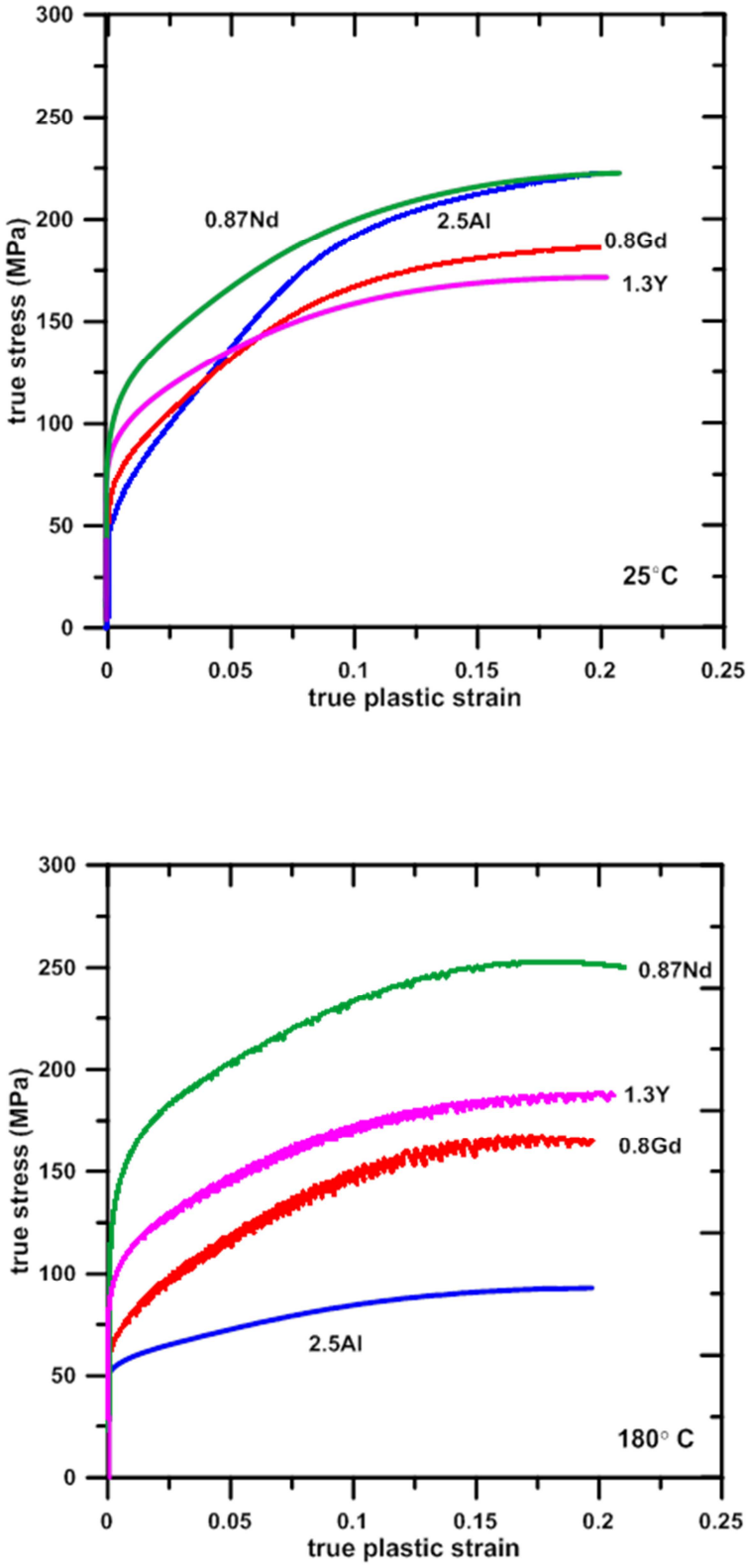

Figure 5-1. Compressive flow curves of the alloys studied, at 25°C and 180°C.

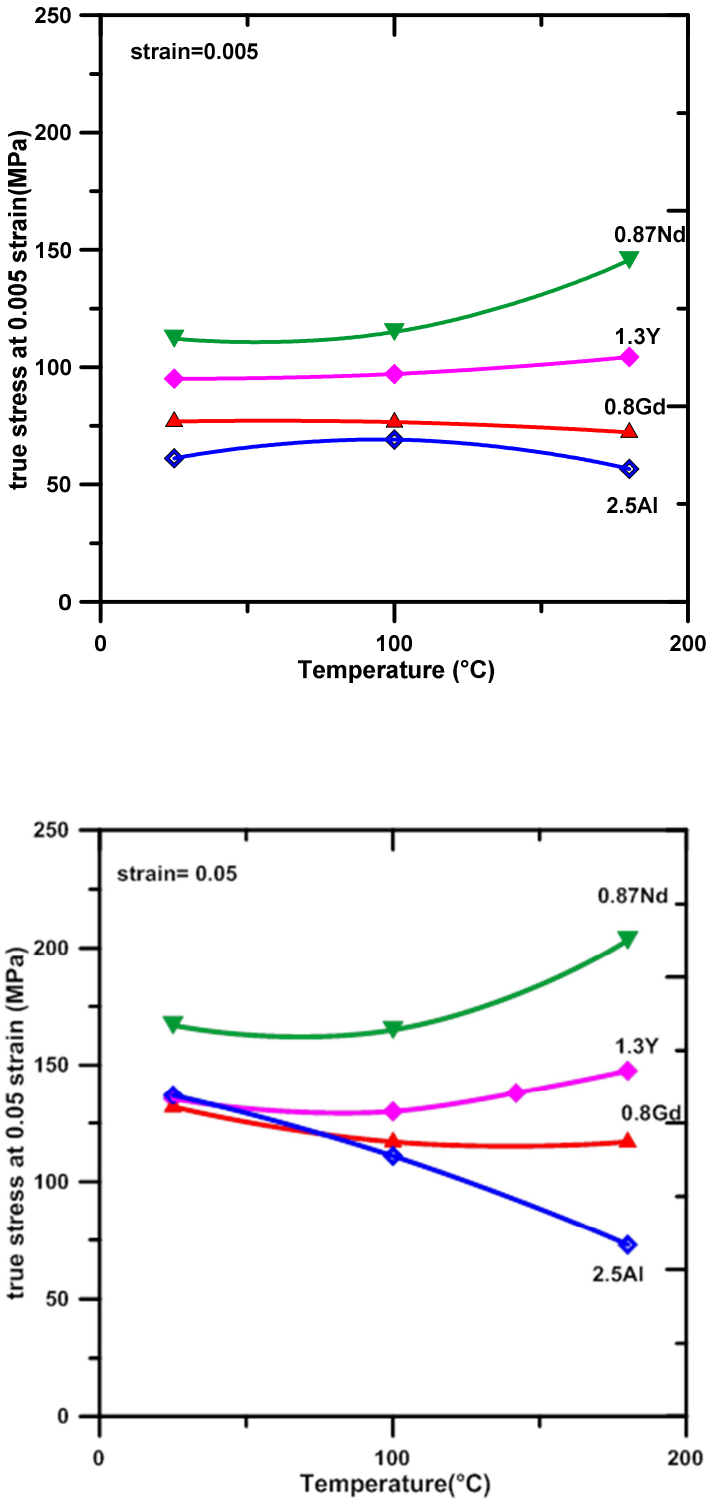

Figure 5-2. The strength as a function of temperature, determined at a strain of 0.5% and 5%

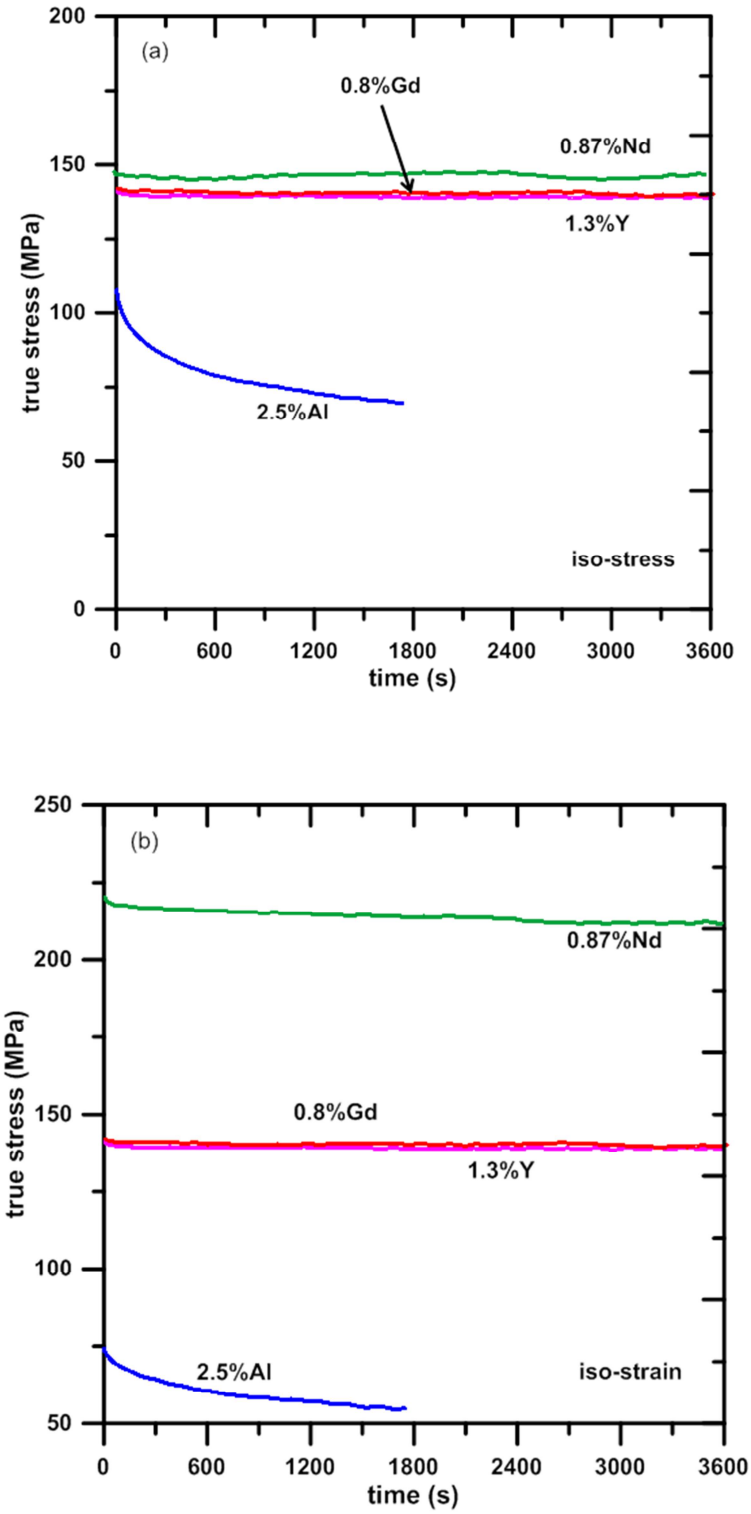

Figure 5-3. Stress relaxation tests a)iso-stress(all tests started at 150 MPa), b)at 5% strain

.

5.5 Conclusions

The Mg-2.5Al alloy showed no athermal regime in the temperature range studied. The strength dropped substantially during stress relaxation as expected for a random solid solution.

The remarkably athermal behaviour of Mg-0.8Gd Mg-1.3Y and Mg-0.87Nd alloys, despite their low solute content, appears consistent with a strong tendency to develop SRO.

5.6 References

[1] D. Hull, D.J. Bacon, 3rd ed., Pergamon Press, Oxford, 1984.

[2] D. Kuhlmann-Wilsdorf, H.G.F. Wilsdorf, J.A. Wert, Scripta Metallurgica et Materialia, 31 (1994) 729-734.

[3] A. Seeger, in: J.C. Fisher, W.G. Johnston, R. Thomson, T. Vreeland (Eds.) Dislocations and mechanical properties of crystals, Chapman and Hall, London, 1957, pp. 243-329.

[4] A. Akhtar, E. Teghtsoonian, Acta Metallurgica, 17 (1969) 1351-1356.

[5] S. Ando, H. Tonda, Materials Science Forum, 419-422 (2003) 87-92.

[6] C.H. Cáceres, D.M. Rovera, Journal of Light Metals, 1/3 (2001) 151-156.

[7] S. Abaspour, C.H. Caceres, in: (Ed.) *TMS 2013*, TMS, 2013, pp.

[8] C.H. Caceres, S. Abaspour, in: (Ed.) *TMS 2013*, 2013, pp.

[9] F.R.N. Nabarro, H.L. de Villiers, Taylor and Francis London, 1995.

[10] Y. Chino, M. Kado, T. Ueda, M. Mabuchi, Metallurgical and Materials Transactions A, 42 (2011) 1965-1973. 10.1007/s11661-010-0563-1

[11] P. Haasen, Cambridge University Press, Cambridge, 1996.

Chapter 6 Thermodynamics-Based Selection and Design of Age-hardenable and Creep Resistant Cast Mg Alloys

Thermodynamics-based selection and design of age-hardenable and creep resistant cast Mg alloys

Saeideh Abaspour, Carlos H. Cáceres

ARC Centre of Excellence for Design in Light Metals

Materials Engineering, School of Engineering

The University of Queensland, QLD 4072, Australia

Abstract:

Atomic level thermodynamics arguments that account for the generally weak age-hardening response while suggesting that extending the athermal regime through short range order (SRO) is a most feasible path to increasing the creep strength of many current alloys are presented. The tendency of many solutes to develop SRO in dilute solid solutions rationalizes a number of observations in current multicomponent Mg alloys while it disputes the viability of several micromechanisms often considered active, such as pinning of edge dislocations by mobile solute clouds, dynamic precipitation of thermally stable precipitates or atomic size effects on the diffusivity. Potential solutes are sorted out and ranked based on the sign and value of the enthalpy of mixing of binary solid solutions using the Miedema's phenomenological scheme. Due to their large negative energy of mixing and reasonable solubility (>1*at*.%) at ~473K (200^{o}C), Y and Gd appear as the best candidates to increase the creep strength through SRO, in close agreement with data reported in the literature. The feasibility of enhancing the age hardening response through homogeneously nucleated, coherent precipitates, in some cases despite the alloy's negative energy of mixing, or via internally ordered precipitates mimicking those present in Mg-Th alloys is considered by making parallels with the Al-Zn and the Al-Cu alloy systems. The possible optimization of the strengthening of high-pressure die cast alloys combining SRO and intergranular eutectics or of heat treatable cast alloys through internally ordered precipitates and SRO is discussed.

Keywords: Mg alloys; Creep strength; Precipitation hardening; Short range order; Miedema Scheme.

6.1 Introduction:

Although there are no evident structural reasons for either one, weak ageing response and low creep resistance are still major stumbling blocks on the way to advanced structural applications of Mg alloys. Consistently, it has been pointed out that these issues have more to do with the solutes' nature than with the host itself [1-4].

Since the solubility of many solutes decreases with the temperature in the same fashion as in age-hardenable Al-based alloys, at first sight most Mg-based alloys appear as suitable candidates for precipitation hardening through controlled ageing [2, 5-13]. Following the Al alloys model, ageing of Mg alloys is carried out by a combination of solution heat treatment within the single phase field in the relevant phase diagram, followed by quenching to create a super saturated solid solution. Subsequent ageing at an intermediate temperature is expected to harden the alloy through a mixture of coherent and non-coherent precipitates finely distributed in the α-Mg matrix. As shown by Fig. 6-1, more often than not the results hardly meet the expectations: whereas aged Al-Cu alloys can reach in excess of 150HV and Al-Zn alloys 200HV, most aged Mg alloys remain well below 100HV. Among them, the binary Mg-Al and Mg-Zn alloys are textbook examples of weak ageing response [3, 4]. The overall behaviour in Fig.1 is in line with the classical experiments by DeLuca and Byrne [14], who concluded that while age hardening can make Al alloys 200 times harder than the pure metal, a mere increase of a factor ~30 is normally achieved with Mg-based alloys. At ~130HV, recently developed quaternary alloys such as Mg-Gd-Y-Zr and Mg-Y-Nd-Zr can be quoted as acceptably examples of age hardening [13], although still well below Al-Zn alloys.

A fairly similar situation exists regarding creep strength, with many Mg alloys softening at about 393-422K (~120-150^{o}C) [1, 8, 12, 13, 17-19], as shown in Fig. 6-2. Mg-Al is again a case in point: despite Al's high solid solubility and measurable strengthening effects at room temperature [20], solid solution hardening does not extend to high temperatures. Figure 6-2 also shows that the Mg-Th alloys, which are currently being phased out due to Th's radioactivity, remain stable up to 573-623K (300-350°C) [12, 19]. On the positive side, some of the most recently developed alloys, WE43, WE54 and EZ43 approach a service temperature of 523K (250°C) [11, 19, 21, 22] and new alloys are under consideration [11] .

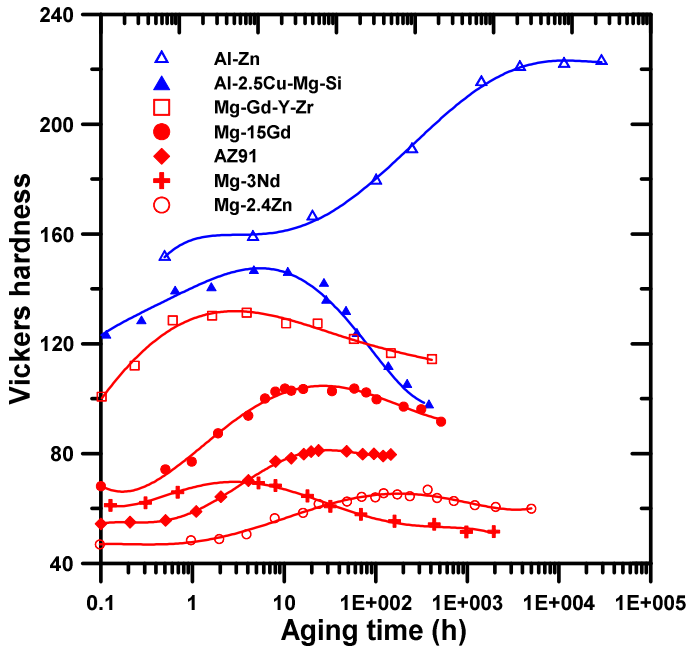

Figure 6-1. Comparison of the ageing response of Al- and Mg-based alloys. Data replotted from: Mg alloys, [13]; Al-Cu [15], Al-Zn [16].

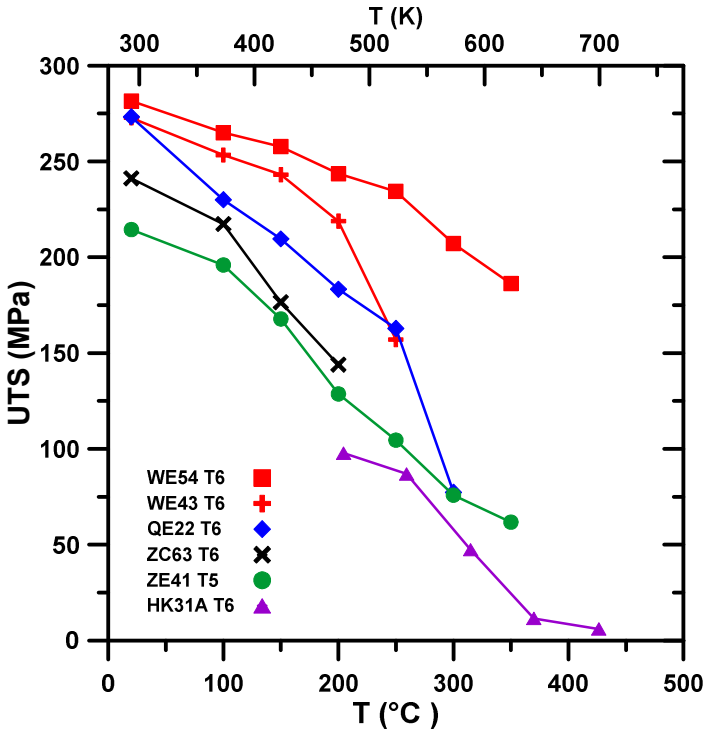

Figure 6-2. The strength of Mg alloys as a function of temperature. Data replotted from [12], save for Mg-Th (alloy HK31A, 2.5-4%Th-1%Zr-0.3%Zn), and for which the points represent the strength at 0.5% strain after 10h at temperature [23].

Another distinguishing feature of the Mg alloys' field is that many micromechanisms proposed to account for the observed improvements in either hardness or creep strength, frequently are little more than *ad-hoc*, after-the-facts explanations, valid at best for the particular system under consideration. Hence, extrapolation to other alloy-systems is either not possible or contradictory, as discussed in the next sections. In practice, trial and error rather than systematic approaches distinguish the field when it comes to alloy selection and design [7, 12, 13, 18, 24].

In what follows several strengthening mechanisms in Mg alloys, at both room and high temperature, are briefly reviewed. Subsequently, atomic level thermodynamics, through the classical Miedema *et al*.'s [25-28] phenomenological scheme, is used to sort out solutes according to the expected behaviour during age hardening or their potential effect on the creep strength of binary solid solutions. It is shown that due to the strongly electropositive nature of Mg, most alloy systems can be expected to develop short range order (SRO), on the one hand curtailing the nucleation of finely dispersed coherent precipitation, hence preventing a strong response to artificial ageing, while on the other, potentially increasing the creep strength. The tendency of solutes to develop SRO rationalises most, if not all, of the observed behaviours in current multicomponent alloys, ranging from weak-to-strong ageing response and from low-to-high creep resistance, dismissing many of the micromechanisms currently invoked as explanations. The Miedema scheme naturally suggests a rational approach to solute selection, hence, to alloy design, derived from the relevant binary phase diagrams. The predictions are corroborated using data from the literature in the last sections of this paper, and by experiments involving binary solid solutions described in a companion paper [29].

6.2 Room Temperature Strength

6.2.1 Solid Solution Hardening

Mg-based binary solid solutions can be broadly sorted out into two groups, as illustrated by Fig. 6-3, one represented by Mg-Al alloys and which exhibit strengthening in line with random solid solution [20], and one in which the solid solution hardening rate is several times higher, exemplified by alloys containing Zn [30], Gd or Y [31, 32].

A number of works [31-34] concluded that the high strengthening efficiency of Y and Gd cannot be explained by elastic interactions as would be expected for random solid solution hardening (cf., the Mg-Al case [20]), but active mechanisms, other than an unverified valence mechanism[1] [35] have not been put forward. The hardening in Mg-Gd-Zn alloy has been ascribed to the formation of Gd-Zn dimers that presumably block the movement of the basal dislocations' edge components [36].

Alternatively, the high solution hardening rate introduced by Zn has been accounted for through SRO, [30] consistently with what the alloy's phase diagram indicates [37]. The presence of SRO has been confirmed by diffuse x-ray scattering in a number of binary Mg solid solutions, namely, Mg-Gd [38], Mg-Er [38], Mg-Sn [39], Mg-Tb [40] and Mg-In [41], as well as in liquid Mg-Zn [42] and in aged Mg-5*at*.%Gd [43], suggesting that the similar behaviours of Zn, Y and Gd in Fig. 3 are indeed due to SRO in all three alloy systems.[2,3,4,5]

---

[1] *The alleged valence mechanism is supposed to increase the yield strength of Mg-RE solutions through the introduction of a covalent component in the atomic bonding. The model also predicts that Zn should harden Mg at the same rate as Al, in contradiction with Fig. 6-3.*

[2] *SRO is expected in Mg-Al as well, but its strength is bounded by the low melting point of the $Mg_{17}Al_{12}$ intermetallic [30].*

[3] *The low values of the Hall-Petch friction stress in Mg-Zn [44], and which are also accounted for by SRO effects on twinning, led some authors [31, 34] to conclude that solid solution by Zn is below that of the RE, against what Fig. 3 shows.*

[4] *It has been recently pointed out [45] that the RE increase the ductility more than Zn, which is not correct as can be seen by comparing the data of Refs. [30-32]. That the alloys are more ductile than the pure Mg metal is yet another classic conclusion [46-49], stemming in this case from the solid solution softening of the prism planes, which being a general solid solution effect should apply equally well to all kinds of solutes, including the RE.*

[5] *Mg-Sn is known to develop SRO [39], hence its hardening rate should match that of Mg-Zn in Fig. 6-3, but recent experiments [50] suggest otherwise. It is noted however that the specimens used in those experiments had only 4-5 grains across the cross sections, questioning the validity of the results for polycrystals.*

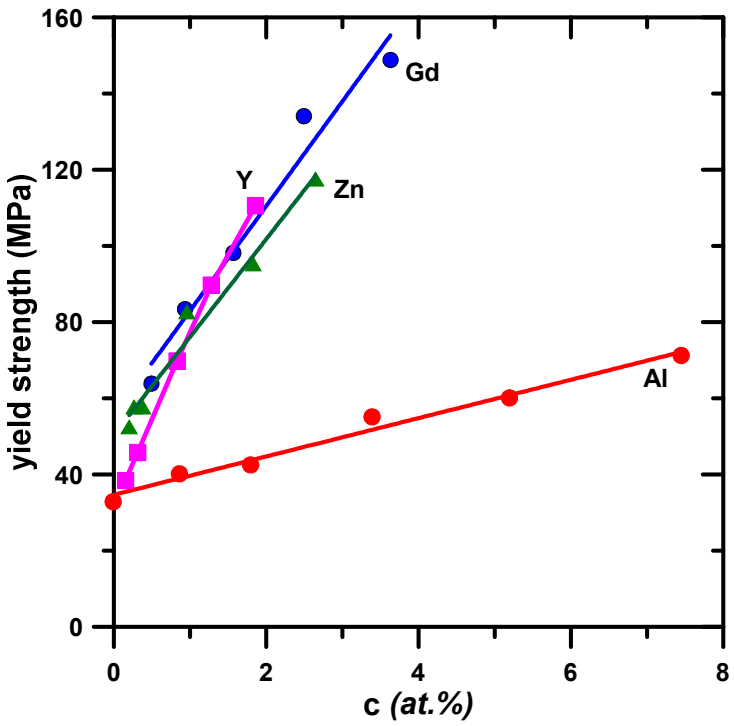

Figure 6-3. The strength of Mg-based solid solutions. Data sourced from:[30] (Mg-Zn);[20] (Mg-Al);[31] (Mg-Gd); [32] (Mg-Y).

6.2.2 Precipitation hardening

In their pioneering work, Sturkey and Clark [2-4, 51] pointed out that Mg-Al and Mg-Zn alloys were reluctant to form the homogeneously distributed clusters which act as precursors to precipitation in Al-based alloys. The lack of a suitable precursor, hence of finely distributed intermediate phases equivalent to the GP zones in Al-Zn or Al-Cu, means that the equilibrium phase, which in most Mg alloys forms straight from the solid solution, is ultimately responsible for age hardening through the Orowan mechanism [2-4, 51]. The Orowan mechanism requires a disproportionate large volume fraction of finely distributed, hard (normally non-coherent) particles to achieve the strengthening that internally ordered, coherent precipitates can achieve with orders of magnitude less due to the elastic coherency strains which repel dislocations [52-54]. An additional drawback affecting precipitation strengthening of Mg alloys, and of which Mg-Al alloys are again a textbook example, relates to the fact that the precipitates often lie flat on the basal plane [3, 51], making them morphologically inefficient for interacting with the dominant form of slip. It has been noted, however, that in aged Mg-Zn solid solutions [2, 4] the $MgZn_2$ phase precipitates with the right orientation, i.e., perpendicular to the basal plane, but still the alloys' performance is hardly any

better than that of Mg-Al. In practical terms, the highly inefficient Orowan mechanism is a last resort when it comes to artificial ageing: detailed calculations by Nie and Muddle [52] and Hutchinson *et al*.[17] show the extent to which both comminution and reorientation of precipitates should occur in order to significantly increase the strength of most Mg alloys.

The early literature suggested the use of ternary additions as a way to increase the precipitates' number density [3, 4, 51, 55], and numerous experiments followed this path time and again, with uneven success [5, 17, 55-58]. Likewise, sophisticated efforts to reorientate precipitates in Mg-Y alloys by edge-to-edge matching through trace element additions led to an increase of about 10~20 HV at best [59].

In the specific case of AZ91 alloy, trace elements such as Si, Sb, Sr, Ca, Na, Ag, Mo, Ba, Pb, B and Cu [7, 8, 60-63] have been tried in order to either refine the precipitates, alter their morphology or enhance the kinetics of precipitation, again with varied success [13, 18].

It has also been suggested that increasing the density of precipitates requires trace elements with atomic size larger than the host's so as to attract vacancies [13]. This mechanism seems unlikely to work, though, as, on the one hand, controlled quenching experiments by Pike and Noble [64] already showed that increased diffusivity through enhanced vacancy concentration makes for coarser rather than finer precipitation whereas, on the other, when additional (heterogeneous) nucleation sites are provided, e.g., through predeformation, the precipitation scale is reduced [17, 65]. That is, the coarseness of the precipitation stems from the lack of suitable nuclei in the early ageing stages rather than from insufficient diffusivity. Possible ways around the weak ageing hardening response of many Mg alloys are discussed in sections IV and V.

6.3 . Creep strength

Mordike [12] pointed out that efforts aimed at increasing the creep strength of Mg alloys have followed two complementary paths: incremental strengthening of existing alloys, AZ91 in particular, through minor chemical additions, and the development of alternatives to Mg-Th alloys.

Examples of the first path involve trace additions of, e.g., Ca [66], Sr [18], RE [8], Si [61, 67], and Sb [62, 68] to Mg-Al, aimed at either strengthening the α-Mg matrix by solid solution or precipitation hardening, or at preventing grain boundary sliding through thermally stable intergranular intermetallic particles. As already stated, most of these attempts met with limited success.

The other path resulted in new alloys containing RE [1, 12, 18, 32, 69-76] and was significantly more successful: e.g., the creep rate of Mg-Y alloys is some 3 orders of magnitude lower [1] than that of Mg-Al. Further improvements have been possible through the addition of Nd to Mg-Y alloys, leading to the current WE54 and WE43 alloys [12, 18]. Other cases are described in section VII. Despite the experimental success, the micromechanics accounting for the high creep resistance of Mg-RE alloys, as well as those active in some of the Mg-Al alloys [67] is still a matter of debate, as evident from the wide variety of proposed mechanisms which often are either in contradiction with each other, or lack specific structural support, as discussed below.

6.3.1 Solid Solution hardening

As expected from Fig. 3, two different situations are observed: Al in solution leads to a minor increase in creep resistance [77, 78], even when ternary elements like Sn in MRI230D alloy shift the solute partitioning during solidification, increasing the final amount of Al in solid solution [77]. Moreno *et al.*[79] pointed out that the solid solution strengthening by Al leads only to short term increases in the strength in AE42 (Mg-4Al-2RE) alloy compared to MEZ (Mg-2.5RE-0.35Zn-0.3Mn) alloy.

It has also been claimed that the low creep resistance of AZ91 alloy mainly stems from the low melting temperature (735K (462°C)) of the intermetallic [67, 80-83]. Addition of RE elements [84, 85] or Si [67] aiming at introducing thermally stable intermetallics improves the creep somewhat. However, since the presence of harder intergranular particles provides no additional solid solution strengthening across the α-Mg matrix, the dislocation substructure remain virtually free to cross slip or climb, as discussed in more detail with reference to Figs. 4 and 5 later on. By and large, the poor creep performance of AZ91 alloy, which with as much as 9% Al in solution is hardly any better than that of Mg-2%Al [1, 67, 82, 86], denies in principle any beneficial effects ascribed to solution hardening by Al on the creep strength of any Mg alloy. [6]

RE in solution, on the other hand, perform much better: Maruyama *et al*. and Mordike showed that Y in solution is much more effective than Al [1, 12] when it comes to improving creep strength.

[6] *Many studies, e.g., [80, 82, 86] based their conclusions on specimens tested in the as-cast condition. Cast microstructures are strongly geometry dependent, and since coring creates strong concentration gradients and disproportionate amounts of interdendritic eutectics, as-cast specimens seem hardly suitable to properly quantify solid solution strengthening, or any other micromechanism, for that matter. This criticism does not apply to studies based on high-pressure die-cast specimens, since in those cases what is measured, rather than material properties, are the properties of the casting cross-section [87].*

Zhu *et al*.[88] and Gibson *et al*.[76] showed that the creep strength of Mg-RE alloys increases with the content of the RE and concluded that both solid solution and precipitation hardening are major factors in the creep strength of these alloys, in decreasing order for Nd, Ce and La. Xu *et al*.[89] showed that partly replacing Gd by Y in a Mg-Gd alloy leads to decreased number density of precipitates while still increasing the creep strength, an indication of the stronger effect of solid solution over precipitation in these alloys.

6.3.2 Dynamic precipitation

This is one the most often quoted mechanisms to account for the increased creep resistance [1, 13, 18, 90] of Mg alloys, with or without RE, and possibly one of the least defendable. The logic behind dynamic precipitation is that the mutual intersection of dislocations increases the vacancy concentration during creep, enhancing diffusion, and ultimately leading to finer, hence more effective, precipitation occurring concurrently with the deformation [91]. As mentioned in relation to (static) precipitation hardening, Pike and Noble classic experiments [64] showed through controlled quenching that an increased concentration of vacancies led to coarser rather than finer precipitates. The strengthening effects observed during creep, when they indeed occur, are thus more likely to be accountable through the introduction of heterogeneous nucleation sites (dislocations) rather than through enhanced diffusivity. Maruyama *et al*. [1] made this point explicit as well regarding Mg-Y. Again, ECAP experiments show that saturating the matrix with dislocations prior to ageing leads to a highly refined precipitate microstructure [65] without the need for enhanced vacancy concentration. More significantly, deformation-enhanced precipitation occurs in AZ91 alloy as well [17, 62, 92] but it does not lead to hardening during creep, further disputing the fundamentals of this mechanism as a general strengthening mechanism.

6.3.3 Solute dragging / Solute clustering

Serrated flow in Mg-Y and Mg-Gd alloys [12, 93] has been mentioned as evidence of solute dragging and locking of dislocations, therefore accounting for these alloys' enhanced creep resistance. Against the alleged efficiency of this mechanism it may be argued that serrated flow is also observed in many other Mg alloys [12, 32, 94-96], including AZ91 alloy [92, 97, 98], which, again, hardly qualifies as creep resistant. Along the same lines, it has been suggested [99] that small additions of Zn (0.3*at*.%) to Mg-Nd-La improves the alloy's creep strength through Cottrell

atmospheres of Zn atoms around dislocations.[7] Solute clustering requires thermodynamic conditions which are in principle excluded by most of these alloys' phase diagrams (e.g., positive energy of mixing), and of RE in particular, as discussed in more detail in Sections IV-VI, questioning the fundamentals of the cloud forming mechanism.

A more direct criticism can be levered to the hypothesis of dislocation pinning by solute clouds. Since solute dragging stems from atomic size differences, it should affect mainly the edge component of dislocation loops, leading to loops elongated in the direction of the screw components [102]. Such elongated loops have been observed, e.g., after prism slip in pure Mg single crystals [103] and in the bcc metals [102], and correctly ascribed to the anisotropy of the Peierls–Nabarro friction, but have not been reported regarding basal dislocations in Mg alloys.[8]

6.3.4 Atomic size controlled diffusivity

More recently it has been speculated [13] that the slower creep of Mg-RE alloys stems from the reduced diffusivity of RE atoms, ascribed, through as unspecified atomic mechanism, to the larger solute's atomic size in relation to the host's. This hypothesis was put forward in relation to Nd, Y, Gd, Ce and La [13, 88], and by extension, it should explain why Al, being smaller in size, hence able to diffuse at a faster rate, does not increase the alloys creep strength when present in solution [76, 88]. Likewise, it has been argued [89] that when Gd is partially replaced by Y in the Mg-Gd-Zn-Zr alloy the precipitates become smaller due to the lower diffusion rate of the (larger than Gd) Y atoms. Similar arguments have been applied to Ca [100]. However, no direct evidence of size related effects on the diffusivity of substitutional solutes in Mg alloys, or any other alloy system for that matter, seems to be available in the literature. On the contrary, comprehensive work on (HCP) Zr by Tendler and Abriata [104] showed that while the diffusivity of interstitial solutes is closely correlated with atomic size (and indeed much faster for smaller solutes as would be expected), it is independent of the atomic size for substitutional ones.[9]

---

[7] *The formation of the so called RE texture in Mg-RE alloys [100] has also been ascribed to solute dragging effects stemming from the larger atomic size of RE elements. A similar texture weakening has also been ascribed to the atomic size effects of Ca [96, 101].*

[8] *This criticism can also be levered to the hypothesis that Gd-Zn dimmers form in Mg-Gd-Zn alloys and block the edge components of mobile dislocations on the basal plane [36].*

9 Using the Meidema-Niessen model, Bakker [105]showed that for solutes much smaller than the alloy's host, the reduction of effective atomic volume due to the charge transfer enables a significant fraction of the solute atoms to fast-diffuse as interstitials, i.e., the solute exhibits on average a faster than expected diffusion rate. However, when the difference in size between solute and host is less than the Hume-Rothery limit of ±15% the solute beha ves strictly as

Alternatively, drawing from Brouwer *et al.*'s [107] work on Ti, it can be argued that any reduction in the diffusivity of RE atoms, which is certainly possible, is likely the result of the increased activation energy for diffusion due to the formation of SRO.

Two other possible strengthening mechanisms are described below for completeness. Unlike the ones discussed so far, these mechanisms are well supported by experiments.

6.3.5 Coherent, internally ordered ppt

Mg-Th alloys are in a class by themselves due to the ordered precipitates which are at the core of their remarkable creep strength [108, 109]. In these alloys a Laves transition phase with the composition Mg_2Th, which differs from the equilibrium phase (Mg_4Th) [108], forms during ageing. The formation of a semi-coherent ordered transition lattice has also been reported in Mg-3.7%Th-0.4%Zr by Mushovic and Stoloff [109] with the probable composition of Mg_3Th. The precipitation behaviour of Mg-Th differs in a fundamental aspect from that of most other alloys, such as Mg-Al, Mg-Zn or the Mg-RE: it involves homogeneously nucleated, finely dispersed, coherent precursor phases, closely mimicking those observed in age hardenable Al-Zn alloys. As shown in Section IV, these diverging behaviours, i.e., whether a binary Mg alloy can be expected to develop fine precipitation or otherwise, can be anticipated from the respective phase diagrams.

6.3.6 Percolating eutectic microstructure

The spatially interconnected eutectic microstructure that forms in most High Pressure Die Cast (HPDC) Mg-alloys [10, 110-113] has been shown to introduce hardening effects ranging from a few MPa in AZ91 to ~40 MPa in some Mg-RE alloys. In a Mg-RE alloy, strengthening of the α-Mg matrix in which the eutectic structure was embedded, a ternary addition [112] which higher terminal solubility added ~30MPa to the alloy's room temperature strength on top of what the eutectic percolating microstructure did on its own.

Needless to say, to take advantage of a thermally stable intermetallic microstructure, a thermally stable dislocation substructure in the α-Mg matrix is also necessary, as discussed in relation to Figs.

---

substitutional and the diffusion is normally slow and size-independent. Considering the similar atomic radius and c/a ratio of Mg and Zr [106] the diffusivity behaviour of any solutes can in principle be expected to be similar for both hosts. Tendler and Abriata's results also suggest that for solutes larger than the 15% limit, increased rather than decreased diffusivity can be expected, further denying the possibility of slower diffusivity of the larger RE, or any other larger substitutional solute, for that matter.

4 and 5. Dedicated experiments and further discussion involving these hypotheses can be found in the companion paper [29].

6.4 Thermodynamics-based analysis

6.4.1 The athermal strength regime

Figure 6-4 schematically shows the strength of a solid solution as a function of temperature. The plateau at intermediate temperatures identifies the so called athermal strength regime. The overall behaviour can be rationalised by dividing the flow strength into two components [114-117]:

$$\tau = \tau_i + \tau^* \qquad (1)$$

where τ_i is the athermal component of the stress arising from long range stress fields, and τ^* is the thermally activated component connected with short range obstacles that can be overcome by thermal energy. At temperatures above about 1/3 of the melting point, T_m, the flow stress decreases rapidly again, approaching the critical resolved shear stress of the pure metal, a behaviour attributed to the onset of dislocation's dynamic recovery through first cross slip and then climbing, the latter through increased atomic diffusivity.

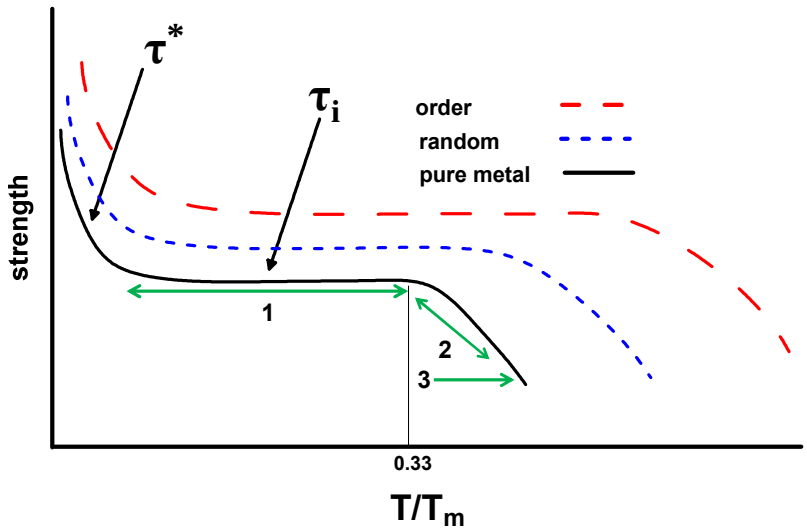

Figure 6-4. Solid solution and precipitates effects on the extent of the athermal regime. (schematic) [47, 118]. The numerals are a link to the flow curves of Fig. 6-5.

Figure 6-5 exemplifies with actual data for alloy AZ91 the correlation between an alloy's deformation behaviour and the schematics of Fig. 4. At room temperature the deformation curve (#1) exhibits a linear strain hardening regime extending to nearly 10% strain, consistent with

hardening by athermal accumulation of forest dislocations [119, 120]. At 373K (100°C) partial activation of dynamic recovery lowers the slope and shortens the linear hardening stage (#2). At 473K (200°C) extensive recovery prevents strain hardening altogether (#3). The deformation behaviour of solid solutions of Y, Gd, Nd, Zn and Sn are compared in the terms of Figs. 6-4 and 6-5 in the companion paper [29].

The extent of the athermal strength regime determines the alloy's maximum service temperature. Consequently alloy design for creep strength aims at rising and extending the athermal regime as much as possible [121] as schematized in Fig. 6-4. Hardening mechanisms to consider are solid solution, precipitation and atomic scale order [49, 114-116, 122], sorted out through the length scale of the interaction with dislocations as:

Short range interactions: these include elastic interactions between solute and solvent involving the shear modulus and atomic size misfit (i.e., random solid solution effects). Being amenable of thermal activation, they are not expected to significantly widen the athermal regime. Random solid solution effects dominate the strength of Mg-Al [30] and by extension AM and AZ91 alloys, which, consistently, have virtually no mentionable strength above 120-150^{o}C [18].

Long range interactions: order in solid solutions, in either the long or the short range scale, or through coherent, internally ordered precipitates, increases the strength and curtails cross slip, generally suppressing dynamic recovery, hence introducing athermal forest hardening [116, 118, 121] upon the deforming alloy. Order in a solid solution also lowers the diffusion rate by increasing its activation energy [107] as already mentioned, decreasing the climbing rate. Thus, order is expected to significantly lift and widen the alloy's athermal regime. Top examples of these types of interactions are the alloys containing RE discussed with regards to Fig. 6-3 and the internally ordered coherent precipitates which are the core of the creep strength of Mg-Th alloys [108]. Solutes that lower the stacking fault energy are expected to have similar effects [114, 123]. Possible RE effects on the SFE of Mg at the nanoscale have been considered in recent works [45, 124].

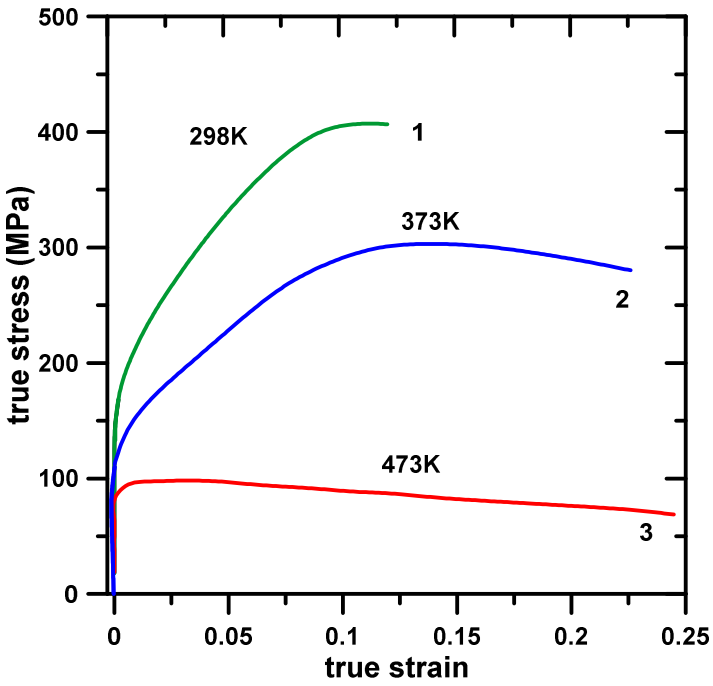

Figure 6-5. Deformation curves for AZ91 alloy at different temperatures, replotted from [125] (The numerals link the alloy's behaviour to the strength's stages in Fig. 6-4).

6.5 Atomic Order vs. Clustering

As the energy of mixing [126-131] of a binary solution becomes increasingly positive, a solubility gap appears, then a congruently solidifying alloy and finally a single eutectic system. Conversely, increasingly negative energy of mixing leads to multiple electronic compound formation and ultimately to a high melting point intermetallic solidifying congruently from the melt bounded by two eutectics. The extreme cases are illustrated by Fig. 6-6.

A supersaturated solid solution involving elements that keep a positive interaction (i.e, single eutectic phase diagrams alloys such as in Al-Zn, Fig. 6-6b) leads, upon ageing, to segregation of the solute into small and uniformly distributed clusters (GP zones), which act as precursors to the subsequent, equally fine precipitates that ultimately strengthen the alloy [54]. In the opposite case [127], a negative interaction (i.e., two eutectic phase diagrams, Fig. 6-6c) leads to the development of short range order (SRO) at dilute concentrations. Upon ageing, the reluctance to form solute clusters leads to heterogeneously nucleated, and ultimately coarse second phase particles, often with

the equilibrium phase composition [130], exemplified by Mg-Al, Mg-Zn and Mg-Sn alloys [2, 4, 30, 76, 132].[10]

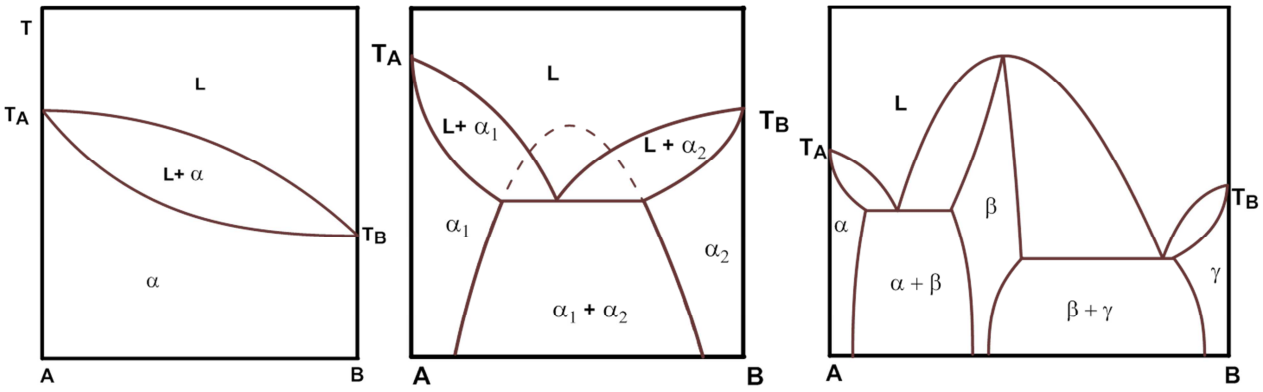

(a) (b) (c)

Figure 6-6. Changes in the phase diagram from (a) complete solubility to either (b) large positive energy of mixing or (c) large negative energy of mixing [127].

The sign and magnitude of the enthalpy of mixing can be used to sort out alloys of any given host, Mg in this case, and predict which alloys are prone to exhibit either solute clustering or SRO, i.e., which alloys can be expected to exhibith either strong precipitation hardening or high creep strength. The cellullar scheme laid out by Miedema *et al*. [25-28] will be used to this purpose.

6.6 Miedema's Cellular Scheme

Miedema *et al.*'s [25-28, 133-136] phenomenological scheme, introduced in the 1970's, involves two parameters: the work function, ϕ^*, (closely related to Pauling's electronegativity value), and the electron density at the boundary of the Wigner–Seitz (WS) cell, $n_{WS}^{1/3}$. The sign and magnitude of the enthalpy of formation of metallic solutions can be calculated based on these two parameters alone, therefore anticipating the relative tendency to form either ordered, random or immiscible solutions, as schematized by the phase diagrams Figs. 6-6. *Ab-initio* and Calphad calculations normally reproduced closely Miedema *et al.*'s values, providing the approach with strong independent

[10] *Deep eutectics and the development of SRO already in the liquid correlate with the tendency to form metallic glasses in many Mg alloys [127].*

support [134-136]. The scheme has also been successfully used to calculate the enthalpy of formation of Laves phases [135] with the accuracy of results confirmed by *ab-initio* calculations in most cases, e.g. [136]. A limitation often pointed out is the Scheme's fundamentally isotropic nature, i.e., it applies most accurately to liquid metals, where elastic energy related to any size mismatch is negligible. Further developments in the *ab-initio* methods enabled overcoming some of these limitations (e.g., see [134]).[11]

In the Miedema's scheme an atom in the metallic state is assumed as a macroscopic piece of metal within the Wigner-Seitz cell. The macroscopic atomic model for alloy formation is shown in Fig. 6-7. The Wigner-Seitz atomic cells of the pure metals A and B, with a small change in the shape, form the AB alloy system. If the molar volume remains unchanged (Fig. 6-7b) the energy of alloying would be close to zero. However, the boundary conditions impose a redistribution of charge within and between the atomic cells leading to a change in the cells volume, as in Fig. 6-7c (cf. footnote #9 re. atomic size and diffusivity). The equilibrium state is thus achieved through two contributions of opposite sign to the enthalpy of formation [25, 28].

The negative term, proportional to $(\Delta\phi^*)^2$, stems from the difference between the host's and solute's work functions, leading to a charge transfer from the more electropositive element to the more electronegative one providing the main driving force to form either a phase separating system or many ordered intermetallic compounds. The positive contribution stems from the need to remove any discontinuity of the electron density at the boundary of the WS cell between solute and solvent and is proportional to $(\Delta n_{WS}^{1/3})^2$.

[11] *Pettifor's Quantum Mechanics analysis [137] showed some contradiction in the fundamentals, but which do not detract from the practical value of the scheme as a (powerful) sorting and ranking tool.*

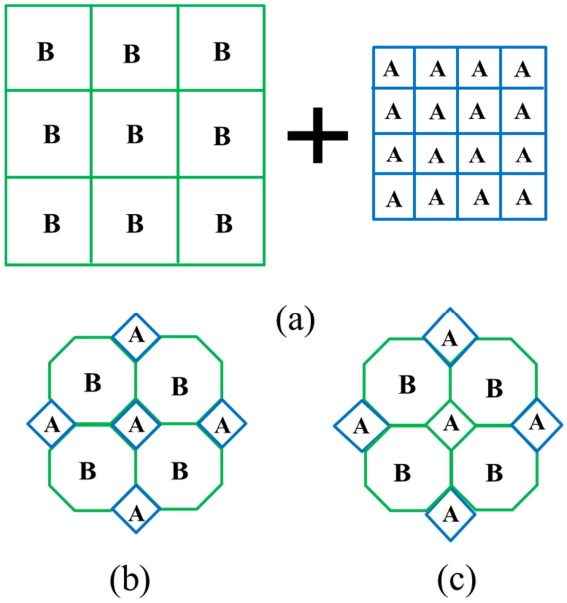

Figure 6-7. Miedema Scheme's macroscopic atomic model for alloy formation: the pure metals (a) form an alloy with (b) no change in the volume fraction. In (c) A expands and B shrinks due to the transfer of charge.

The enthalpy of formation, ΔH, in both the solid and liquid state, involved when forming an equi-atomic compound [28, 138, 139] is thus given by [26, 27, 140, 141]:

$$\Delta H = -P(\Delta\varphi^*)^2 + Q(\Delta n_{WS}^{1/3})^2 - R\,, \qquad (2)$$

where P and Q are constants,[12] related to each other through $Q/P = 9.4\ (eV)^2(d.u.)^{2/3}$, the slope of the straight line separating positive and negative ΔH- values (i.e., for $\Delta H = 0$) as explained in relation to Fig. 6-8 in the next section. R, called the hybridization term, is a constant for given groups of alloys, and enters the equation only when transition metals are alloyed with non-transition metals, hence its name.

[12] *For consistency with the original formulation, non-SI units (eV and d.u.) are used for the scheme.*

6.6.1 Application to Mg alloys

A diagram using Miedema's coordinates was created in Fig. 6-8 for binary Mg-based alloys involving both transition and non-transition elements. [13] R is small when Mg is the host and can be neglected [27], so Fig. 6-8 was created assuming R = 0 for all solutes. The effect of neglecting the R-value on particular (borderline) solutes is discussed in Appendix A.

The two diagonal lines, drawn through Mg with slope Q/P = +/- 9.4 $(eV)^2(d.u.)^{2/3}$, sort out solutes as follows: elements sitting right on the lines show zero enthalpy of mixing; the upper (or "North) and lower, (or "South") sectors identify solutes with a negative energy of mixing; those lying on the East/West sectors have a positive energy of mixing. Consequently, solutes located right on the lines are expected to exhibit complete miscibility; those on the North or South sectors should show a tendency to develop phase diagrams with either "multiple electronic compounds", or "two-eutectics" similar to that of Fig. 6-6c; those on the East-West sectors should form single eutectic diagrams akin to that of Fig. 6-6b. Figure 6-9 shows how these distinguishing features of the phase diagrams vary consistently, and systematically, according to the elements' location in the periodic table. [14]

[13] *Diagrams similar to that of Fig. 8 can be seen in [139] for Fe, in [27] for Mg and a generic one in [133].*

[14] *With exception of Ni and B, the sorting of solutes in Fig. 6-8 is consistent with the respective phase diagrams as per Figs. 6(a-c). The mismatches are discussed in Appendix A.*

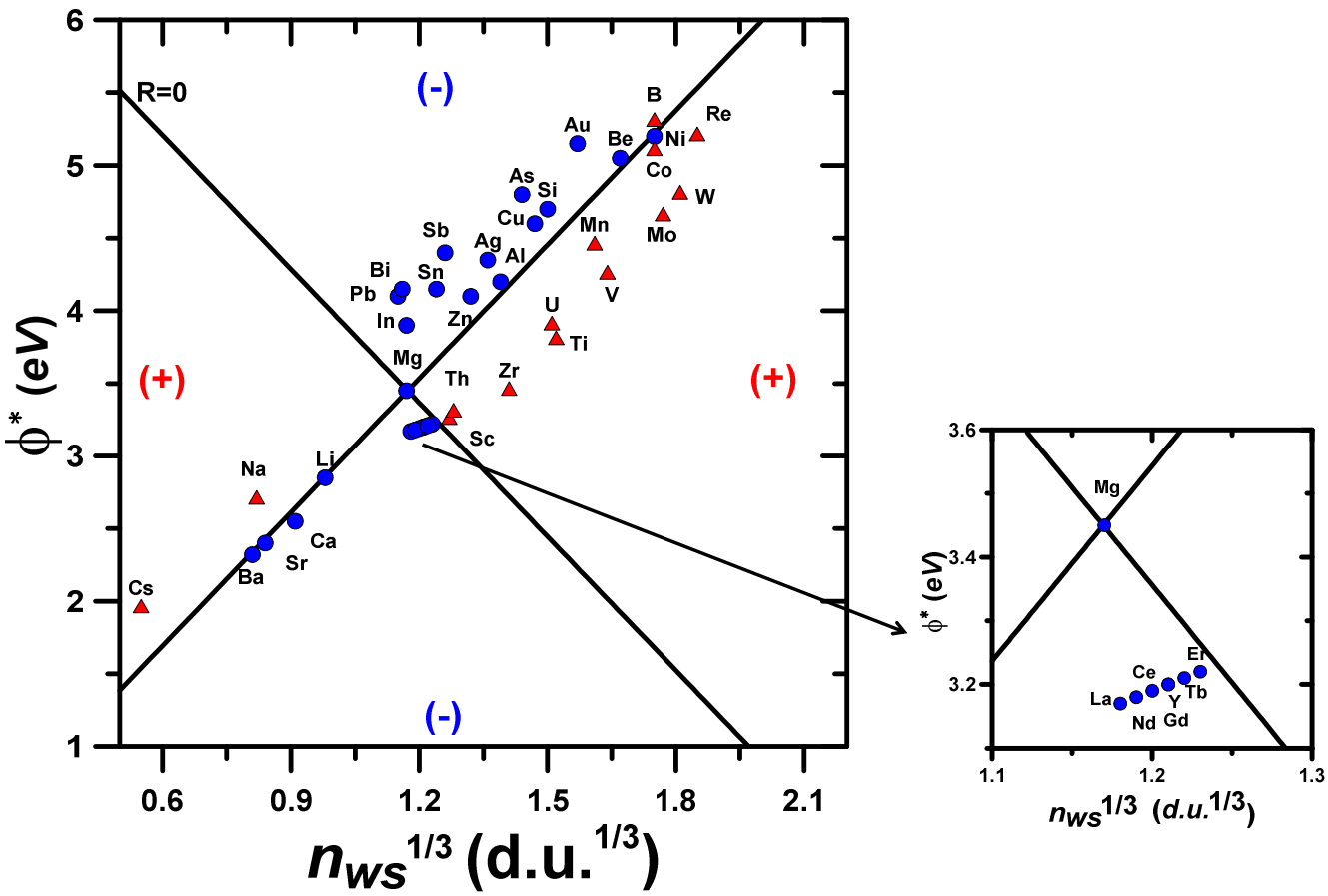

Figure 6-8. The Miedema scheme for Mg alloys, assuming R=0 in Eq. 2. Coordinates data from [26].

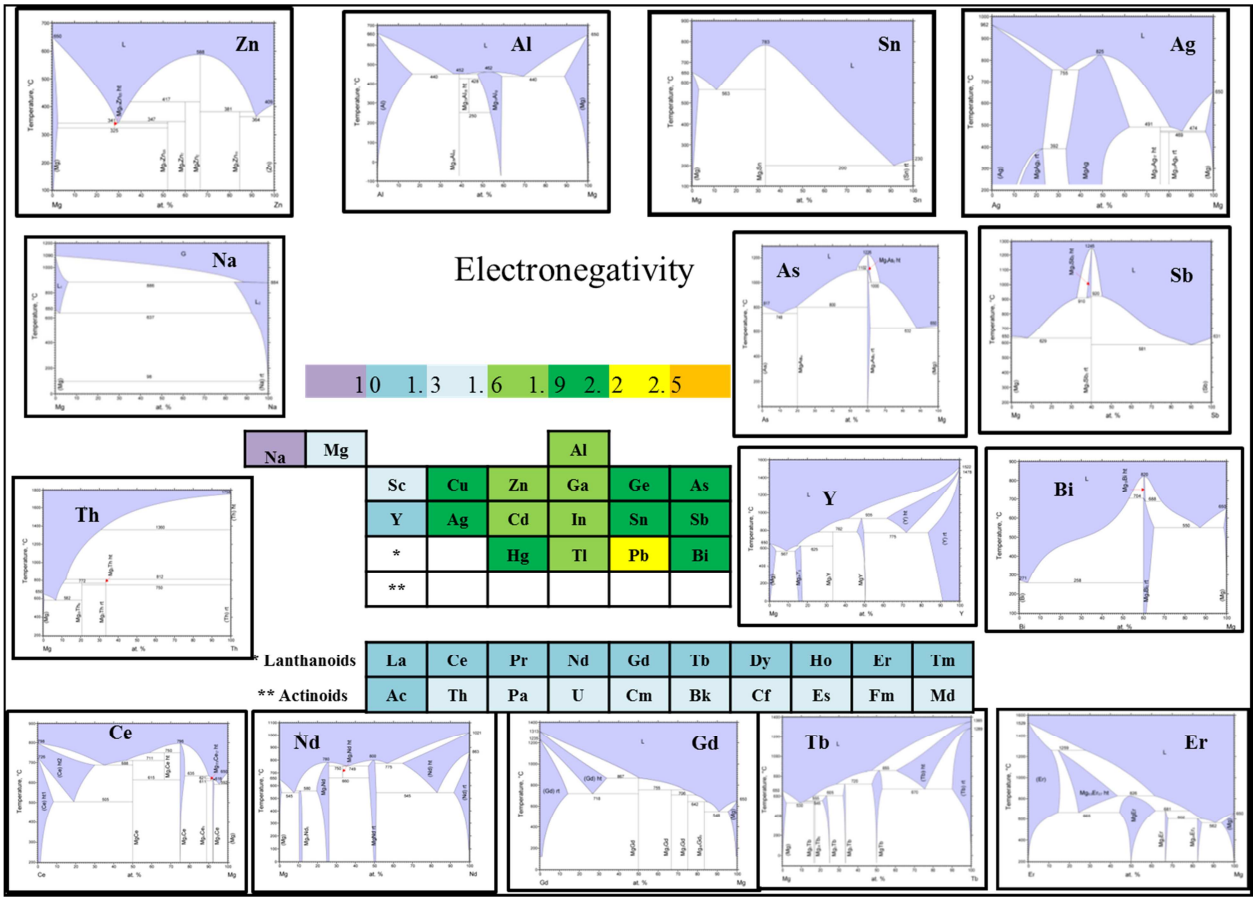

Figure 6-9. Selected solutes' electronegativity and their phase diagrams (the later from the ASM phase diagram centre[142], diagrams # 979988, 103456, 979989, 980984, 101029, 101007, 900643, 102127, 104161, 907783, 900170, 101162, 901583, 2002147, 102125).

Elements more electropositive than Mg's (e.g., the RE), are likely to sit on the South sector of Fig. 6-8, whereas the more electronegative ones (e.g., Al and Zn) are likely to sit on the North. Figure 6-9 shows that the RE elements generally exhibit a sequence of electronic compounds [130] with an increasing tendency to develop a single maximum at intermediate (equiatomic) composition, in order Er, Tb, Y, Gd, Nd, Ce.

In the North sector the phase diagrams mostly conform to Fig. 6-6c, e.g., those of Ag, Zn, Pb, Sn or Al, with a single or dominant compound forming congruently at near equiatomic concentration. Since the terminal solubility is also limited by the difference in electronegativity, consistently with Hume-Rothery's rules, the most electronegative elements such as As, Sb and Bi (group VA of the periodic table, all in the North sector), exhibit negligible solid solubility, in comparison with, e.g. Al, which exhibits extensive solubility (cf. footnote # 2 concerning Fig. 6-3).

For many of the alloy systems in the North/South sectors the tendency to develop SRO has been recognised in early studies and was ascribed to the large difference in electronegativity between solvent and solute [130]. Alloy systems where SRO was confirmed by x-ray diffraction were already mentioned in section II. Consistently with these assertions, Nie [13] pointed out that there is no evidence of solute clustering in binary solid solutions of Gd or Nd, nor in the ternary solutions Mg-Y-Nd, Mg-Gd-Y or Mg-Gd-Nd. Maruyama *et al.* [1] made a similar assertion concerning Mg-Y.

The magnitude of the (negative) enthalpy of formation measures both the thermal stability of the intermetallics in the concentrated alloys[135] and the tendency to develop SRO in the dilute compositions [127, 130]. Figure 10 shows that the melting temperature of the intermetallics of approximate equiatomic composition for Ag, Gd, Nd and Y and of the Laves phase for Sn and Zn generally scales with the enthalpy of formation (see also Table 1). [15]

The tendency to developing SRO naturally explains the weak ageing response of binary alloys containing Zn, Al, Sn, and R in general as already discussed, and accounts at the same time for the solid solution hardening results of Fig. 6-3. The already mentioned success, or otherwise, of solutes and trace elements aimed at increasing the age hardening response of Mg alloys [13] can now be understood through Fig. 6-8. Belonging to the East/West sectors, solutes such as Th, Mn, Na, and Co can be expected to exhibit homogenous clustering and fine coherent precipitation from the solid solution, along the line Al-Zn alloys follow. Most other trace elements mentioned in the literature, namely, Si, Sb, Ca, Ag, Ba, Cu etc., belong in the North/South sectors, hence should tend to form SRO and are not necessarily suitable for improving the ageing response through clustering. The fact that some of them do, e.g., Ca and Ag improve the age hardening of Mg-Zn alloys [143] whereas Pb and Sb do so in AZ91 [60, 144], suggests that further options are available. These possibilities are considered, together with the SRO effects on the creep strength, in the next two sections.

[15] *In a sense, the phase diagrams on the South sector are temperate forms of the more extreme ones on the North, e.g., Bi, As and Sb, and in which intermetallics form congruently at temperatures as high as 1518K (1245^{o}C, Sb).*

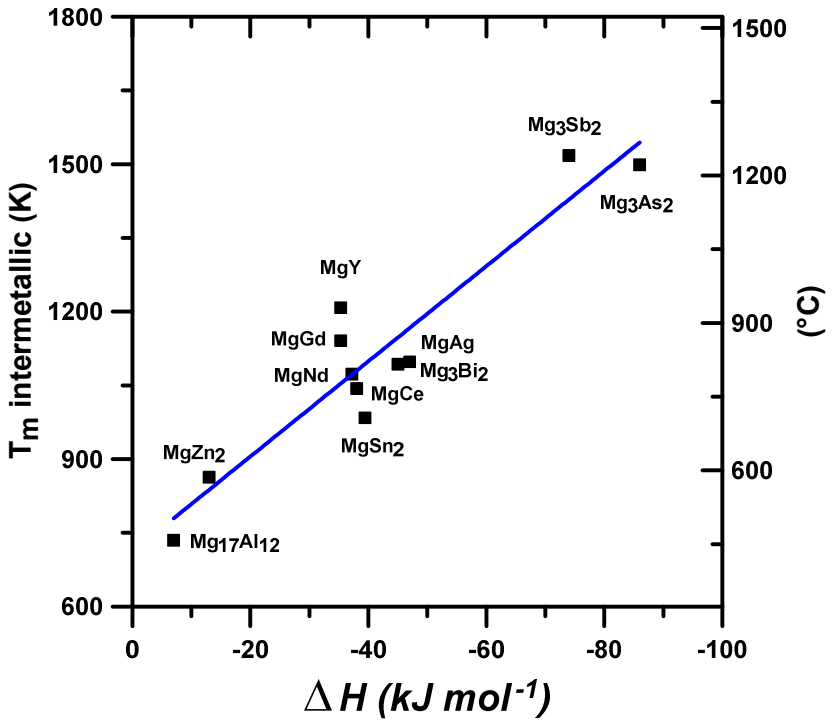

Figure 6-10. The melting point of intermetallics (at nearly equiatomic compositions for Ag, Gd, Nd and Y and Laves phases for Sn and Zn) as a function of the enthalpy of formation. Melting point data from the phase diagrams of Fig. 6-9 and enthalpies of formation from [134].

6.7 Ranking for Creep Strength

Being an athermal strengthening mechanism [118], SRO is expected to increase the alloy's creep strength by both lifting and widening the alloy's athermal regime as schematised in Fig. 6-4. Following the analysis of Refs. [30, 145] the enthalpy of formation, scaled by the concentration effects on SRO can be used to rank the alloys strength as [146]:

$$\tau_{SRO} \sim [\Delta H * c(1-c)]^2 \qquad (3)$$

where τ_{SRO} is the expected contribution to the shear strength stemming from the SRO and c is the atomic concentration. Numerical values for the parameters of Eq. 3 are given in Table 6-1 for a number of solutes. The c values, read from Fig. 6-11, represent the respective solubilities at 473-573K (200-300°C) unless stated otherwise.

Table 6-1. Approximate solute solubilities (at. %) at 473K (200°C) for the alloys studied (read from Fig. 6-11) and the respective Miedema's coordinates values[26] used to create Figs. 6-8 and 6-12. (Solutes in bold were used in the experiments described in the companion paper[29].

Solute	**Solutes used in dilute concentration experiments** [29]								Low solubility solutes				
Solute	**Mg**	**Al**	**Zn**	**Sn**	**Gd**	**Nd**	**Y**	Ca	Si	Sr	Ce	Ag	Sb
c @ 473K (200°C) [a]	-	2.5	1.5	0.5	1.0	0.8	1.5	0.05	0.05	0.05	0.05	0.5	0.05
ϕ^*	3.45	4.20	4.10	4.15	3.20	3.19	3.20	2.55	4.70	2.40	3.18	4.35	4.40
$n_{WS}^{1/3}$	1.17	1.39	1.32	1.24	1.21	1.20	1.21	0.91	1.50	0.84	1.19	1.36	1.26
ΔH [b] *(kJ/mol)*	-	-7	-13	-38	-35.3	-37.2	-35.3	-26	-34	-19	-39.4	-38.6	-74
IM forming upon ageing [c]	-	$Mg_{17}Al_{12}$	$MgZn_2$	Mg_2Sn	Mg_3Gd	Mg_3Nd	$Mg_{24}Y_5$	-	-	-	-		-

[a] *the c-values were bound by the solid solubilities at either ~ 473K (200°C) as per Fig. 11 (solutes in bold in this table), the solid solution heat treatment temperature (Nd), a maximum of 2.5 at.% (Al), or a nominal value of 0.05at.% for Ca, Si, Sr, Sb and Ce. For Ag a solubility of 0.5% was assumed following [13, 147]. See also footnote 16.*

[b] ΔH *values for non-transition elements, Al ,Zn, Sn, Ca, Si, Sr and Sb from [25] and for transition solutes, Y, Gd, Nd and Ce from[134].*

[c] *References: [11, 35, 74, 81, 83, 84, 148, 149].*

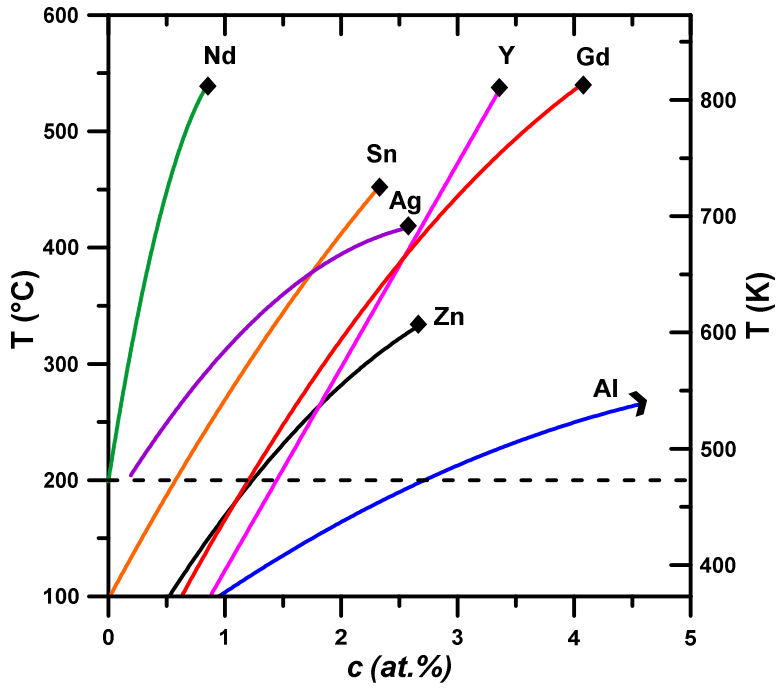

Figure 6-11. Temperature vs Solid solubility for selected solutes (data replotted from ASM phase diagrams # 979988, 103456, 979989, 980984, 100220 and 101029) except for Ag [147]. The diamonds at the top end of each line indicate the solution heat treatment temperature used in the experiments of the companion paper [29] except for Zn, from which it indicates the terminal solubility (see also footnote 16).

Considering that the two terms of Eq. 3 vary in opposing directions (i.e., for large ΔH the maximum solubility c becomes negligible, and vice-versa), the Pareto plot [150] of Fig. 12 enables ranking the solutes based on the combined tendency of both parameters.

Being closest to the origin Y and Gd appear as the most effective solutes, followed by Sn, Zn, Ag and Nd, in that order. Al represents a solute with very high solubility but very small ΔH^2 hence its low strengthening effect. Towards the high ΔH^2 end the low terminal solubilities of Sr, Ca, Si, Ce, and particularly Sb determine an equally low strengthening potential. Any other solute sitting in the North-South sectors of Fig. 6-8 thus can be expected to fit in between the Mg-Al or the Mg-Sb bounds, with its overall contribution modulated by its solubility at the operating temperature (~473K (200°C)). The combination of high ΔH^2 and relatively high solubility of Y thus accounts for

its high ranking, followed by Gd. Nd and Ag appear[16] better than they would, should the actual solubility at 473K (200°C) be considered. The higher solubility for Nd (0.8*at*.%) assumed in Table 2 and Figs. 12-13 approximates the supersaturated solid solution of the α-Mg grains in a HPDC alloy [88, 112].

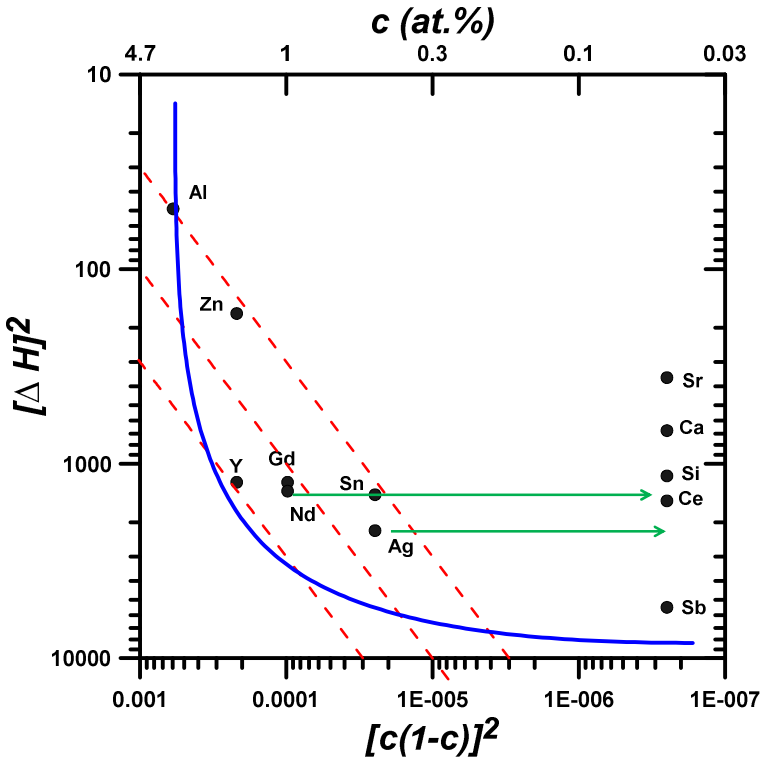

Figure 6-12. A Pareto plot created based on Eq. 3 (note the decreasing order of the scales). The dashed lines represent constant τ_{SRO}. The strength of the expected SRO, increases towards the origin of the plot. The solid line (or Pareto front) identifies the solutes (or non-dominated solutions [150]) that maximise SRO by either one of the two parameters of Eq. 3. The solutes closer to the origin, Y and Gd, appear as optimal solutions. The arrows point to the locii of Nd and Ag corresponding to their room temperature solid solubilities (cf. footnote 16).

In Fig. 6-13 the Pareto plot of Fig. 6-12 was overlapped to a graph of minimum creep rates of binary and multicomponent commercial alloys containing RE [12, 76] using a common

[16] *The lack of reliable solid solubility data at the temperatures of interest (~473K, (200°C)) is an important issue affecting this analysis, as exemplified by Ag: whereas the ASM phase diagram (#101007) indicates negligible solubility, Refs.[147] and [13] indicate 0.2 and 0.35at.% respectively.*

concentration scale. The close agreement between the Pareto plot's predictions and the experimental data concerning both the binary and multicomponent alloys strongly supports the assumptions behind the present analysis. Experiments in the companion paper involving binary alloys with the concentrations of Table 1 (**bold solutes**) further confirm the predictions.

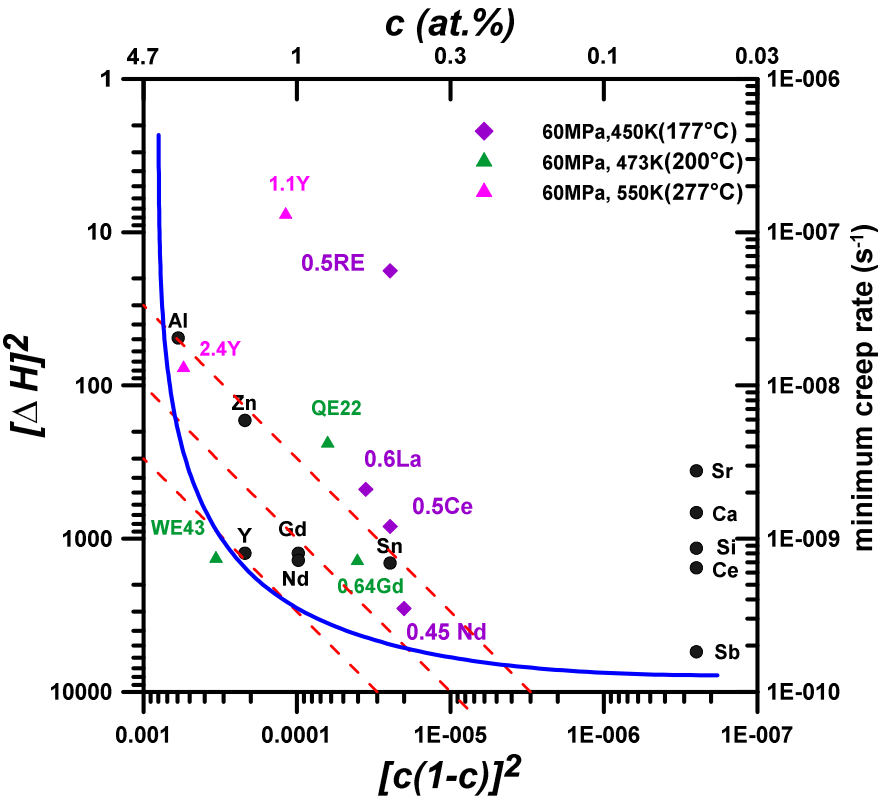

Figure 6-13. The Pareto plot of Fig. 6-12 superimposed to minimum creep rate data for a range of binary and commercial alloys from [1, 12, 76, 151]. The Y-axes scales are in arbitrary relationship with each other. The circles are measured on the left hand y-axis, the diamonds and triangles on the right hand y-axis). Compositions: QE22 (0.35Nd-0.46Ag); WE43 (assumed):1.16Y-0.57Nd-0.14Zr.

6.8 Alloy Selection and Design

The sorting of solutes as per the Miedema scheme suggest the following possible strategies, depending on whether the alloy is meant for HPDC applications or is amenable of solid solution/aging heat treatment.

6.8.1 High Pressure Die Castings

In HPDC Mg alloys, segregation during solidification leaves the core of the grains largely denuded of solute whereas it leads to the formation of a percolating eutectic network [76, 112, 152, 153]. As already mentioned, Zhang *et al*. [112, 152] proposed a microstructure combining a eutectic forming solute with one providing efficient solid solution hardening even at the low concentrations feasible for most HPDC alloys. A working example was shown through a ternary Mg-La-Nd alloy in which (supersaturated) solid solution strengthening by Nd through SRO and eutectic reinforcement through La added their strengthening contributions in a linear fashion [112, 113, 152]. Experiments by Gavras *et al*. and Nie *et al*. showed that replacing Gd and/or Y by Nd further improved the creep resistant of these alloys despite decreased precipitation [13, 154]. Thus, it seems safe to assert that solutes such as Y and Gd, which combine a measurable solid solubility at high temperature with a strong tendency to develop SRO in the terms of Fig. 6-12, are a straightforward way of strengthening the core of the α-Mg grains on top of any reinforcement by intergranular eutectics.

6.8.2 Heat treatable alloys

As for HPDC alloys, solid solution hardening through SRO via Y and Gd is an obvious choice. Working examples for binary and ternary combinations are those presented by [1, 12, 32].

Alternatively, solutes with positive enthalpy of mixing, i.e., sitting in the East/West sectors of Fig. 6-8 such as Th, Mn and Sc can be expected to mimic the behaviour of Al-Zn alloys upon ageing. Of these, Mg-Th is the best available example due its thermally stable, internally ordered precipitates. Manganese appears as the next suitable candidate, although classic experiments [14, 155] showed that precipitates in Mg-Mn alloys are only soft pure Mn. Turning the Mn precipitates into internally ordered, stronger and thermally stable precipitates, while preserving coherency at the interfaces is an attractive option. Mordike and Smola anticipated this approach with good success [12] in their experimental Mg-Sc-Mn alloys. Subsequent experiments led to Mg-Gd-Sc-Mn [12] and Mg-Y-Sc-Mn [156] alloys with creep strength superior to that of WE43, suggesting that the ordered Mn_2Sc precipitates added their strengthening effects to the SRO introduced by either Y or Gd in the α-Mg

matrix as for the HPDC case. The Mg-Sc system appears equally promising, but dedicated experiments [12, 156] showed that the binary alloys were very hard to cast and the results were inconclusive.

Wolverton *et al*. [54, 131, 157] showed that while the Al-Cu system is expected to develop SRO, hence, in principle it should not exhibit the strong age hardening it does, the formation of a coherent metastable Al_3Cu phase rather than the equilibrium Al_2Cu phase leads to its remarkable precipitation hardening. SRO parameters for fully ordered Al-2%Cu alloy calculated by Müller *et al.* [129] show negative values except for the first two real-space shells, consistent with those of the fully ordered Al_3Cu coherent ground state. That is, against expectations due to its negative energy of mixing, clustering occurs on a fine scale through an unexpected precursor phase which leads to coherent precipitation and efficient age hardening, on a comparable scale to Al-Zn. Along this line, and with the implicit or explicit intention of creating fine precursor phases, solutes from either the East/West or North/South sectors of Fig. 6-8 have been tried in the literature as trace elements. Mendis *et al*. and Gibson *et al.* [55, 76] showed that traces of Na improve the age hardening response Mg-Sn through to the formation of clusters of Na which act as precursors to finely distributed Mg_2Sn precipitates**.** The increased age hardening response of Mg-Zn through trace additions of Co has been ascribed to the higher solution treatment temperature used, hence to the higher concentration of quenched-in vacancies [158]. However, and similarly to Na, Co should be expected to introduce clustering, thus accounting for the enhanced precipitation behaviour without the need to appeal to an increased vacancy concentration mechanism likely to lead to coarser rather than finer precipitation [64].

The use of trace additions with negative energy of mixing, e,g., Ag, Cu, Si, Sb, Ca, have already been mentioned. Successful examples of this approach are Ag, Ca [143] and Cu [73] which have been shown to improve the age hardening response of Mg-Zn, or Ag added to Mg-Gd [159] and Mg-Y [160].

Recent work by Wolverton *et al.* [161] shows that first principles calculations can be used to advantage in order to understand the thermodynamic and elastic properties of metastable precipitation in Mg-RE alloys.

By and large, the present analysis shows that a rational approach to alloys selection and design is possible, stemming from the binary phase diagrams of Mg-solid solutions, and based on the sorting/ranking of solutes by their expected tendency to develop either clustering or order at the short range atomic scale. The thermodynamics-based approach naturally accounts for most of the

observed ageing or creep behaviors in current multicomponent Mg alloys, while dismissing many unsupported or contradictory micromechanisms often assumed active. The data from the literature strongly supports the main hypotheses of the present approach. Further supporting evidence involving dilute binary alloys for a range of representative solutes is presented in the companion paper [29].

6.9 Conclusions:

- The Miedema's phenomenological scheme was used to sort out and rank potential solutes based on their respective tendency to developing either clustering or SRO when present in dilute concentrations.

- The relative tendency to developing SRO or otherwise of the main solutes rationalises many of the observed behaviours of multicomponent alloys, including the wide difference in solid solution hardening, weak for Al-, and strong for Zn-, Y- and Gd-containing alloys while dismissing a number of micromechanisms which lack structural support, such as solute dragging, dynamic precipitation and atomic size controlled diffusivity.

- Two main strategies for the selection and design of high strength, creep resistant Mg alloys are suggested, exemplified by experiments from the literature.

- For HPDC alloys, the use of solutes with significant solubility yet strong tendency to develop SRO, such as Y or Gd, should be used to reinforce the core of the solute depleted α-Mg grains. On top, the strengthening resulting from a high volume fraction of percolating, high melting point eutectic microstructure formed by low-solubility, eutectic forming solutes, such as Ce or La should be added.

- For heat treatable cast alloys, aside from strengthening trough SRO on its own, e.g, as in Mg-Y or Mg-Gd binary alloys, one option is through a parallel with the Al-Zn alloy

system in order to reproduce the Mg-Th alloys. One example is the Mg-Mn-Sc system, in which traces of Sc introduce order and harden the fine pure Mn precipitates. The combined (efficient ageing + SRO) approach is exemplified by Mg-RE-Sc-Mn experimental alloys. Traces of Na and Co also serve to induce homogeneously nucleated clusters that refine subsequent precipitation in other alloys systems. Alternatively, and inspired in the Al-Cu alloys system, ternary trace additions which in principle should not do so might also introduce a precursor phase to refine the subsequent precipitation in existing alloy systems. Trace additions of Ag, Ca, Cu, etc. already proved their worth along this line.

6.10 References

[1] K. Maruyama, M. Suzuki, S. HIROYUKI, Metallurgical and Materials Transactions A, 33 (2002) 875-882.

[2] L. Sturkey, J.B. Clark, Journal of the Institute of Metals, 88 (1959) 177-181.

[3] J.B. Clark, Acta Metallurgica, 13 (1965) 1281-1289.

[4] J.B. Clark, Transactions of Japan Institute of Metals, 9 Supplement (1968) 354-355.

[5] J. van der Planken, A. Deruyttere, Acta Metallurgica, 17 (1969) 451-454. 10.1016/0001-6160(69)90026-1

[6] G. Mima, Y. Tanaka, Transactions of Japan Institute of Metals, 12 (1971) 323-328.

[7] C. Bettles, M. Gibson, ADVANCED ENGINEERING MATERIALS, 5 (2003) 859-865.

[8] Z. Yang, J.P. Li, J.X. Zhang, G.W. Lorimer, J. Robson, Acta Metallurgica Sinica (English Letters), 21 (2008) 313-328. 10.1016/s1006-7191(08)60054-x

[9] L.Y. Wei, G.L. Dunlop, H. Westengen, Metallurgical and Materials Transactions A, 26 (1995) 1705-1716. 10.1007/bf02670757

[10] R. Wilson, C. Bettles, B.C. Muddle, J.F. Nie, in: T. Aizawa Y. Kojima, K. Higashi, S. Kamado (Ed.) Materials Science Forum, Trans Tech Publ, 2003, pp. 267-272.

[11] B. Smola, I. Stulıková, F. Von Buch, B. Mordike, Materials Science and Engineering: A, 324 (2002) 113-117.

[12] B.L. Mordike, Materials Science and Engineering: A, 324 (2002) 103-112. http://dx.doi.org/10.1016/S0921-5093(01)01290-4

[13] J.-F. Nie, Metallurgical and Materials Transactions A, 43 (2012) 3891-3939. 10.1007/s11661-012-1217-2

[14] R. DeLuca, J.G. Byrne, Transactions of Japan Institute of Metals, 9 (supplement) (1968) 514-520.

[15] C.R. Hutchinson, S.P. Ringer, Metallurgical and Materials Transactions A, 31 (2000) 2721-2733. 10.1007/bf02830331

[16] I. Polmear, in: A.J. Morton and B.C. Muddle J.F. Nie (Ed.) Materials Forum, 2004, pp. 1-14.

[17] C.R. Hutchinson, J.F. Nie, S. Gorsse, Metallurgical and Materials Transactions A, 36 (2005) 2093-2105. 10.1007/s11661-005-0330-x

[18] M. Pekguleryuz, M. Celikin, International Materials Reviews, 55 (2010) 197-217. doi:10.1179/095066010X12646898728327

[19] L.B. Duffy, Foundry Trade Journal, (1991) 319-321.

[20] C.H. Cáceres, D.M. Rovera, Journal of Light Metals, 1/3 (2001) 151-156.

[21] R. Khosrhoshahi, in: (Ed.) Proceedings of the Third International Magnesium Conference, 1996, pp. 241-256.

[22] I.J. Polmear, 3rd ed., Edward Arnold, London, 1995.

[23] K.E. Nelson, Transactions of the American Foundrymen's Society, 67 (1959) 610-613.

[24] Q. Han, B.K. Kad¶, S. Viswanathan, Philosophical Magazine, 84 (2004) 3843-3860.

[25] A.R. Miedema, F.R. de Boer, R. Boom, Calphad, 1 (1977) 341-359. 10.1016/0364-5916(77)90011-6

[26] F.R. de Boer, R. Boom, W.C.M. Mattens, A.R. Miedema, A.K. Niessen, North-Holland, Amsterdam, 1989.

[27] A.R. Miedema, Journal of the Less Common Metals, 32 (1973) 117-136. 10.1016/0022-5088(73)90078-7

[28] A.R. Miedema, R. Boom, F.R. De Boer, Journal of the Less Common Metals, 41 (1975) 283-298. 10.1016/0022-5088(75)90034-x

[29] S. Abaspour, C. Cáceres, submitted (2014)

[30] C.H. Cáceres, A. Blake, physica status solidi, 194 (a) (2002) 147-158.

[31] L. Gao, R.S. Chen, E.H. Han, Journal of Alloys and Compounds, 481 (2009) 379-384. 10.1016/j.jallcom.2009.02.131

[32] L. Gao, R.S. Chen, E.H. Han, Journal of Alloys and Compounds, 472 (2009) 234-240.

[33] S. Miura, S. Imagawa, T. Toyoda, K. Ohkubo, T. Mohri, Materials Transactions, 49 (2008) 952-956.

[34] I. Toda-Caraballo, E.I. Galindo-Nava, P.E.J. Rivera-Díaz-del-Castillo, Acta Materialia, 75 (2014) 287-296. http://dx.doi.org/10.1016/j.actamat.2014.04.064

[35] L. Gao, J. Zhou, Z. Sun, R. Chen, E. Han, Chinese Science Bulletin, 56 (2011) 1038-1042. 10.1007/s11434-010-4052-0

[36] J. Nie, K. Oh-Ishi, X. Gao, K. Hono, Acta Materialia, 56 (2008) 6061-6076.

[37] P. Haasen, in: R. W. Cahn, P. Haasen (Eds.) Physical Metallurgy, Elsevier Science, Amsterdam, 1996, pp. 2009-2073.

[38] D.S. Gencheva, A.A. Katsnel'son, L.L. Rokhlin, V.M. Silonov, F.A. Khavadzha, Fiz. metal. metalloved., 51 (1981) 788-793.

[39] S. Henes, V. Gerold, Zeitschrift fur Metallkunde, 53 (1962) 703-708.

[40] V.M. Silonov, E.V. Evlyukhina, L.L. Rokhlin, Russian Physics Journal, 39 (1996) 622-625.

[41] L.A. Safronova, A.A. Katsnel'son, S.V. Sveshnikov, Y.M. L'Vov, Fiz. metal. metalloved., 43 (1977) 76-80.

[42] N. Jha, A.K. Mishra, Journal of Alloys and Compounds, 329 (2001) 224-229.

[43] M. Nishijima, K. Hiraga, Materials Transactions, 48 (2007) 10-15.

[44] C.H. Caceres, G.E. Mann, J.R. Griffiths, Metallurgical and Materials Transactions A, 42 (2011) 1950-1959. 10.1007/s11661-010-0599-2

[45] S. Sandlöbes, Z. Pei, M. Friák, L.F. Zhu, F. Wang, S. Zaefferer, D. Raabe, J. Neugebauer, Acta Materialia, 70 (2014) 92-104. http://dx.doi.org/10.1016/j.actamat.2014.02.011

[46] A. Akhtar, E. Teghtsoonian, Materials Transactions (JIM), 9, supplement (1968) 692-697.

[47] A. Akhtar, E. Teghtsoonian, Acta Metallurgica, 17 (1969) 1339-1349. 10.1016/0001-6160(69)90151-5

[48] A. Akhtar, E. Teghtsoonian, Acta Metallurgica, 17 (1969) 1351-1356.

[49] A. Akhtar, E. Teghtsoonian, Philosophical Magazine, 25 (1972) 897-916.

[50] B.Q. Shi, R.S. Chen, W. Ke, Journal of Alloys and Compounds, 509 (2011) 3357-3362. 10.1016/j.jallcom.2010.12.065

[51] J.B. Clark, Acta Metallurgica, 16 (1968) 141-152.

[52] J.F. Nie, B.C. Muddle, in: M. Ferry (Ed.) Materials 98, Institute of Materials Engineering Australasia, Melbourne, 1998, pp. 567-571.

[53] J.W. Martin, Cambridge University Press, Cambridge, 1980.

[54] C. Wolverton, Philosophical Magazine Letters, 79 (1999) 683-690. 10.1080/095008399176724

[55] C. Mendis, C. Bettles, M. Gibson, S. Gorsse, C. Hutchinson, Philosophical Magazine Letters, 86 (2006) 443-456.

[56] C.L. Mendis, C.J. Bettles, M.A. Gibson, C.R. Hutchinson, Materials Science & Engineering A, 435 (2006) 163-171. 10.1016/j.msea.2006.07.090

[57] H. Liu, Y. Chen, Y. Tang, S. Wei, G. Niu, Journal of Alloys and Compounds, 440 (2007) 122-126. 10.1016/j.jallcom.2006.09.024

[58] F.R. Elsayed, T.T. Sasaki, C.L. Mendis, T. Ohkubo, K. Hono, Materials Science and Engineering: A, 566 (2013) 22-29. http://dx.doi.org/10.1016/j.msea.2012.12.041

[59] M.X. Zhang, P.M. Kelly, Acta Materialia, 53 (2005) 1085-1096. http://dx.doi.org/10.1016/j.actamat.2004.11.005

[60] N. Balasubramani, A. Srinivasan, U.T.S. Pillai, B.C. Pai, Materials Science and Engineering: A, 457 (2007) 275-281. http://dx.doi.org/10.1016/j.msea.2006.12.132

[61] A. Srinivasan, U.T.S. Pillai, B.C. Pai, Materials Science & Engineering A, 527 (2010) 6543-6550. 10.1016/j.msea.2010.07.020

[62] A. Srinivasan, J. Swaminathan, M.K. Gunjan, U.T.S. Pillai, B.C. Pai, Materials Science & Engineering A, 527 (2010) 1395-1403. 10.1016/j.msea.2009.10.008

[63] G. Feng, H. Yu, in: (Ed.) Electronic and Mechanical Engineering and Information Technology (EMEIT), 2011 International Conference on, IEEE, 2011, pp. 4763-4765.

[64] T.J. Pike, B. Noble, Journal of the Less Common Metals, 30 (1973) 63-74. 10.1016/0022-5088(73)90007-6

[65] K. Máthis, J. Gubicza, N.H. Nam, Journal of Alloys and Compounds, 394 (2005) 194-199. http://dx.doi.org/10.1016/j.jallcom.2004.10.050

[66] A.A. Luo, in: JOM Journal of the Minerals, Metals and Materials Society, TMS (The Minerals, Metals and Materials Society), Nashville, 2002, pp. 42-48 DOI: 10.1007/BF02701073.

[67] M.S. Dargusch, G.L. Dunlop, A.L. Bowles, K. Pettersen, P. Bakke, Metallurgical and Materials Transactions A, 35 (2004) 1905-1909. 10.1007/s11661-004-0099-3

[68] Y. Guangyin, S. Yangshan, Z. Weiming, Journal of Materials Science Letters, 18 (1999) 2055-2057.

[69] S.L. Couling, Metals Engineering Quarterly, May (1972) 7-13.

[70] G.S. Foerster, Metals Engineering Quarterly, February (1973) 19-22.

[71] I.A. Anyanwu, S. Kamado, Y. Kojima, Materials Transactions, 42 (2001) 1212-1218.

[72] A. Luo, Materials Science Forum, 419-422 (2003) 57-66.

[73] M.O. Pekguleryuz, A.A. Kaya, ADVANCED ENGINEERING MATERIALS, 5 (2003) 866-878. 10.1002/adem.200300403

[74] B. Mordike, I. Stulikova, B. Smola, Metallurgical and Materials Transactions A, 36 (2005) 1729-1736.

[75] B. Smola, I. Stulíková, J. Pelcová, B.L. Mordike, in: (Ed.) Magnesium: Proceedings of the 6th International Conference-Magnesium Alloys and Their Applications, John Wiley & Sons, 2006, pp. 43.

[76] M.A. Gibson, X. Fang, C.J. Bettles, C.R. Hutchinson, Scripta Materialia, 63 (2010) 899-902. http://dx.doi.org/10.1016/j.scriptamat.2010.07.002

[77] J.R. Terbush, N.D. Saddock, J.W. Jones, T.M. Pollock, Metallurgical and Materials Transactions A, 41 (2010) 2435-2442.

[78] S.W. Chung, H. Watanabe, W.-J. Kim, K. Higashi, Materials Transactions, 45 (2004) 1266-1271.

[79] L. Moreno, T. Nandy, J. Jones, J. Allison, T. Pollock, in: (Ed.) Magnesium Technology 2002 TMS Annual Meeting, 2002, pp. 111-116.

[80] Y. Zhang, L. Yang, J. Dai, J. Ge, G. Guo, Z. Liu, Materials & Design, 63 (2014) 439-445.

[81] F. Czerwinski, Springer, 2008.

[82] J. Bai, Y. Sun, F. Xue, S. Xue, J. Qiang, T. Zhu, Journal of Alloys and Compounds, 437 (2007) 247-253.

[83] G.V. Raynor, Pergamon, 1959.

[84] G. Nayyeri, R. Mahmudi, F. Salehi, Materials Science and Engineering: A, 527 (2010) 5353-5359.

[85] R. Alizadeh, R. Mahmudi, Journal of Alloys and Compounds, 509 (2011) 9195-9199.

[86] B.-G. Moon, B.-S. You, Y.-D. Hahn, Current Nanoscience, 10 (2014) 108-113.

[87] K. Yang, C. Cáceres, M. Easton, Metallurgical and Materials Transactions A, 45 (2014) 4117-4128. 10.1007/s11661-014-2326-x

[88] S.M. Zhu, M.A. Gibson, M.A. Easton, J.F. Nie, Scripta Materialia, 63 (2010) 698-703.

[89] W.-F. Xu, Y. Zhang, J. TerBush, L.-M. Peng, W.-J. Ding, J.-F. Nie, Metallurgical and Materials Transactions A, 45 (2014) 4103-4116. 10.1007/s11661-014-2335-9

[90] M. Suzuki, H. Sato, K. Maruyama, H. Oikawa, MATERIALS SCIENCE AND ENGINEERING A-STRUCTURAL MATERIALS PROPERTIES MICROSTRUCTURE AND PROCESSING, 252 (1998) 248-255.

[91] W.P. Sun, J.J. Jonas, Acta Metallurgica et Materialia, 42 (1994) 283-292.

[92] S.M. Zhu, M.A. Gibson, J.F. Nie, M.A. Easton, T.B. Abbott, Scripta Materialia, 58 (2008) 477-480.

[93] L. Gao, R. Chen, E. Han, Stress, 250 (2009) 300oC.

[94] C. Wang, Y. Xu, E. Han, Journal of Metallurgy, 2012 (2012)

[95] X.Y. Fang, D.Q. Yi, J.F. Nie, Metallurgical and Materials Transactions A, 40 (2009) 2761-2771. 10.1007/s11661-009-9967-1

[96] N. Stanford, D. Atwell, M.R. Barnett, Acta Materialia, 58 (2010) 6773-6783. http://dx.doi.org/10.1016/j.actamat.2010.09.003

[97] C. Corby, C.H. Cáceres, P. Lukác, Mater. Sci. Eng. A, 387-389 (2004) 22-24.

[98] Z. Trojanova, C.H. Caceres, Scripta Materialia, 56 (2007) 793-796.

[99] D. Choudhuri, D. Jaeger, M.A. Gibson, R. Banerjee, Scripta Materialia, 86 (2014) 32-35. http://dx.doi.org/10.1016/j.scriptamat.2014.04.026

[100] T. Wang, L. Jiang, R. Mishra, J. Jonas, Metallurgical and Materials Transactions A, 45 (2014) 4698-4709. 10.1007/s11661-014-2371-5

[101] N. Stanford, Materials Science and Engineering: A, 528 (2010) 314-322.

[102] L.J. Cuddy, W.C. Leslie, Acta Metallurgica, 20 (1972) 1157-1167.

[103] A. Couret, D. Caillard, Acta Metallurgica, 33 (1985) 1447-1454.

[104] R. Tendler, J.P. Abriata, Journal of Nuclear Materials, 150 (1987) 251-258. http://dx.doi.org/10.1016/0022-3115(87)90001-8

[105] H. Bakker, Journal of the Less Common Metals, 105 (1985) 129-138.

[106] P.G. Partridge, Metallurgical Reviews, 12 (1967) 169-194.

[107] R. Brouwer, J. Rector, N. Koeman, R. Griessen, Physical Review B, 40 (1989) 3546.

[108] L. Sturkey, Trans. Met. Soc. AIME, 218 (1960)

[109] J. Mushovic, N. Stoloff, (1968)

[110] D. Amberger, P. Eisenlohr, M. Göken, Acta Materialia, 60 (2012) 2277-2289. 10.1016/j.actamat.2012.01.017

[111] K.V. Yang, C.H. Caceres, A.V. Nagasekhar, M.A. Easton, Materials Science and Engineering A, (2012)

[112] B. Zhang, S. Gavras, A.V. Nagasekhar, C.H. Cáceres, M.A. Easton, Metallurgical and Materials Transactions A, (2014) 1-12.

[113] B. Zhang, A.V. Nagasekhar, T. Sivarupan, C.H. Caceres, ADVANCED ENGINEERING MATERIALS, 15 (2013) 1059-1067.

[114] D. Kuhlmann-Wilsdorf, H.G.F. Wilsdorf, J.A. Wert, Scripta Metallurgica et Materialia, 31 (1994) 729-734.

[115] D. Hull, D.J. Bacon, 3rd ed., Pergamon Press, Oxford, 1984.

[116] A. Seeger, in: J. C. Fisher, W. G. Johnston, R. Thomson, T. Vreeland (Eds.) Dislocations and mechanical properties of crystals, Chapman and Hall, London, 1957, pp. 243-329.

[117] C.G. Schmidt, A.K. Miller, Acta Metallurgica, 30 (1982) 615-625.

[118] H. Suzuki, in: J C Fisher, W G Johnston, R Thomson, T Vreeland (Eds.) Dislocations and mechanical properties of crystals, John Wiley, New York, 1957, pp. 361-390.
[119] C.H. Cáceres, P. Lukác, Philosophical Magazine A, 88 (2008) 977-989. http://dx.doi.org/10.1080/14786430801968611
[120] H. Mecking, U.F. Kocks, Acta Metallurgica, 29 (1981) 1865-1875.
[121] F.R.N. Nabarro, H.L. de Villiers, Taylor and Francis London, 1995.
[122] Y. Chino, M. Kado, T. Ueda, M. Mabuchi, Metallurgical and Materials Transactions A, 42 (2011) 1965-1973. 10.1007/s11661-010-0563-1
[123] U.F. Kocks, H. Mecking, Progress in Materials Science, 48 (2003) 171-273.
[124] W.W. Jian, G.M. Cheng, W.Z. Xu, H. Yuan, M.H. Tsai, Q.D. Wang, C.C. Koch, Y.T. Zhu, S.N. Mathaudhu, Materials Research Letters, 1 (2013) 61-66. 10.1080/21663831.2013.765927
[125] Z. Trojanová, P. Lukác, Journal of Materials Processing Technology, 162-163 (2005) 416-421.
[126] J.C. Fisher, Acta Metallurgica, 2 (1954) 9-10.
[127] P. Haasen, Cambridge University Press, Cambridge, 1996.
[128] T.C. Tiearney, N.J. Grant, Metallurgical Transactions A, 13 (1982) 1827-1836. 10.1007/bf02647839
[129] S. Müller, L.W. Wang, A. Zunger, C. Wolverton, Physical Review B, 60 (1999) 16448-16462.
[130] W. Hume-Rothery, Institute of Metals, London, 1946.
[131] C. Wolverton, V. Ozolin, A. Zunger, Journal of Physics: Condensed Matter, 12 (2000) 2749-2768.
[132] J.S. Chun, J.G. Byrne, Journal of Materials Science, 4 (1969) 861-872.
[133] K.C. Russell, in, DTIC Document, 1989.
[134] R.F. Zhang, S.H. Sheng, B.X. Liu, Chemical Physics Letters 442 (2007) 511.
[135] J.H. Zhu, C.T. Liu, L.M. Pike, P.K. Liaw, Intermetallics, 10 (2002) 579-595. http://dx.doi.org/10.1016/S0966-9795(02)00030-4
[136] X.-Q. Chen, W. Wolf, R. Podloucky, P. Rogl, Intermetallics, 12 (2004) 59-62. http://dx.doi.org/10.1016/j.intermet.2003.07.003
[137] D.G. Pettifor, in: Ehrenreich Henry, Turnbull David (Eds.) Solid State Physics, Academic Press, 1987, pp. 43-92.
[138] Y.M. Zhang, J.R.G. Evans, Y. Shoufeng, The Journal of Crystallization Physics and Chemistry, 1 (2010) 103-119.

[139] A.R. Miedema, P.F. de Châtel, F.R. de Boer, Physica B+C, 100 (1980) 1-28. http://dx.doi.org/10.1016/0378-4363(80)90054-6

[140] A.R. Miedema, F.R. De Boer, R. Boom, Physica B+C, 103 (1981) 67-81. 10.1016/0378-4363(81)91003-2

[141] A.R. Miedema, Physica B: Condensed Matter, 182 (1992) 1-17. http://dx.doi.org/10.1016/0921-4526(92)90565-A

[142] P. Villars, H. Okamoto, K. Cenzual, ASM International, Materials Park, (2006)

[143] C. Bettles, M. Gibson, K. Venkatesan, Scripta Materialia, 51 (2004) 193-197.

[144] Q. Wang, W. Chen, W. Ding, Y. Zhu, M. Mabuchi, Metallurgical and Materials Transactions A, 32 (2001) 787-794. 10.1007/s11661-001-1013-x

[145] C.H. Caceres, S. Abaspour, in: (Ed.) TMS 2013, 2013, pp.

[146] P.A. Flinn, Acta Metallurgica, 6 (1958) 631-635.

[147] A.A. Nayeb-Hashemi, J.B. Clark, Bulletin of Alloy Phase Diagrams, 5 (1984) 348-358. 10.1007/bf02872949

[148] P. Chen, D.-L. Li, J.-X. Yi, L. Wen, B.-Y. Tang, L.-M. Peng, W.-J. Ding, Solid State Sciences, 11 (2009) 2156-2161.

[149] H. Zhou, W. Xu, W. Jian, G. Cheng, X. Ma, W. Guo, S. Mathaudhu, Q. Wang, Y. Zhu, Philosophical Magazine, (2014) 1-7.

[150] M.F. Ashby, 3 ed., Butterworth-Heinemann, Oxford, 2005.

[151] A.A. Luo, B.R. Powell, M.P. Balogh, Metallurgical and Materials Transactions A, 33 (2002) 567-574. 10.1007/s11661-002-0118-1

[152] B. Zhang, A.V. Nagasekhar, X. Tao, Y. Ouyang, C.H. Cáceres, M. Easton, Materials Science and Engineering: A, 599 (2014) 204-211. http://dx.doi.org/10.1016/j.msea.2014.01.074

[153] T.L. Chia, M.A. Easton, S.M. Zhu, M.A. Gibson, N. Birbilis, J.F. Nie, Intermetallics, 17 (2009) 481-490. 10.1016/j.intermet.2008.12.009

[154] S. Gavras, S. Zhu, M.A. Gibson, M.A. Easton, J.-F. Nie, in: (Ed.) 9th International Conference on Magnesium alloys and their Applications, 2012, pp.

[155] R. De Luca, J.G. Byrne, Acta Metallurgica, 13 (1965) 1187-1195.

[156] B. Smola, I. Stulíková, J. Pelcová, B.L. Mordike, Journal of Alloys and Compounds, 378 (2004) 196-201. http://dx.doi.org/10.1016/j.jallcom.2003.10.099

[157] C. Wolverton, Acta Materialia, 49 (2001) 3129-3142. http://dx.doi.org/10.1016/S1359-6454(01)00229-4

[158] J. Geng, X. Gao, X.Y. Fang, J.F. Nie, Scripta Materialia, 64 (2011) 506-509. http://dx.doi.org/10.1016/j.scriptamat.2010.11.027

[159] X. Gao, J. Nie, Scripta Materialia, 58 (2008) 619-622.

[160] Y. Zhu, A. Morton, J. Nie, Scripta Materialia, 58 (2008) 525-528.

[161] A. Issa, J.E. Saal, C. Wolverton, Acta Materialia, 65 (2014) 240-250. http://dx.doi.org/10.1016/j.actamat.2013.10.066

Appendix

The Miedema scheme for R ≠ 0

In alloys of a transition metal (d-electron-type) and one of the polyvalent non-transition (p-electron-type) metals, the solutes can be sorted out in the same way as non-transition elements. However, in this case the lines which separate the positive enthalpy of mixing regions from negative ones are not straight through the origin, but take a hyperbolic shape because of an additional, negative term, R. This term indicates that a large negative energy stemming from hybridisation between the valence d and p electrons contributes to the heat of formation. Using equation 2, Fig. A-1 was created for different R values according to the solutes, listed in Table A-1.

Table A-1: R-values for different elements [26]. In alloys of a transition metal and non-transition metal R (or indeed R/P in units of eV2) is obtained by multiplying the values of R corresponding to each elements and to the solid or liquid state.

Mg	Solid	Liquid
0.4	1.0	0.73

Ca	Sc	Ti	V	Cr	Mn	Fe	Co	Ni	Cu
0.4	0.7	1.0	1.0	1.0	1.0	1.0	1.0	1.0	0.3
Sr	Y	Zr	Nb	Mo	Tc	Ru	Rh	Pd	Ag
0.4	0.7	1.0	1.0	1.0	1.0	1.0	1.0	1.0	0.15
Ba	La	Hf	Ta	W	Re	Os	Ir	Pt	Au
0.4	0.7	1.0	1.0	1.0	1.0	1.0	1.0	1.0	0.3

Th	U	Pu
0.7	1.0	1.0

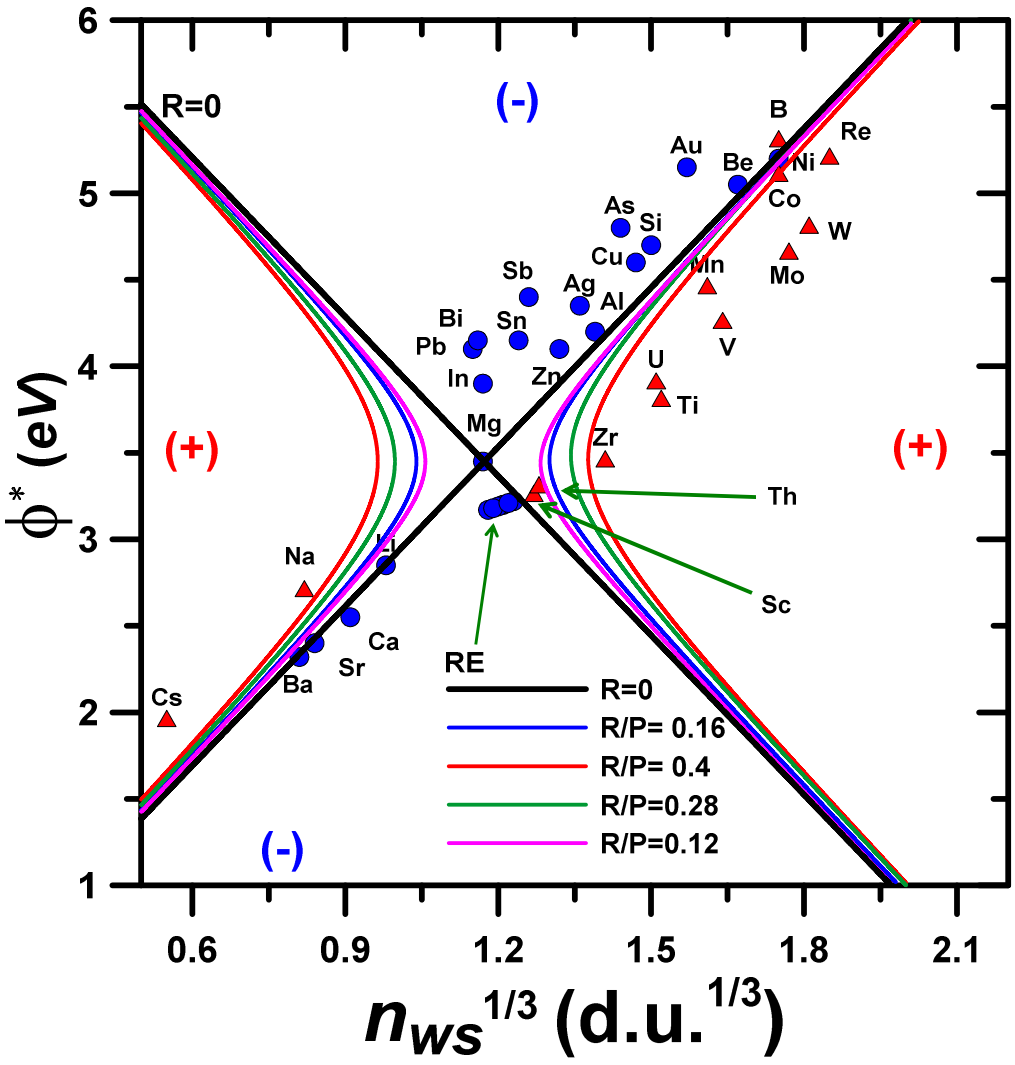

Fig. A-1. The Miedema Scheme for Mg alloys, for different R values (given as R/P ratios) in Eq. 2. Coordinates data from [26]. R=0 corresponds to Fig. 8.

Replacing the diagonal lines of Fig. 8 by the lines for different R/P values shits a few elements borderline elements, e.g. Th and Sc, from the East sector to the North-South. In those cases examination of the phase diagrams determines to which sector the element actually belongs. Thus, Th and Sc, both with a single eutectic phase diagram, belong to the West-East sector, consistently with assuming R=0 for Fig. 6-8.

The Mg-Ni phase diagram, with two eutectics, belongs in the North sector, which is correct as per the R/P = 0.4 line. On the other hand, B, with a single-eutectic phase diagram is expected to sit on the West sector while it appears on the North sector.

Chapter 7 High Temperature Strength and Stress Relaxation Behaviour of Dilute Binary Mg Alloys

High Temperature Strength and Stress Relaxation Behaviour of Dilute Binary Mg Alloys

Saeideh Abaspour, Carlos H. Cáceres[*]

ARC Centre of Excellence Design in Light Metals

Materials Engineering, School of Engineering

The University of Queensland, QLD 4072, Australia

Abstract

Monotonic compression and stress relaxation tests were carried out on specimens of 6 cast binary alloys with (*at*.%) 2.5 Al, 0.6 Sn, 2.2 Zn, 0.9 Nd, 0.8 Gd and 1.3 Y, and of a similarly cast AZ91D alloy for reference. The solute concentration of the binary alloys was kept deliberately low to limit precipitation hardening effects during the testing, done in the solution heat-treated and quenched condition. Compression testing was carried out at 298K (25°C), 373K (100°C) and 453K (180°C) for all of the alloys and at 493K (220°C) and 523K (250°C) for the Nd-, Gd-, and Y- containing ones. Stress relaxation was done at 453K (180°C) at either a predetermined strain (0.05) or stress (150 MPa). The Mg-Al and the AZ91 alloys softened considerably above 373K (100°C). The rest of the alloys exhibited extended linear strain hardening in compression and reduced relaxation, in the order Sn, Zn, Nd, Gd and Y, an indication of a progressively stable dislocation substructure, hence of an increasingly extended athermal regime in the strength-temperature relationship. The overall behaviour, which matched those of commercial alloys involving the same solutes, can be accounted for through the respective solutes' tendency to develop short range order, lowest for the near-random solid solution introduced by Al, and highest for Gd and Y, in agreement with what the respective phase diagrams suggest. The implications for creep resistant alloy selection and design are discussed.

Keywords: Athermal Regime, Linear Hardening, Stress Relaxation, Short Range Order

7.1 Introduction

The importance of solid solution hardening to the creep strength of Mg alloys has often been stressed in the literature [1-10]. This assertion, however, calls for some qualification considering that AZ91, the commercial alloy with the highest solid solubility of its main solute, is also a textbook example of poor creep performance, even in the solution-heat-treated state in which as much as ~9 at.% of Al is in solution at the start of the test. That is, solid solution effects on the creep behavior of Mg alloys are rather related to the nature of the solute itself than to just its mere presence. Obvious as the preceding conclusion may seem, its practical value for cast alloys is made evident next.

In high-pressure die cast (HPDC) Mg alloys pronounced coring leaves the center of the α-Mg grains largely denuded of solute [10, 11]. Solute profiles of HPDC Mg-Al alloys created using the Scheil-Gulliver equation (e.g., Fig. 2-a of [12]) or obtained through microprobe profiles (Fig. 4 of [1]), show that even for a solute like Al with very high terminal solubility, the core of the grains retains only a minute fraction in solution. Thus, unless heat treated, the core of the α-Mg grains is little more than pure Mg, constituting an inherent weakest link in the alloy's microstructure. It follows that the relative efficiency of the solid solution strengthening at dilute (~1*at.*%) concentrations is crucial when it comes to optimizing the microstructural design of all cast (i.e., not heat treated) Mg alloys, and particularly so in HPDC alloys.

A relevant case study concerning HPDC binary Mg-La and Mg-Nd alloys was recently described by Zhang *et al*. [13, 14]. FIB sectioning was used to show that the segregation of solute towards the grain boundaries during solidification results in the formation of a percolating 3D eutectic microstructure. For the La-containing alloy the terminal solubility is very limited and the eutectic represented as much as 30% by volume of the alloy's microstructure whereas the remaining 70% was nearly pure Mg. Comparison with reference alloys showed that the percolating eutectic contributed ~40 MPa to the alloy's total strength. In contradistinction, the higher terminal solubility of Nd led to virtually no intergranular eutectic in the Mg-Nd alloy, with ~30 MPa of the alloy's strength accounted for by the supersaturated solid solution. Zhang *et al*. concluded that an optimal design of the microstructure should therefore include a eutectic forming solute as well as one able to provide efficient solid solution hardening to the alpha-Mg matrix at the low concentrations feasible for most RE-solutes. A working example was shown through a ternary Mg-La-Nd alloy in which both solid solution and eutectic reinforcement added their strengthening contributions in a linear fashion[13]. It is implicit in these assertions that both the percolating eutectic microstructure and the

solid solution hardening of the alpha-Mg grains' core must be effective, i.e., stable, at high temperatures if they are to make the alloys creep resistant.

With the ultimate goal of designing creep resistant HPDC Mg alloys, a close examination of the high temperature strength of dilute binary alloys seems then to be a necessary first step. In the companion paper [15] it is argued that solutes with a strong tendency to develop short range order (SRO)should be sought after, since, for given concentration, they should extend the alloy's athermal regime well above what can be expected for similar concentrations of solutes leading to random solid solutions, such as Al. Potential solutes were ranked as per their potential strengthening effects by combining their tendency to develop SRO with their solubility at the testing temperature. Such a ranking for a range of selected solutes can be seen in the Pareto plots of Figs. 12 and 13 of the companion paper, and which suggest, in decreasing order of expected strength of SRO, hence of potential contribution to the creep strength of a solid solution, the following sequence:

$$\text{Y, Gd} > \text{Nd, Zn, Ag, Sn} > \text{Al} > \text{Sb, Sr} \qquad (1)$$

In this work the strength and stress relaxation behavior of six representative dilute binary alloys, namely, alloys with Y, Gd, Nd, Zn, Sn and Al, was assessed to verify the extent to which Eq. 1 represented reality at the temperatures at which Mg alloys are expected to be useful (453-523K (180-250°C)). The concentrations used for the study were set at, or slightly above, the respective solute solubilities at ~ 473K (200°C) so as to limit precipitation during the testing while representing the solute-depleted core of the grains of HPDC alloys [12]. Specimens of AZ91D alloy were included in the study to provide a straightforward comparison with existing data in the literature. Preliminary results of this study were presented in [16, 17].

7.2 Experimental Details

Melting was done in a steel crucible coated with boron nitride loaded with predetermined proportions of commercially pure Mg, Zn, Al, Sn, Nd, Y and a Mg-Gd master alloy (2:3 Gd:Mg) using an electric furnace. SF6+CO2 was used as protective atmosphere. The liquid alloys were stirred mechanically for ~20 minutes to ensure the dissolution of the solute and subsequently poured at 1008-1023K (735-750°C) under an argon atmosphere into 80 x 80 x 10 mm^3 steel moulds preheated to 573K (300°C). Commercial AZ91D alloy was similarly cast. The cast plates were solution heat treated under Ar atmosphere as per the times and temperatures given in Table 1, and

quenched into water. Samples for grain size measurement were polished following standard procedures and etched using an acetic–picric acid mixture [20 ml acetic acid, 3 g picric acid, 20 ml H_2O and 50 ml Ethanol] for Mg-Zn and Nital [5% nitric acid and 95% ethanol] for the rest of the alloys. The linear intercept method in accordance with ASTM E112-88 was used to determine the grain size, counting not fewer than 200 boundaries (see Table 7-1). The nominal and actual compositions are also listed in Table 1.

Testing was carried out using cylindrical specimens, 18 mm in height and 9 mm in diameter, on a screw-driven machine at 298K (25°C), 373K (100°C) and 453K (180°C) in a temperature controlled chamber. All of the alloys were tested in the solid solution heat treated and quenched condition.The more creep resistant solid solutions, namely, those with the three RE solutes (Y, Gd and Nd) were also tested at 493K (220°C) and 523K (250°C). The crosshead speed for compression testing was 0.016 mm/min (initial strain rate = $1.5x10^{-5}s^{-1}$). All tests were repeated at least once.

Stress relaxation tests were performed at 453K (180°C). The specimens were deformed at an applied crosshead speed of 0.2 mm/min (initial strain rate = $1.85x10^{-4}$ s^{-1}) up to a predetermined strain and stress, and the machine stopped allowing the stress to relax for 1800s (30 min) for the less creep resistant alloys (Al, Zn and AZ91) or 3600s (60 min) for the rest.

Table 7-1 Chemical composition of the binary alloys studied determined by inductively coupled plasma atomic emission spectroscopy (ICP-AES), (AZ91 the nominal composition is quoted) and the respective grain sizes and solution heat treatment (time and temperature) schedules.

Alloy (*at.*%)	Solute (*at.*%)	*c* @ 473K (200°C)[a]	Grain size (μm)	Time(h)	Temperature K (°C)
Mg-1.5%Zn	2.2	1.5	123	4	653 (380)
Mg-2.5%Al	2.5	2.5	129	10	686 (413)
Mg-1%Gd	0.8	1.0	119	4	808 (535)
Mg-1.5%Y	1.3	1.5	108	2	813 (540)
Mg-1%Nd	0.9	0.8	120	6	813(540)
Mg-0.6%Sn	0.63	0.5	130	8	723 (450)
AZ91	(nominal) 8Al-0.4Zn	-	130	20	686 (413)

[a] *the c-values were bound by the solid solubilities at either ~ 473K (200°C) as per Fig. 11 in the companion paper[15] , or the solid solution heat treatment temperature (Nd), or by a maximum of 2.5 at.% (Al).*

7.3 Results

Compression curves of the alloys of Table 7-1 are shown in Figs. 7-1(a-c). Figure 7-2 compares the respective strengths at strains of 0.005 and 0.05 (identified by vertical lines in Fig. 7-1). Figure 7-3 shows the alloys' stress relaxation behaviour.

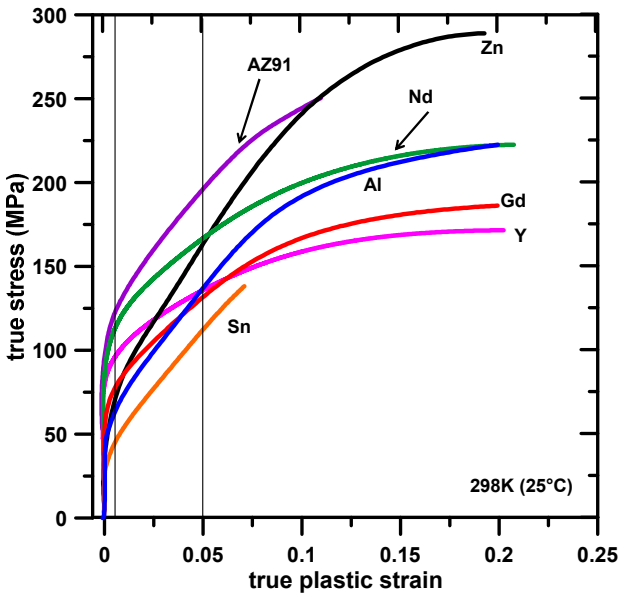

(a)

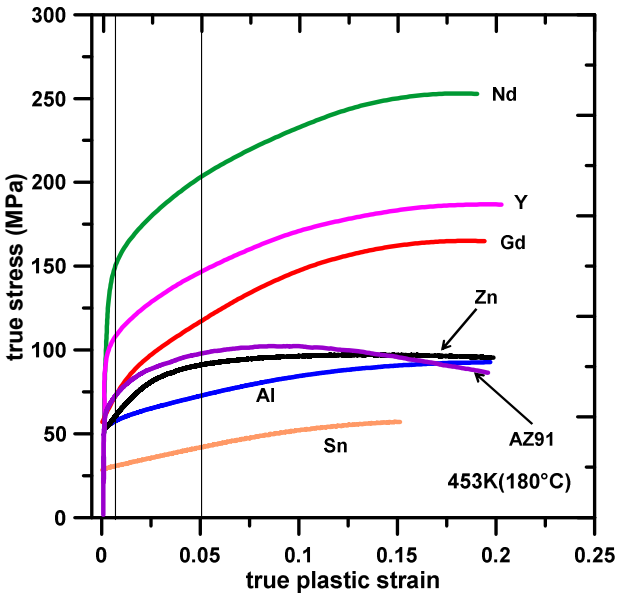

(b)

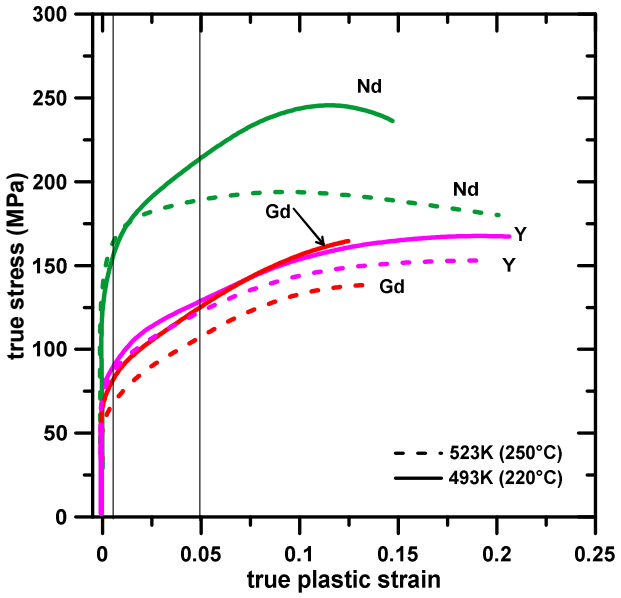

(c)

Figure 7-1. The compressive flow behaviour of the alloys studied, at (a): 298K (25°C); (b): 453K (180°C); (c): 493K (220°C) and 523K (250°C). The vertical lines identify the 0.005 and 0.05 strains used for creating Figs. 7-2(a) and (b).

At room temperature (Fig. 7-1a), a linear hardening stage of comparable slope was observed in the flow curve of all of the alloys between yield and ~10 % strain. At 453K (180°C), Mg-Al exhibited

the largest loss of strength (Figs. 7-1b and 7-2b), or the fastest relaxation (Fig. 7-3), followed by Mg-Sn, Mg-Zn and AZ91D. The loss of strength was limited for Gd as the testing temperature increased, whereas a small gain was observed for both Y and Nd containing alloys (Fig. 7-2). The linear strain hardening regime was observed at 493K (220°C) for Nd, whereas at 523K (250°C) only the Gd- and Y-containing alloys (Fig. 7-1c) exhibited it.

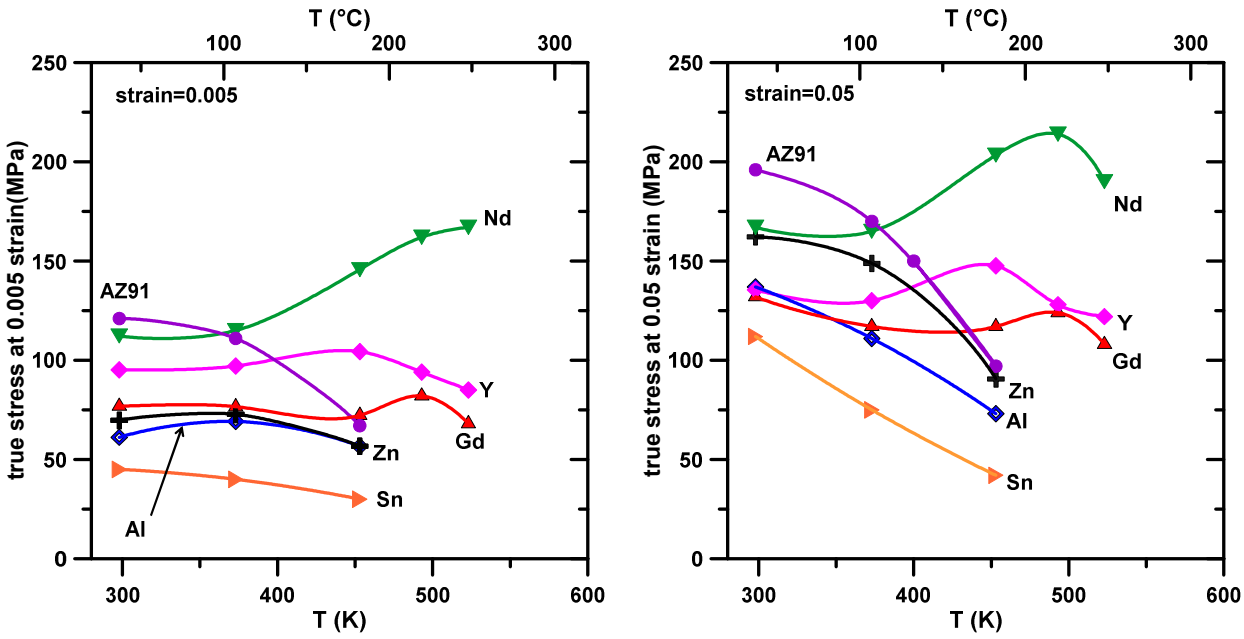

(a) *(b)*

Figure 7-2. The flow stress of the alloys of Table 1 as a function of the test temperature, for applied compressive strains (the vertical lines in Figures 7-1) of (a) 0.005 and (b) 0.05.

Figure 7-2a identifies an athermal regime up to about 373K (100°C) for AZ91, Mg-Sn and Mg-Zn, and up to 493K (250°C) for the rest of the alloys at low stress and strain. At higher stress and strain (Fig. 7-2b) the athermal regime was virtually non-existing in the weaker alloys (Al, Sn and Zn), whereas it extended to over 473K (220°C**)** for the RE's, making the differentiation between the two groups of alloys much more explicit. The stress relaxation behaviour (Fig. 7-3) was generally consistent with the monotonic strength data of Fig. 7-2, i.e., Al-, Sn- and Zn-containing alloys as well as AZ91 exhibited pronounced stress relaxation, whereas the RE's did it on a much limited scale despite the very high applied stresses applied (>150 MPa for Y, Gd and >200 MPa for Nd). In the iso-stress test (Fig. 7-3b) the difference in behaviour between the RE's specimens and that of

the AZ91 is again much more evident (the Al, Sn and Zn specimens did not reach the required flow stress of 150 MPa to be included in Fig. 7-3b.).

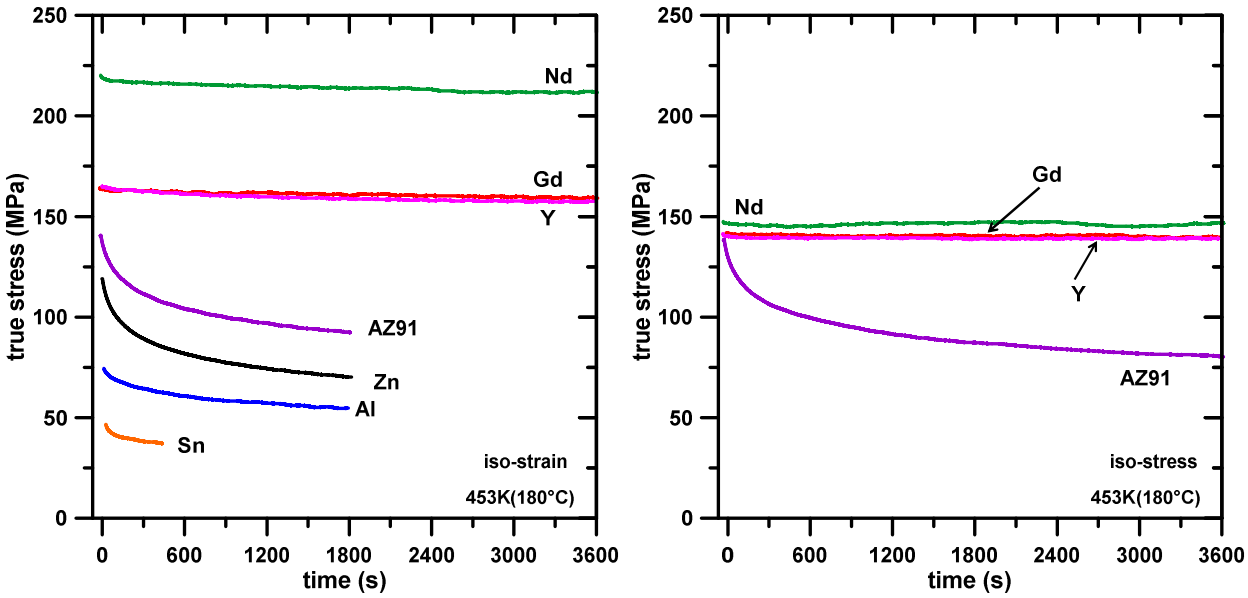

(a) *(b)*

Figure 7-3. Stress relaxation curves at 453K (180°C) at an applied (a) strain of 5%, (b) stress of 150 MPa for the alloys of Table 7-1.

7.4 Discussion

The difference in behaviour between the two sets solutes, i.e., Al, Sn and Zn versus Nd, Gd and Y, evidence the difference in intensity of dynamic recovery within the respective dislocation substructures, greater in the weaker alloys [18, 19]. The linear strain hardening regime exhibited by the deformation curves in Fig. 7-1, when present, is consistent with an athermal forest mechanism stemming from a stable dislocation substructure [7, 18-20]. This is the case up to ~273K (100°C) for the weakest alloys (Al), up to 493K (220°C) for Nd (Fig. 7-2c) and up to 523K (250°C) for the Y and Gd containing alloys.

The linear hardening stage in the flow curves, and the extended athermal behaviour observed in Figs. 7-2 and 7-3 for the RE's are both closely consistent with an increasingly stronger SRO, which imposes an additional activation energy to the relevant dynamic recovery reactions, as predicted by

Eq. 1. A strong SRO makes these alloys to behave as if they were tested at a lower temperature [21] hence a more difficult prismatic slip, affecting cross slip of screw dislocations, and a slower diffusion rate, hence a slower climbing of edge components can be expected [22] as discussed in more details in chapter 6.

The increase in strength during testing at high temperature made evident by Figs. 7-1 and 7-2 for the Y- and Nd-containing alloys is an indication of an additional strengthening mechanism, which is normally ascribed to either dynamic precipitation or strain induced precipitation [2, 7, 23, 24]. However, Fig. 7-1c shows that despite its higher yield strength at 523K (250°C), the linear strain hardening stage of the Mg-Nd alloy virtually disappeared, in contrast with Mg-Y and Mg-Gd, for which it still prevails. Precipitates can only act efficiently in pinning dislocations if the whole of the dislocation substructure is stable at the working temperature, since otherwise the long range stresses which determine the material's flow stress will decrease over time. The behaviour of Mg-Nd, which loses the ability to strain harden linearly at 523K (250°C) despite its high yield strength is an example of this situation: although the dislocations are hard to move at yield, the freshly generated dislocation substructure of the deformed alloy is generally unstable, hence strain hardening is negligible and the overall strength collapses. The overall behaviour of the Mg-Nd alloy appears consistent with the weaker SRO predicted by Eq. 1 for Nd (due to its lower solubility at high temperature) in comparison with Y and Gd, which, as Fig. 7-1c shows, retain the ability to strain harden linearly (i.e., athermally) at 523K (250°C). A related example is discussed below in relation to alloy AE42. Consistently with these conclusions, Maruyama *et al.*[7] pointed out that secondary (non-basal) slip predominates in Mg-Y solid solutions tested at 500K (277^{o}C), accounting for the alloy's strain hardening.

Figure 7-4 compares the compression behaviour of the present dilute solid solutions with several commercial alloys from the literature (tested at comparable strain rate (1.33×10^{-4} s^{-1})). The strengths of the present binary RE solid solutions, with only ~ 1*at.*%, closely match those of the Ag-RE- (QE22) and Al-RE- containing (AE42) alloys, and are higher than that of Al-Si (S21) alloy, providing support to the present SRO-based hypothesis that the strength and the strain hardening behaviour of the alloys is determined by the relatively small amount of solute in solution.

In connection with the loss of the linear strain hardening of Mg-Nd at the higher emperatures mentioned above, the opposite effect can be seen in Fig. 7-4: the addition of RE results in the recovery of the linear hardening stage in AE42 in comparison with AZ91, an indication of increased thermal stability of the dislocation substructure in the former.

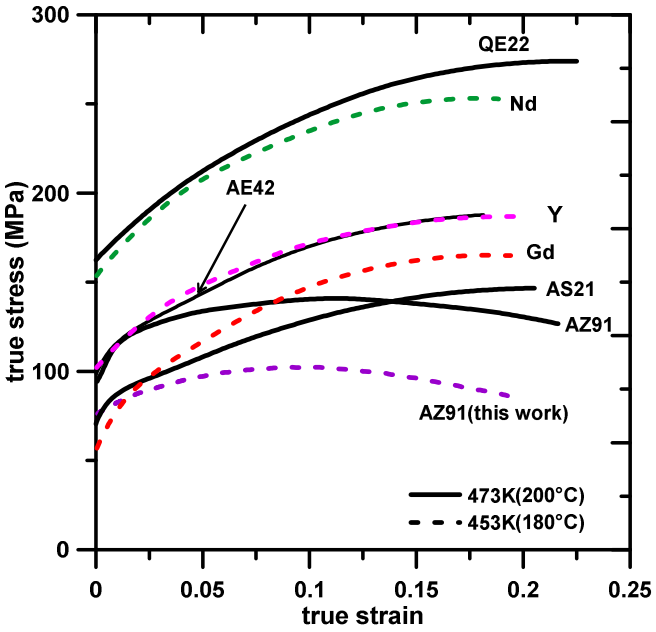

Figure 7-4. Compression behaviour of squeeze-cast alloys AZ91, AS21, QE22 and AE42 (solid lines) replotted from [25] and selected solid solutions from the present work (dashed lines).

Following the analysis of Ref. [26], the alloys of the present study have been ranked based on the strength of the respective SRO as:

$$\tau_{SRO} \sim [\Delta H * c(1-c)]^2 \quad , \qquad (2)$$

where ΔH is the enthalpy of formation of the solid solution and c is the solute concentration listed in Table 7-1. The calculated data, which reproduces the ranking of Eq. 1, have been plotted in Fig. 7-5 as a function of ΔH to make evident that the most effective solutes, i.e., Y and Gd, are those that combine a high ΔH with high solubility at the test temperature. Figure 7-5 includes also the stress relaxation data of Fig. 7-3, expressed as the reciprocal of the stress drop for each alloy. The experimental data closely conforms to the predicted behaviour, locating Y at the top and Al at the bottom, i.e., consistently with the high SRO strength of the former and the near-random solid solution hardening of the latter. Again, the agreement between the calculated and experimental data are all the more remarkable considering that the concentrations of the alloys studied are all in the order of 1*at*.%.

In the introduction the speculation by Zhang *et al*. [13, 14] on the need to ensure that the solid solution component is stable at the testing temperature was mentioned. Experiments by Gavras *et al*.[24] show that Mg-La-Y and Mg-La-Gd are indeed much more creep resistant than the Mg-La-Nd alloy, in close consistency with Fig. 7-5, which rates Y and Gd well above Nd. The overall predictions of Fig. 7-5 also match the creep results obtained by Maruyama *et al*.[7] concerning Mg-Y being much better than Mg-Al already mentioned.

By and large, the data from either the present experiments or the open literature support the assertions that, on the one hand, the creep resistance of cast Mg alloys is ultimately determined by the strength of their weakest link represented by solute depleted core of the α-Mg grains. On the other, solutes with measurable solubility at the testing temperature and a strong tendency to develop SRO, such as Gd and Y, appear as the most suitable candidates for increasing the creep strength of cast Mg alloys.

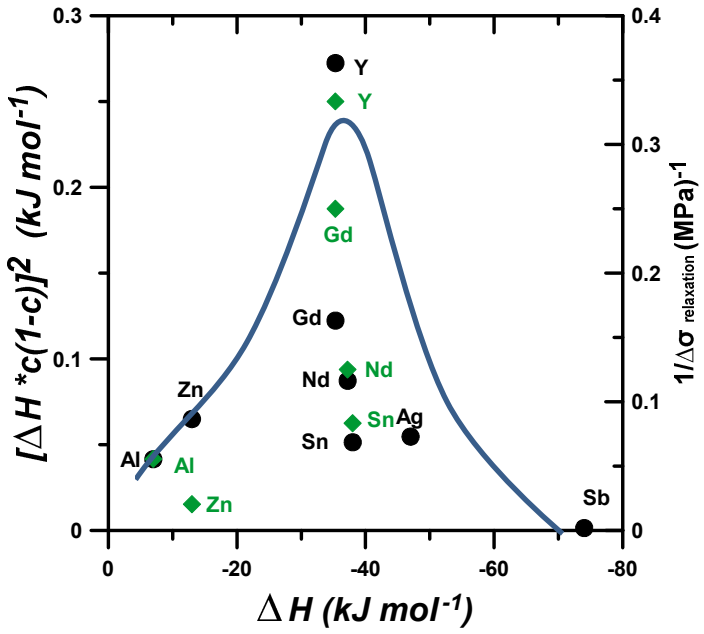

Figure 7-5.The predicted strength of SRO (solid circles) according to Eq.2 and stress relaxation data from Fig. 7-2a (diamonds). Ag and Sb are included for completeness, assuming a concentration of 0.5at.% for Ag and 0.05at.% for Sb (see Table1 in the companion paper). The solid line is arbitrary. Likewise, the respective scales of the left and right hand side Y-axes were adjusted for the data to fit within comparable spans.

7.5 Conclusions

- Specimens of six dilute binary Mg-based solid solutions containing (at.%) 2.5Al, 2.2Zn, 0.6Sn, 0.8Gd, 0.9Nd and 1.3Y and of AZ91D alloy were tested in compression at 298K (25°C), 373K (100°C) and 453K (180°C) and stress relaxation at 453K (180°C) at a preset strain or stress, in order to determine the extent of the alloys' athermal regimes.

- The athermal behaviour extended only to about 373K (100°C) for the Mg-2.5Al and AZ91 alloys, consistently with the random solid solution hardening introduced by Al.

- The RE containing alloys exhibited an extended athermal regime, up to 493K (220°C) for Nd and past 523K (250°C) for Y and Gd. Zn and Sn exhibited an intermediate behavior between the RE and Al.

- The compression and relaxation behaviour of the alloys ranked the solutes in decreasing order of strength efficiency as: Y ➔ Gd ➔ Nd➔ Zn ➔Sn➔ Al. This behaviour closely matched the expected behaviour considering the relative tendencies to develop short range order combined with each solute's solubility at ~473K (200°C).

- The high temperature strength of the present binary RE alloys, despite containing only about 1*at*.% solute in solution, either matched or surpassed that of typical ternary and quaternary commercial alloys (AS21, QE22, AE42), supporting the hypothesis that short range order introduced by suitable solutes that remain in solution ultimately determines the high temperature strength of current creep resistant cast Mg alloys.

7.6 References

[1] J.R. Terbush, N.D. Saddock, J.W. Jones, T.M. Pollock, Metallurgical and Materials Transactions A, 41 (2010) 2435-2442.

[2] J.-F. Nie, Metallurgical and Materials Transactions A, 43 (2012) 3891-3939. 10.1007/s11661-012-1217-2

[3] B.L. Mordike, Materials Science and Engineering: A, 324 (2002) 103-112. http://dx.doi.org/10.1016/S0921-5093(01)01290-4

[4] M.O. Pekguleryuz, A.A. Kaya, ADVANCED ENGINEERING MATERIALS, 5 (2003) 866-878. 10.1002/adem.200300403

[5] M. Pekguleryuz, M. Celikin, International Materials Reviews, 55 (2010) 197-217. doi:10.1179/095066010X12646898728327

[6] M.S. Dargusch, G.L. Dunlop, A.L. Bowles, K. Pettersen, P. Bakke, Metallurgical and Materials Transactions A, 35 (2004) 1905-1909. 10.1007/s11661-004-0099-3

[7] K. Maruyama, M. Suzuki, S. HIROYUKI, Metallurgical and Materials Transactions A, 33 (2002) 875-882.

[8] I. Moreno, T. Nandy, J. Jones, J. Allison, T. Pollock, Scripta Materialia, 45 (2001) 1423-1429.

[9] M.A. Gibson, X. Fang, C.J. Bettles, C.R. Hutchinson, Scripta Materialia, 63 (2010) 899-902. http://dx.doi.org/10.1016/j.scriptamat.2010.07.002

[10] S.M. Zhu, M.A. Gibson, M.A. Easton, J.F. Nie, Scripta Materialia, 63 (2010) 698-703. http://dx.doi.org/10.1016/j.scriptamat.2010.02.005

[11] T.L. Chia, M.A. Easton, S.M. Zhu, M.A. Gibson, N. Birbilis, J.F. Nie, Intermetallics, 17 (2009) 481-490. 10.1016/j.intermet.2008.12.009

[12] K. Yang, C. Cáceres, M. Easton, Metallurgical and Materials Transactions A, 45 (2014) 4117-4128. 10.1007/s11661-014-2326-x

[13] B. Zhang, S. Gavras, A.V. Nagasekhar, C.H. Cáceres, M.A. Easton, Metallurgical and Materials Transactions A, (2014) 1-12.

[14] B. Zhang, A.V. Nagasekhar, X. Tao, Y. Ouyang, C.H. Cáceres, M. Easton, Materials Science and Engineering: A, 599 (2014) 204-211. http://dx.doi.org/10.1016/j.msea.2014.01.074

[15] S. Abaspour, C. Cáceres, Metallurgical and Materials Transactions A, submitted (2014)

[16] S. Abaspour, C. Cáceres, in: Martyn Alderman, Michele V. Manuel, Norbert Hort, Neale R. Neelameggham (Ed.) *Magnesium Technology 2014*, 2014, pp. 71-75.

[17] S. Abaspour, C.H. Caceres, in: (Ed.) *TMS 2013*, TMS, 2013, pp.

[18] U.F. Kocks, H. Mecking, Progress in Materials Science, 48 (2003) 171-273.

[19] D. Kuhlmann-Wilsdorf, Metallurgical and Materials Transactions, 35A (2004) 369-418.

[20] C.H. Cáceres, P. Lukác, Philosophical Magazine A, 88 (2008) 977-989. http://dx.doi.org/10.1080/14786430801968611

[21] H. Suzuki, in: J C Fisher, W G Johnston, R Thomson, T Vreeland (Eds.) Dislocations and mechanical properties of crystals, John Wiley, New York, 1957, pp. 361-390.

[22] K. Sadananda , M.J. Marcinkowski, Journal of Applied Physics, 44 (1973) 1989- 1996; DOI:1910.1063/1981.1662504

[23] T.J. Pike, B. Noble, Journal of the Less Common Metals, 30 (1973) 63-74. 10.1016/0022-5088(73)90007-6

[24] S. Gavras, in, Monash University. Faculty of Engineering. Department of Materials Engineering, 2014.

[25] Z. Trojanová, P. Lukác, Journal of Materials Processing Technology, 162-163 (2005) 416-421.

[26] C.H. Cáceres, A. Blake, physica status solidi, 194 (a) (2002) 147-158.

Chapter 8 Conclusions

This study focused mainly on the structural reasons for poor creep resistance and low age hardening response of Mg alloys. Atomic level thermodynamics arguments suggesting that extending the athermal regime through short range order (SRO) is a most feasible path to increasing the creep strength of Mg alloys were used. Potential solutes were sorted out and ranked based on their tendency to developing SRO. The predictions were corroborated by experiments involving binary alloys. Specimens of six dilute binary solid solutions, Mg-2.5Al, Mg-2.2Zn, Mg-0.6Sn, Mg-0.8Gd, Mg-0.9Nd and Mg-1.3Y and of AZ91D alloy were tested in compression at 298K (25°C), 373K (100°C) and 453K (180°C) and stress relaxation at 453K (180°C) at preset strain and stress, in order to determine the extent of the alloys' athermal regime. The following conclusions were obtained.

- The Miedema *et al.*'s scheme rationalizes most, if not all, of the observed behavior in current multicomponent alloys, ranging from weak-to-strong ageing response and from low-to-high creep resistance. The scheme naturally suggests a rational approach to solute selection, hence, to alloy design, derived from the relevant binary phase diagrams.

- The relative tendency, of most solutes to develop SRO disputes the viability of several other micromechanisms often considered, such as pinning of edge dislocations by mobile solute clouds, dynamic precipitation of thermally stable precipitates, or atomic size effects on the diffusivity of rare-earths solutes.

- It was shown that due to the strongly electropositive nature of Mg, most alloy systems can be expected to develop short range order (SRO), on the one hand curtailing the nucleation of finely dispersed coherent precipitation, hence preventing a strong response to artificial ageing whereas on the other time potentially increasing the creep strength.

- The ranking of the strengthening by SRO is: Y ➔ Gd ➔ Nd ➔ Zn ➔Sn➔ Al. Rare earths appeared as the strongest candidates, particularly Y, Gd and Nd, consistently with the high melting point of the intermetallics they form with the host, and in close agreement with the alloys' creep behavior reported in the literature.

- The creep strength of the present binary alloys, despite containing only about 1at.% RE, closely matches the strength of commercial ternary alloys (AS21, QE22, AE42) indicating that SRO is indeed the dominant strengthening mechanism in current creep resistant Mg alloys.

Alloy Selection and Design

Three strategies for selection and design likely to lead to high strength alloys were suggested.

- The first one points to the need to incorporate solutes such as Y, with significant solubility yet strong tendency to develop SRO, to reinforce the core of the grains in HPDC alloys. On top of this basic solid solution strength, other strengthening mechanisms can be added, such as those resulting from a percolating eutectic microstructure.

- The second strategy, derived from the Al-Cu alloys system, consists in inducing homogeneous precipitation through a ternary addition that naturally tends to cluster, hence provide a homogeneously nucleated precursor phase that would lead to subsequent coherent or at least fine incoherent precipitation (e.g., adding Na to Mg-Sn or Mg-Sb).

- The third path, inspired in the Mg-Th system, starts with a suitable (although inherently weak) alloy such as Mg-Mn, but requires a ternary addition (e.g. Sc) to create order in the pre-existing coherent precipitates.